University of Southampton
Optoelectronic Research Centre

High Power Pulsed Ytterbium Doped Fibre Lasers And Their Applications

by

Kang Kang Chen

Thesis submitted for the degree of
Doctor of Philosophy

Jan, 2011

UNIVERSITY OF SOUTHAMPTON

ABSTRACT

FACULTY OF ENGINEERING AND APPLIED SCIENCE
OPTOELECTRONICS RESEARCH CENTRE

Doctor of Philosophy

HIGH POWER PULSED YTTERBIUM DOPED FIBRE LASERS AND THEIR APPLICATIONS

by Kang Kang Chen

The aim of my project is to develop pulsed Ytterbium (Yb) doped fibre master oscillator power amplifier (MOPA) systems seeded by semiconductor lasers. I was principally focused on two specific projects aligned to sponsored programs of research within the ORC pulsed fibre laser group:

The first project, TSB funded project LAMPS, aimed to develop an important class of next generation laser system capable of average output powers of more than 100 W when operating in both the nanosecond and picosecond regimes. The goal was to develop a fully fiberized, polarisation maintaining, single transverse mode system. The full project included the development of the necessary diode & micro-optic systems, fibre beam delivery technology and with application focused evaluations in collaboration with our industrial partners. The main project partners were BAE Systems, Selex, Ceram, Intense Photonics, ORC, Herriot Watt University, Power Photonics, OptoCap and Rofin Sinar. I contributed to the development of the single transverse mode Ytterbium (Yb)-doped fibre system and achieved the full target specifications of 100 W of output power with single mode and single polarisation operation in both the nanosecond and picosecond regimes. In addition, second harmonic generation pumped by the fundamental beam at 1.06 μm was also achieved. In order to transfer from picosecond pulses to nanosecond pulses it is only necessary to switch the seed laser, the power amplifier system remaining unchanged making for a highly flexible system. Both fundamental and second harmonic beam were successfully used to do material processing and various high

power frequency conversion experiments (visible, broadband supercontinuum and mid-IR).

The second project, called HEGAC (also funded by the TSB), was a collaboration with the University of Cambridge and SPI Lasers Ltd. The aim of the HEGAC project was to develop a high power nanosecond fibre laser with an active pulse shaping capability suitable for cutting metals. This project targeted mJ pulses with more than 100 W average power at the final output – with a 200 W stretch objective. We first achieved more than 310 W using a free space seeding and pumping configuration in our laboratories proving power scaling of our proposed approach. I subsequently rebuilt and improved this system and developed a fully-fiberized version (including all pump launches). The laser was capable of generating >100 W of output power and pulse energies up to 2.5 mJ. This project also involved spatial mode as well as temporal pulse shaping. Using a pair of axicon lenses the normal Gaussian beam profile was converted to a ring shaped profile as required and the system tested up to average powers of 100 W. In addition to the normal temporal pulse shapes required using our pulse shaping system (square, triangle and step), I also achieved high average power pulses with smooth shaped pulses (Parabolic and Gaussian) using an adaptive pulse shaping technique. The laser was transported and successfully used in materials processing experiments at Cambridge, proving the robustness of the design and implementation. I also did some novel experiments on high efficiency Raman conversion exploiting the square shaped pulses possible using this laser.

List of contents

List of figures

DECLARATION OF AUTHORSHIP

I, KANG KANG CHEN declare that the thesis entitled

HIGH POWER PULSED YTTERBIUM DOPED FIBRE LASERS AND THEIR APPLICATIONS.

and the work presented in it are my own. I confirm that:

- this work was done wholly or mainly while in candidature for a research degree at this University;
- where any part of this thesis has previously been submitted for a degree or any other qualification at this University or any other institution, this has been clearly stated;
- where I have consulted the published work of others, this is always clearly attributed;
- where I have quoted from the work of others, the source is always given. With the exception of such quotations, this thesis is entirely my own work;
- I have acknowledged all main sources of help;
- where the thesis is based on work done by myself jointly with others, I have made clear exactly what was done by others and what I have contributed myself;
- Parts of this work have been published (see list of publications).

Signed: ....

Date: ....

Acknowledgements

First of all, I would like to thank my supervisor Professor David Richardson.

I greatly appreciate that he gave me the chance to start my PhD at the ORC. Without this the rest would not have happened! Prof. Richardson has given me all of the guidance that I needed throughout my project. My co-supervisor Dr Andy Malinowski has helped greatly, especially at the beginning of my study. He was always there for me to ask for help and advice. My supervisors have been very encouraging to me. I am also very grateful to Mr Khu Tri Vu who spent a great amount of time teaching me during the first few months of my study and which enabled me to get off to a quick start. Dr Shaif-ul Alam accelerated my study tremendously and he gave me a lot of fantastic advice along the way - without him I would not have finished my studies so quickly and with such success.

I would like to specially thank Dr Fei He and Dr Jonathan Price for the many useful discussions. Thanks also go to Mr John R. Hayes and Dr Dejiao Lin with whom I shared a lot of good experiences during our work together.

In addition, I acknowledge others who have directly helped me during my whole study.

I would like to thank Dr Jayanta Sahu for fabricating many of the fibres that I used. I thank Dr Christophe Codemard and Dr Yoonchan Jeong for their generous sharing of their experience. I am grateful for Dr Morten Ibsen for fabricating the chirped fibre Bragg Gratings used in my picosecond seed laser. Also, I would like to thank PhD student Florian Kienle in the Ultrafast Optical Parametric Oscillators group for the collaborative OPO work.

I thank all of the technicians, IT and support staff for their help during the time I studied at the ORC - especially Simon Butler and Trevor Austin who I bothered very often during my PhD. I send my special thanks to Mrs Eve Smith for being such a good student coordinator.

I acknowledge the ORC for supporting my PhD studies through a precious ORC studentship, and I thank Prof. Rob Eason, Prof. David Shepherd and other members of the ORC Graduate Board for their great support.

Last but not least, I wish to thank my wife and my parents for all their solid support throughout my studies.

List of Abbreviations

AOM	Accousto-Optics Modulator
ASE	Amplified Spontaneous Emission
AWG	Arbitrary Waveform Generator
BDO	Beam Deliver Optics
CFBG	Chirped Fibre Bragg Gratings
CPA	Chirped Pulse Amplification
CW	Continuous Wave
DCA	Digital Communication Analyser
DCF	Double-Clad Fibre
DFB	Distributed Feedback
EOM	Electro-Optics Modulator
ESA	Excited State Absorption
FROG	Frequency-Resolved Optical Gating
FP	Fabry-Prot
FWHM	Full Width at Half Maximum
LMA	Large Mode Aera
MCVD	Modified Chemical Vapour Deposition
MFD	Mode Field Diameter
MOPA	Master Oscillator Power Amplifier
NA	Numerical Aperture
OD	Outer Diameter
OPO	Optical Parametric Oscillator
ORC	Optoelectronics Research Centre
OSA	Optical Spectrum Analyser
PBGF	Photonics Band Gap Fibre
PC	Polarisation Controller
SA	Simulated Annealing
SBS	Stimulated Brillouin Scattering
SHG	Second Harmonic Generation
SMSR	Side-Mode Suppression Ratio
SPI	Southampton Photonics Inc.
SPM	Self-Phase Modulation
SRS	Stimulated Raman Scattering
TFB	Taper Fibre Bundle
WDM	Wavelength Division Multiplexing

Chapter 1 Introduction

Overview

This chapter gives a brief overview of why high power pulsed fibre MOPA laser systems are of great interest. In section 1.1 the general motivations are introduced. A short review of the state of the art in this area is given in section 1.2. Finally, an outline of the thesis structure is given in section 1.3.

1.1 Motivation for the project

Pulsed laser systems have found widespread application in both the scientific research and commercial worlds. At present, the workhorse lasers are solid-state and gas lasers. However, there are problems associated with these lasers such as the management of thermal effects sufficient to preserve mode quality, low efficiency, the large physical size as well as the cost of manufacture and ownership. Rare-earth doped fibre lasers have much higher efficiency than crystal host solid-state lasers. In addition, the spectral transitions in glass are much broader than in crystals, which mean that is possible to amplify very short optical pulses [1]. Furthermore, the management of thermal effects and the effect on mode quality of the output is much easier since in fibre thermal lensing is generally negligible due to the inherent waveguiding in the core. The beam quality of the output is purely determined by the fibre structure and fibre configuration (at least up to the several 10's of kW average power regime). The development of fully-fiberized lasers and amplifier will lead to cheap, robust and compact replacements for expensive, complicated solid-state and gas lasers.

At present, the cost of solid state laser systems is limiting many applications of ultrafast pulsed lasers. Most of these ultrafast pulsed lasers are based on mode locked Ti:Sapphire cavities. They are bulky, expensive and are not readily scalable to the multi-watt average power levels required by many applications. Nanosecond high power lasers use Nd-doped glass/crystals which require careful thermal management in order to prevent beam quality distortion caused by thermal lensing effects. Even higher power applications are currently served by even more bulky and expensive gas laser systems (e.g. CO_2 lasers) which cannot provide femtosecond pulses.

Fibre laser systems seem avoid the problems mentioned above. They have good mode quality, high gain efficiency, low cost and compact size. In addition, they are generally pumped with compact semiconductor diode laser sources which are available commercially at low cost. Because of the feasibility of all fiberized integration eliminating free space devices and alignment, fibre lasers potentially require fewer components and mechanical parts making them more robust and compact [2]. However, the high power fibre laser is still a relatively new technology which is not well developed and currently many fibre lasers reported in the literature (particularly many pulsed fibre lasers) still incorporate bulky optics such as lenses, mirrors, dichroic mirrors, acousto-optic/electro-optic modulators, frequency conversion crystals and so on. Practical pump coupling is a major issue and although some all fiberized approaches have been invented (e.g. GT-wave[3]), they still have some drawbacks when it comes to pulsed fibre laser operation since they decrease the pump brightness and increase the fiber length. Pumping schemes using taper fibre bundle (TFB) technology to combine multimode pump and signal beams into a single fibre provide advantages in terms of brightness preservation, simplicity when adding pumps and flexibility when adapting signal and pump to different types of gain fibres – however the limited degree of isolation between laser signal and pumps can be a challenge for certain pulsed systems. Despite these issues all fibre high power pulsed fibre lasers can be built that are very robust and practical to use. As a consequence, fibre lasers, both continuous wave and pulsed, are in the process of moving out of research labs to become the next generation of industrial work horse lasers. With these high power and reliable sources at 1 μm, one can easily frequency convert the power to other wavelengths using traditional conversion techniques such as crystal based Second Harmonic Generation, Third Harmonic Generation, Fourth Harmonic Generation and Optical Parametric Oscillation - as well as novel fibre based techniques such as Stimulated Raman Scattering Conversion and Supercontinuum Generation. Fibre lasers, together with external frequency conversion techniques, can now be used to generate light at essentially any wavelength spanning from the deep UV to the mid-IR over a 4000 nm spectral range [4-7]. Because of their versatility and flexibility, I believe fibre lasers will replace many of the traditional solid state lasers and gas lasers for many applications in the very near future.

The aim of my research was to develop pulsed Yb^{3+}-doped fibre master oscillator power amplifier (MOPA) systems seeded by semiconductor lasers and to develop wavelength conversion schemes based on these systems.

I was principally devoted to working on two Technology Strategy Board (TSB) projects. The first of these projects was known by the acronym 'HEGAC [8]'. The aim of this project was to develop a nanosecond system for materials processing – specifically the gas-assisted cutting of metal. Our group demonstrated active shaping of the electrical drive pulses to a laser diode used as a MO in order to compensate for the pulse shaping effects due to gain saturation in a Yb^{3+}-doped fibre amplifier cascade so as to allow the generation of user defined customized output pulses [9]. This project aimed to generate more than 200 W of average power at the final output. We achieved more than 310 W of average output power using a free space pumping scheme [10]. However to make the system reliable and robust, we built a fully fiberized system (including pump delivery) capable of generating 100 W of output power and nanosecond pulses with up to 2.5 mJ of energy. A polarisation maintaining version was also built to make the system more versatile and suitable for frequency conversion uses. This project required both temporal shaped pulses and a ring-shaped output beam. In order to generate this ring mode we used a pair of external axicon lenses designed by another group in the ORC to reshape the normal Gaussian beam profile generated by the laser. In addition to the normal pulse shapes (square, triangular and step profile), we also achieved high average power with smooth shaped pulses (Parabolic and Gaussian) [10].

The other project was referred to be the acronym 'LAMPS[8]', which aimed to develop an important class of next generation laser system capable of delivering more than 100 W average output power but with the flexibility to work either in the nanosecond or picosecond pulse regimes, according to the requirements of the different applications pursued within the project (various materials processing and defence applications) . The aim was to build a fully fiberized, polarisation maintaining and single transverse mode laser system. I contributed to the development of the Yb^{3+}-doped fibre lasers and amplifiers capable of generating high energy output pulses. To change from picosecond pulses to nanosecond pulses, only the seed laser needed to be modified, keeping the amplifier chain unchanged. I achieved 100 W output power providing single mode and single polarisation operation both in the nanosecond and picosecond regimes. Using these laser sources, I then successfully demonstrated various wavelength conversion experiments. These included nanosecond pulse pumped OPOs, SHG and stimulated Raman conversion, as well as synchronously-pumped picosecond OPOs, SHG and supercontinuum sources. All these results proved pulsed fibre lasers combined with frequency conversion techniques represent practical solutions to various wavelength generation needs.

1.2 Brief review of the state of the art in pulsed fibre lasers at the beginning of my project

To provide some initial perspective of my PhD contribution relative to the development of the field I provide a very brief overview of the state of the art in high power pulsed fibre lasers at the start of my project – further more focussed descriptions of the literature relevant to specific aspects of my project are provided in the chapters that follow.

Fibre lasers were first introduced in the 1960s using multimode Nd-doped fibres by Elias Snitzer [11, 12]. However, due to the lack of appropriate pump sources (the first fibre laser were flash-lamp pumped and thus highly inefficient), the field of fibre lasers developed quite slowly. With the development of single mode doped fibres in the mid-1980s and parallel advances in semiconductor pump lasers the technology finally took off. At the beginning, fibre lasers used core-pumping and most work focused on Nd-doped silica fibre devices operating at 1.06 μm, as well as Er-doped fibre devices operating around 1.55 μm. The invention of the cladding pumping scheme in 1988 was however the key to power scaling [13] and has led to the boom in fibre laser power increases in the following decades. In 1995 2 W was reported [14], followed by 20 W [15] and 35 W [16] in 1997 and thereafter 110 W was reported in 1999 [17] using the Yb-doped gain medium. In 2003, the kilowatt power barrier for a close to diffraction limited beam was broken at the ORC, University of Southampton [18]. Later, several kW class commercial CW lasers with good output beam quality were successfully introduced to the market [19, 20]. The 10kW level was broken for the first by the company IPG in 2009 during my PhD.

Along with the development of CW lasers, short pulse high power Yb^{3+}-doped double-clad fibre lasers have also been intensively investigated due to their high peak power outputs.

In the nanosecond regime, high energy single transverse mode operation in core pumped erbium doped LMA fibres was first studied [21]. The LMA concepts was then applied to the ytterbium system in 2000 [22]. In this experiment, a multimode LMA fibre with V number 7.4 was coiled to a diameter ~1.58 cm: the output beam quality was measured to be M^2=1.09. Single mode pulsed operation was later achieved with pulse energy of 255 μJ, peak power of 300 kW and a pulse duration of 0.8 ns [23]. Several high average power cladding pumped mJ nanosecond Yb^{3+}-doped fibre lasers were reported in 2002: Limpert et al. reported a Yb^{3+}-doped high energy nanosecond fibre MOPA capable of delivering 100 W average output powers and corresponding pulse energies of 2 mJ (90 ns pulse duration) and 15 W average power with 4 mJ pulse energy at a lower repetition rate with near diffraction limited beam quality [24]. None of these systems were fully fiberized or used active pulse shaping.

There has also been a lot of interest in picosecond pulsed sources. In 2001, Limpert et al reported a 10 picosecond, single mode fibre MOPA with 43 W average output power at 80 MHz repetition rate [25]. In 2005, our group transfered some well developed techniques from telecoms such as gain switching and picosecond pulse compression to the 1 micron regime to get short duration pulses in a highly practical manner [26]. Output powers as high as 300 W were reported using cladding-pumped ytterbium doped fibre amplifiers (YDFA) seeded by a 1060 nm gain-switched Faby Perot laser [27, 28]. Later, progress was made using VECSEL mode-locked lasers as the seed source [29]. However, free space pump and signal coupling were used at various stages of the MOPA chain in these experiments.

Another development worthy of mention here in the ultrafast pulse regime is Chirped Pulse Amplification (CPA), which firstly stretches a femtosecond seed pulse to longer duration, then amplifies this stretched pulse to high energy in a chain of amplifiers. At the output end, a diffraction grating pair is used to compress the amplified chirped pulse back to the femtosecond regime. The purpose of this is to avioid having high peak powers in the fibre tereby avoiding fibre nonlinearity. Galvanauskas et al [30] demonstrated a 50 μm-core Yb^{3+}-doped fibre CPA that produced 380 fs pulses with energies of 1.2 mJ. In addition, the development of compact stretchers and compressors in CPA systems has attracted a lot of attention. With the development of high damage threshold dielectric diffraction gratings, millijoule pulse energies in the femtosecond regime were achieved in 2007. This result shows that a Gigawatt peak power level fibre system is feasible. Recently, an 830 W high average power CPA system [31] was reported which demonstrates that the kilowatt-class ultra short pulse fibre system will be available very soon. My work is not focused on CPA systems, but progress here is worth mentioning as the compressor technology developed has proved useful in my picosecond system (although the scale of compression is very different in my work).

1.3 Thesis Structure

My thesis is structured as follows.

Chapter 2 introduces the background knowledge of the Yb^{3+}-doped fibre technology. The basic laser physics and physics of the underpinning technologies are described in this chapter. The constraints encountered in fibre lasers due to various nonlinearities are also discussed in this section.

The development of high power nanosecond MOPA systems with active pulse shaping is described in chapter 3.

Chapter 4 describes the development of high power (100W) picosecond MOPA systems in both non-PM and PM configurations.

Chapter 5 presents experimental studies toward frequency conversion (SHG, OPOs and Raman conversion) using the single mode, single polarisation nanosecond source that I developed.

In Chapter 6 I describe results obtained for wavelength conversion in the picosecond regime. Using the picosecond source I developed 56 W of frequency doubled output source at 530 nm was achieved. A high power synchronously pumped OPO and high power supercontinuum source are also demonstrated using the picosecond source.

Finally, conclusions and possible future work are given in Chapter 7.

References

[1] J. Nilsson, J. K. Sahu, Y. Jeong, W. A. Clarkson, R. Selvas, A. B. Grudinin, and S. Alam, "High-power fiber lasers: new developments," in Advances in Fiber Lasers, San Jose, CA, USA, 2003, pp. 50-59.

[2] F. Gonthier, " All-fiber pump coupling techniques for double-clad fiber amplifiers," presented at the Lasers and Electro-Optics Europe, CLEO/Europe, 2005.

[3] A. B. Grudinin, D. N. Payne, P. W. Turner, L. J. A. Nilsson, M. N. Zervas, M. Ibsen, and M. K. Durkin, "Multi-fibre arrangements for high power fibre lasers and amplifiers " United States Patent 6826335, 2004.

[4] Thomas Südmeyer, Yutaka Imai, Hisashi Masuda, Naoya Eguchi, Masaki Saito, and S. Kubota, "12 W continuous-wave 266-nm deep-UV generation through 24 W single-frequency 1064-nm light from a fiber MOPA," in CLEO/QELS, CTuD1, 2006.

[5] K. K. Chen, S.-u. Alam, J. H. V. Price, J. R. Hayes, D. Lin, A. Malinowski, C. Codemard, D. Ghosh, M. Pal, S. K. Bhadra, and D. J. Richardson, "Picosecond fiber MOPA pumped supercontinuum source with 39 W output power," Opt. Express, vol. 18, pp. 5426-5432, 2010.

[6] S. U. Alam, Kangkang Chen, Dejiao Lin, Yonghang Shen, Shuangshuang Cai, Bo Wu, Peipei Jiang, and A. M. a. D. Richardson, "Externally modulated, diode seeded Yb^{3+}-doped fiber MOPA pumped high power optical parametric oscillator " presented at the Photonics West, San Jose, California, 2009.

[7] F. Kienle, K. K. Chen, S.-u. Alam, C. B. E. Gawith, J. I. Mackenzie, D. C. Hanna, D. J. Richardson, and D. P. Shepherd, "High-power, variable repetition rate, picosecond optical parametric oscillator pumped by an amplified gain-switched diode," Opt. Express, vol. 18, pp. 7602-7610, 2010.

[8] T. S. Board. http://www.innovateuk.org/.

[9] K. T. Vu, A. Malinowski, D. J. Richardson, F. Ghiringhelli, L. M. B. Hickey, and M. N. Zervas, "Adaptive pulse shape control in a diode-seeded nanosecond fiber MOPA system," Optics Express, vol. 14, pp. 10996-11001, 2006.

[10] A. Malinowski, K. T. Vu, K. K. Chen, J. Nilsson, Y. Jeong, S. Alam, D. Lin, and D. J. Richardson, "High power pulsed fiber MOPA system incorporating electro-optic modulator based adaptive pulse shaping," Opt. Express, vol. 17, pp. 20927-20937, 2009.

[11] E. Snitzer, "Optical Maser Action of Nd in Barium Crown Glass," Physical Review Letters, vol. 7, p. 444, December 15 1961.

[12] R. J. Koester and E. Snitzer, "Amplification in Fiber Laser," Optics Letters, vol. 3, p. 1192, October 1964.

[13] E. Snitzer, H. Po, F. Hakimi, R. Tumminelli, and B. C. McCollum, "Double-Clad, offset core Nd fiber Laser," in Proc. Opt. Fiber Sensors Post-deadline power PD5, New Orleans, 1988.

[14] H. M. Pask, R. J. Carman, D. C. Hanna, A. C. Tropper, C. J. Mackechnie, P. R. Barber, and J. M. Dawes, "Ytterbium-doped silica fiber lasers: versatile

sources for the 1-1.2 µm region," IEEE Journal of Selected Topics in Quantum Electronics, vol. 1, pp. 2-13, 1995/04/ 1995.

[15] D. Inniss, D. J. DiGiovanni, T. A. Strasser, A. Hale, C. Headley, A. J. Stentz, R. Pedrazzani, D. Tipton, S. G. Kosinaki, D. L. Brownlow, K. W. Quoi, K. S. Kranz, R. G. Huff, R. Espindola, J. D. LeGrange, and G. Jacobovitz-Veselka, "Ultrahigh-power single-mode fiber lasers from 1.065 to 1.472 µm using Yb-doped cladding-pumped and cascaded Raman lasers," in CLEO 1997, Pastdeadline Paper CPD30, 1997.

[16] M. Muendel, B. Engstrom, D. Kea, B. Laliberte, R. Minns, R. Robinson, B. Rockney, Y. Zhang, R. Collins, P. Gavrilovic, and A. Rowley, "5-watt cw single-mode ytterbium fiber laser at 1.1 µm," in CLEO 1997, Pastdeadline Paper CPD30, 1997.

[17] V. Dominic, S. MacCormack, R. Waarts, S. Sanders, S. Bicknese, R. Dohle, E. Wolak, P. S. Yeh, and E. Zucker, "110 W fibre laser," Electronics Letters, vol. 35, pp. 1158-60, 1999/07/08 1999.

[18] Y. Jeong, J. K. Sahu, D. N. Payne, and J. Nilsson, "Ytterbium-doped large-core fibre laser with 1 kW of continuous-wave output power," Electronics Letters, vol. 40, pp. 470-472, 2004.

[19] SPI. http://www.spilasers.com/.

[20] IPG Photonics. http://www.ipgphotonics.com.

[21] N.G.R. Broderick, H.L. Otterhans, D.J. Richardson, R.A. Sammut, J. Caplan, L. Dong, "Large mode area fibres for high power applications", Optical Fiber Technology, Vol. 5, 185-196, 1999.

[22] J. P. Koplow, D. A. V. Kliner, and L. Goldberg, "Single-mode operation of a coiled multimode fiber amplifier," Optics Letters, vol. 25, pp. 442-4, 2000/04/01 2000.

[23] F. Di Teodoro, J. P. Koplow, and S. W. Moore, "Diffraction-limited, 300-kW peak-power pulses from a coiled multimode fiber amplifier," Optics Letters, vol. 27, pp. 518-20, 2002/04/01 2002.

[24] J. Limpert, S. Hofer, A. Liem, H. Zellmer, A. Tunnermann, S. Knoke, and H. Voelckel, "100-W average-power, high-energy nanosecond fiber amplifier," Applied Physics B (Lasers and Optics), vol. B75, pp. 477-9, 2002/10/ 2002.

[25] J. L. Limpert, A; Gabler, T; Zellmer, H; Tünnermann, A; Unger, S; Jetschke, S; Müller, H -R, "High-average-power picosecond Yb-doped fiber amplifier," Optics Letters, Vol. 26 Issue 23, pp.1849-1851 2001.

[26] A. Piper, A. Malinowski, B. C. Thomsen, D. J. Richardson, L. M. B. Hickey, and M. N. Zervas, "11.1W average power 20ps pulses at 1 GHz repetition rate from a fiber-amplified gain-switched 1.06 um Fabry-Perot laser diode," in CLEO/QELS 2005, Baltimore, USA 23 - 26 May 2005. , 1141-1143, 2005.

[27] P. Dupriez, A. Piper, A. Malinowski, J. K. Sahu, M. Ibsen, Y. Jeong, L. M. B. Hickey, M. N. Zervas, J. Nilsson, and D. J. Richardson, "321 W average power, 1 GHz, 20 ps, 1060 nm pulsed fiber MOPA source," Anaheim, CA, USA, 2005, p. 3 pp. Vol. 5.

[28] P. Dupriez, A. Piper, A. Malinowski, J. K. Sahu, M. Ibsen, B. C. Thomsen, Y. Jeong, L. M. B. Hickey, M. N. Zervas, J. Nilsson, and D. J. Richardson, "High average power, high repetition rate, picosecond pulsed fiber master oscillator

power amplifier source seeded by a gain-switched laser diode at 1060 nm," IEEE Photonics Technology Letters, vol. 18, pp. 1013-15, 2006.

[29] P. Dupriez, C. Finot, A. Malinowski, J. K. Sahu, J. Nilsson, D. J. Richardson, K. G. Wilcox, H. D. Foreman, and A. C. Tropper, "High-power, high repetition rate picosecond and femtosecond sources based on Yb-doped fiber amplification of VECSELs," Opt. Express, vol. 14, pp. 9611-9616, 2006.

[30] A. Galvanauskas, G. C. Cho, A. Hariharan, M. E. Fermann, and D. Harter, "Generation of high-energy femtosecond pulses in multimode-core Yb-fiber chirped-pulse amplification systems," Optics Letters, vol. 26, pp. 935-7, 2001/06/15 2001.

[31] T. Eidam, S. Hanf, E. Seise, T. V. Andersen, T. Gabler, C. Wirth, T. Schreiber, J. Limpert, and A. Tünnermann, "Femtosecond fiber CPA system emitting 830 W average output power," Opt. Lett., vol. 35, pp. 94-96, 2010.

Chapter 2 Background

Overview

This chapter discusses the basic theory of Yb^{3+}-doped fibre lasers and amplifiers. In 2.1 a brief introduction to Yb^{3+}-doped fibres is given. In 2.2 basic techniques and fibres used in fibre amplifiers and lasers are discussed. In 2.3 nonlinearities encountered when developing pulsed fibre amplifiers and lasers are introduced. In 2.4 a conclusion is given.

2.1 Introduction

Rare-Earth (RE) doped fibre lasers were first introduced in the 1960s [1, 2]. Due to poor performance, mainly limited by the pump source and fibre fabrication technology, they were out performed by solid-state lasers. In the 1980s, with the development of the semiconductor pump lasers and RE doped single mode silica fibre with low loss, the RE doped fibre laser became a viable technology. It provides high gain efficiency, low lasing threshold and a wide gain spectrum. Then, a revolutionary optical device, the Erbium Doped Fibre Amplifier (EDFA), changed the whole world by solving the problem of complex electrical regeneration of optical pulses and allowing direct optical pulse amplification in the 1.5 μm window. The ytterbium doped fibre laser and amplifier also got the chance to develop to a new stage when appropriate high power semiconductor pump diodes become available.

Ytterbium is one of the most versatile RE ions in a silica-based host. It provides several very attractive features, particularly an unusually broad absorption band and emission band. This broad absorption allows for ultra-short laser pulses to be amplified.

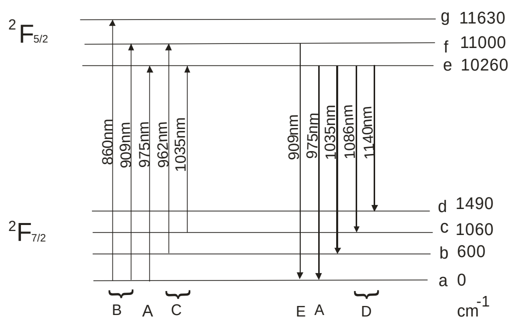

Figure 2.1: Energy level diagram of Yb^{3+} in silica

The energy level graph shown in Fig 2.1 shows the two relevant manifolds. One is the ground-state $^2F_{7/2}$ manifold, the other is $^2F_{5/2}$ excited-state manifold, ~10000 cm^{-1} above the ground level [3, 4]. These manifolds extend to three sub-levels in $^2F_{5/2}$ and four sub-levels in $^2F_{7/2}$. The lack of other energy levels close to these prevents Excited State Absorption (ESA) at either pump or laser wavelength. In addition, the multi-phonon emission from the excited state is reduced [5]. The inversion lifetime of Yb^{3+} ions in pure silicate glass is around 1.5ms. The value of the lifetime is important in MOPA systems with tens of kHz repetition rate as it directly influences the amount of amplified spontaneous emission (ASE). Assuming the pump is constant, the lower the repetition rate is, the larger the amount of ASE is generated as the time without stimulated emission is longer and the population inversion density is higher. ASE powers emitted in forward and backward directions in a fibre amplifier can differ. Usually, ASE is stronger in the direction opposite to that of pumping. The spectral shape of ASE can depend on the pump intensity level. The ASE spectrum shifts toward where the gain grows more quickly. In this work, it was important to consider ASE carefully to avoid unwanted lasing outside the signal wavelength.

Different host glass compositions lead to different optical transition cross sections in the fibre core. Two types of host glasses are popular in high power fibre lasers at present. One is phosphosilicate glass and the other is aluminosilicate glass. The phosphosilicate glass host Yb^{3+}-doped fibre has a property of reduced photodarkening, which is the phenomenon that the optical power losses in a medium grow when the medium is irradiated with light at certain wavelengths [6, 7]. This phenomenon reduces the conversion efficiency of pump to signal and increases heat generation inside the medium. This is very important for laser users who want a laser which can serve for a long time without performance degradation.

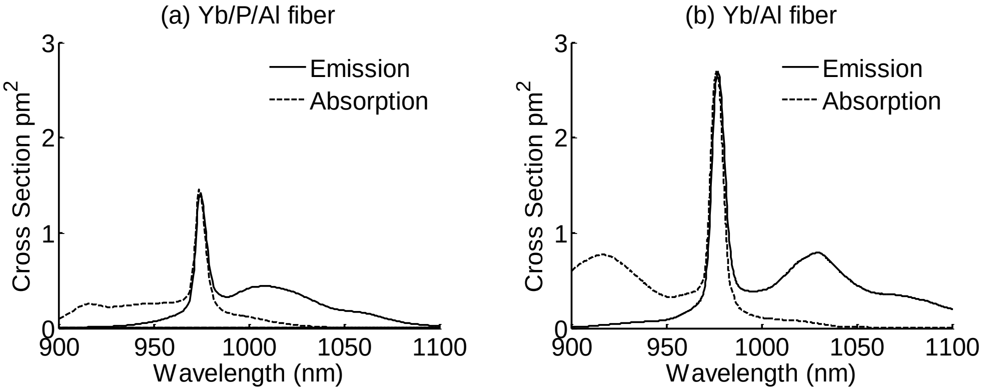

Figure 2.2: Phosphosilicate glass host and aluminosilicate glass host Yb^{3+}-doped fibre ground-state absorption spectrum (dotted line), emission spectrum (solid line)[4]

Figure 2.2 (a) shows the cross section of phosphosilicate glass host Yb^{3+}-doped fibre and (b) shows the cross section of aluminosilicate glass host Yb^{3+}-doped fibre. From Fig 2.2 (a) we can see that Yb^{3+}-doped phosphosilicate glass has relatively flat absorption around 950 nm and a peak absorption at 975 nm. Similarly, from Fig 2.2 (b), we see the aluminosilicate glass host Yb^{3+}-doped fibre has two absorption peaks at 915 nm and 975 nm. Hence, when pumping the phosphosilicate glass host Yb^{3+}-doped fibre, 940 nm pumps are often used. When pumping the aluminosilicate glass host Yb^{3+}-doped fibre, 915 nm pumps are most commonly used. Both phosphosilicate and aluminosilicate glass host Yb^{3+}-doped fibres can be pumped at 975 nm, but due to the relatively narrow spectral range, complex pump wavelength stabilization techniques need to be implemented. It is sometimes worth the effort of stabilizing the pump wavelength when you need to reduce the fibre device length. The higher pump power absorption around 975 nm can significantly reduce the fibre length needed in a system, which is critical to minimize the nonlinearities in the fibre.

2.2 Ytterbium doped fibre lasers and amplifiers

2.2.1 Principles of optical fibres

An optical fibre has the basic structure shown in figure 2.3. It is composed of a core and cladding. It is usually made of highly transparent material such as silica. Light propagates in the core which has the highest refractive index (n_1). The cladding material has a slightly lower refractive index (n_2) than the core, which confines the light in the core due to total internal reflection. The coating is usually made of polymer which can protect the fibre from damage. Normally, this has higher refractive index than silica.

Numerical aperture (NA):

The numerical aperture (NA) is defined as the sine of the half maximum angle of an incident ray that can be coupled into the fibre.

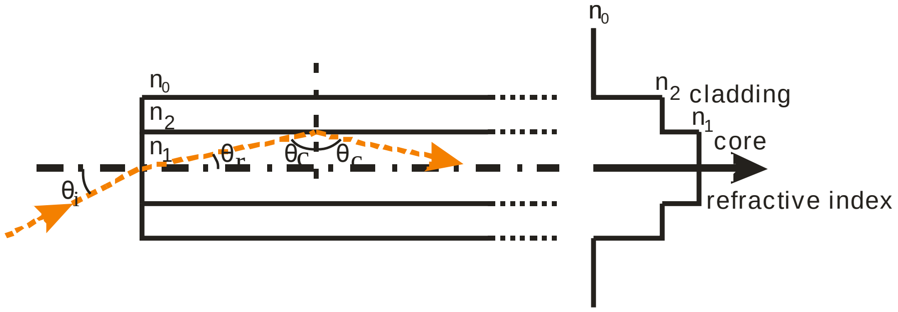

Figure 2.3: The ray picture of fibre NA

In step-index fibres, when a light ray is incident from air with refractive index $n_0 \approx 1$ and enters the fibre core, according to Snell's law.

$$n_0 \sin\theta_i = n_1 \sin\theta_r \tag{2.1}$$

Where θ_i is the incidence angle of the input light ray, while θ_r is the angle of the refracted light ray. According to geometry, $\theta_r = 90^0 - \theta_c$, where θ_c is the critical angle for total internal reflection. Applying Snell's law in the limiting case of a ray which is transmitted parallel to the interface we obtain:

$$\theta_c = \sin^{-1}\frac{n_2}{n_1} \tag{2.2}$$

where n_1 and n_2 are the refractive indices of the core and cladding. From equation (2.1) and (2.2), the NA can be expressed as function of the refractive index of the core and cladding as:

$$NA = n_0 \cdot \sin\theta_{i\_\max} \approx \sqrt{n_1^2 - n_2^2} \tag{2.3}$$

Equation (2.3) provides an approximation of the connection between the NA and the acceptance angle of the fibre. Any light ray that has an incident angle less than θ_i can satisfy the total internal reflection condition, and hence, be guided inside the core of the fibre.

V number:

Single-mode fibres support only the fundamental mode per polarization state for a given wavelength [8]. For step-index fibres, the number of modes supported by the fibre can be determined by a normalized frequency parameter, the V number:

$$V = \frac{2\pi \cdot a}{\lambda} NA = \frac{2\pi \cdot a}{\lambda} \sqrt{n_1^2 - n_2^2} \tag{2.4}$$

where a is the core radius and λ is the wavelength of light. When $V \leq 2.405$, the fibre is single-mode [9, 10]. Single-mode operation of a step-index fibre is limited to a certain wavelength range. The fibre will be single mode only for wavelengths longer than the cut-off wavelength, for which $V = 2.405$. The long wavelength limit, beyond which there are no guided modes, is defined by the bend losses. The core is wrapped by the cladding which is a layer of pure silica glass. Normally, a fibre with high NA has low bending loss, as the light is strongly guided. The bending loss can increase very quickly once a critical bend radius is reached. This bending radius limit can vary from a few millimetres to tens of centimetres depending on the NA of the fibres. In a multimode fibre, at a particular bending radius, the bending loss is typically larger for high order modes than for lower order modes [11]. Therefore, by properly adjusting the bend radius, it is possible to introduce significantly higher losses for higher-order modes, without affecting the lowest-order mode. This technique has been applied in high power fibre amplifiers to achieve single mode operation in a multi-mode fibre [12].

Chromatic dispersion:

First, we need to define phase velocity and group velocity. The phase velocity of light is the velocity with which phase fronts propagate in a medium. It is related to the wavenumber and the optical frequency: $v_p = \frac{\omega}{k}$. In vacuum, the phase velocity is c, independent of the optical frequency, and equals the group velocity. In a medium, the phase velocity is typically smaller by a factor n, called the refractive index, which is frequency dependent. The group velocity is the velocity with which the envelope of a weak narrow-band optical pulse propagates in a medium.

Chromatic dispersion is the variation of phase velocity with the optical frequency or wavelength. Dispersion is often specified by the dispersion parameter D_λ which is equal to $-\frac{2\pi c}{\lambda^2}\beta_2$, β_2 is group velocity dispersion (GVD) parameter. When D_λ <0 ($\beta_2 > 0$) the dispersion is described as normal, while D_λ >0 ($\beta_2 < 0$) the dispersion is described as anomalous. Normal dispersion, where the group velocity decreases with increasing optical frequency, occurs for most transparent media in the visible spectral region. Anomalous dispersion typically occurs at longer wavelengths [8]. At a certain wavelength D_λ =0; this wavelength is known as the zero-dispersion wavelength. For example, in single mode communication fibre SMF-28 the zero-dispersion wavelength is ~1.3 μm.

2.2.2 Core pumping and Clad pumping configurations

2.2.2.1 Core pumping scheme

Initially, Rare-Earth doped fibres used the same configuration as conventional optical fibre. The core of the fibre is doped with Rare-Earth elements like Erbium and Ytterbium. The core has the highest refractive index, the cladding has a lower refractive index, and the coating material is a polymer which has higher refractive index than the cladding, as shown in Fig. 2.4.

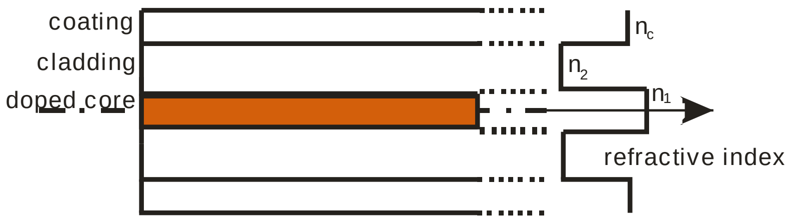

Figure 2.4: Structure of doped fibre

The revolutionary Erbium Doped Fibre Amplifier (EDFA), invented in 1985 at the University of Southampton, used this kind of fibre [13]. Because the pump and signal both propagate in the core of the fibre, this scheme is known as core pumping. This kind of fibre has the drawback that the power of the single mode laser used as the pump is very limited, normally at the sub-watt level. The pump and signal are coupled into the same core using a device called a Wavelength Division Multiplexer (WDM), as shown in Fig. 2.5. The output of the WDM is then spliced to the Rare-Earth doped fibre. The pump then amplifies the signal as they pass along the fibre together.

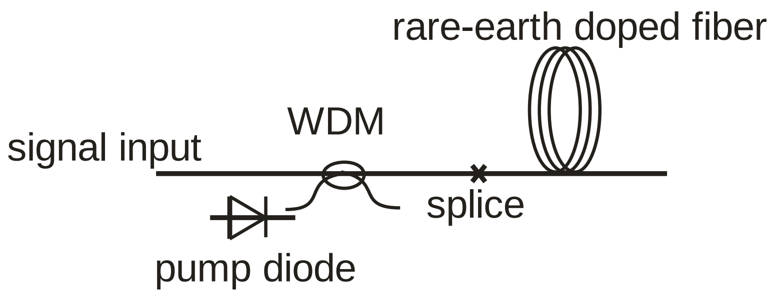

Figure 2.5: Core pumping scheme

Core pumped amplifiers are usually used as pre-amplifiers because the output power is limited to a few hundred milliwatts. Due to the high confinement of pump and signal in the relatively small core, it needs to be carefully designed to minimise nonlinear effects. In my experimental setup, this core pumping scheme is quite common at the beginning of the amplifier cascade, using a fibre pulled at the ORC. This fibre is named HD-406-2. It has a core diameter of 5μm, NA=0.21 and Yb^{3+}-doping concentration about 2000 ppm. The pump is coupled into the Yb^{3+}-doped fibre using a 980 nm/1060 nm WDM coupler.

2.2.2.2 Cladding pumping scheme

To overcome the problem of the unavailability of powerful single mode output fibre-coupled pump diodes, the cladding pumping scheme was invented in 1989 [14]. The cladding-pumping fibre configuration does not require single-mode pump sources, but can still produce a single mode laser output. In this scheme, high power, multimode, diodes/stacks, with output powers scaling from the sub-watt level to the kilowatt level, are used as pumps. With the fast development of pump diodes, fibre laser power has scaled very rapidly in the last 10 years. The typical structure of a double-clad fibre is shown in Figure 2.6.

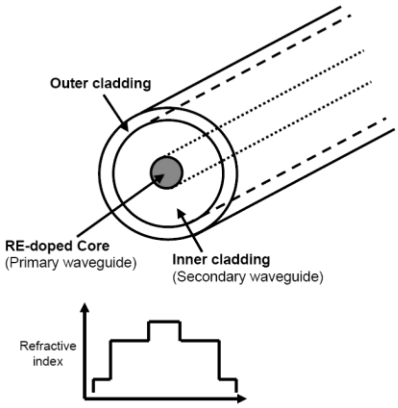

Figure 2.6: Schematic of a double-clad fibre and Refractive index profile

The core is usually doped with a Rare-Earth material such as Ytterbium for guiding the signal and absorbing pump power. The inner cladding has a lower refractive index compared to the core. It is multimode to enable guiding of the high power multimode pump light. To allow guiding in the inner cladding, the outer cladding has a lower refractive index than the inner cladding. It is usually a polymer with a lower refractive index than silica. This Double-Clad Fibre (DCF) allows the launch of high power multimode pump diodes while the core is still small enough to enable single mode operation. Because the cladding modes overlap with the doped core, the pump power is absorbed in the core and amplification of the signal will occur. With DCF, we can convert high power, low brightness, poor beam quality pump light into high power, high brightness, good beam quality signal wavelength light after amplification. But there are problems: the absorption is very low because most of the pump power propagates in modes which do not strongly overlap the core, as shown in the top graphic in Figure 2.7. To improve the absorption, it is necessary to break the circular, centrally symmetrical structure to improve pump overlap with the core and increase absorption by the Rare-earth ions. To achieve this, D shaped and other shapes of DCF were developed.

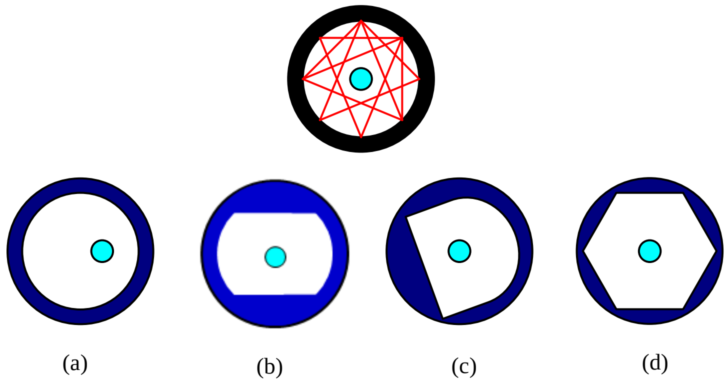

Figure 2.7: Pump propagating in DCF and (a) Offset doped core structure (b) rectangular shape cladding (c) D-shaped cladding (d) hexagonal shape cladding

Figure 2.7 shows different inner cladding geometries; all designs aim to improve the pump coupling into the core.

When practical, it is better to fabricate amplifiers in an all-fibre configuration instead of using free-space end pumping techniques. This is because free-space pumping requires highly stable mechanical parts whilst an all fibre configuration does not. Asymmetrically shaped DCFs will cause many problems when splicing fibres together. It has been found that some symmetrically shaped DCFs such as square or hexagonal shaped DCFs can overcome this problem whilst still improving the pump overlap with the core. Typically, DCFs have pump absorption lengths in the region of a few meters.

Large Mode Area (LMA) fibre

A problem which remains in conventional small core DCF is that the nonlinearities such as Self Phase Modulation (SPM), Stimulated Raman Scattering (SRS), Stimulated Brillouin scattering (SBS) rise quickly due to the high intensity in the relatively small core of the gain fibre. To deal with this problem, the peak intensity of pulse needs to be reduced. One solution is to increase the core area without compromising beam quality. According to Equation 2.4, for normal step index fibre, to keep the V number the same whilst increasing the core radius, the NA has to be decreased. Even with very low NA, large core diameter fibre is still generally multimode.

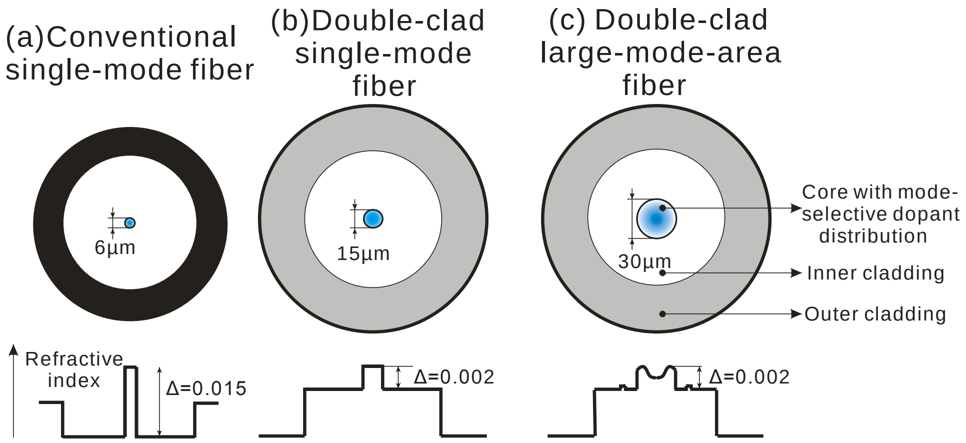

Figure 2.8: Comparison between (a) conventional single mode fibre, (b) double clad single mode fibre and (c) Double clad LMA fibre

The term Large Mode Area (LMA) fibre is used for fibres which have relatively large mode areas but are optimised to propagate a single or small number of modes. They have a much larger core size and less refractive index difference between core and cladding than a conventional single-mode fibre. A typical Yb^{3+}-doped LMA DCF fibre is shown in (c) of Figure 2.8. The LMA fibre has a refractive index profile and doping distribution optimized for single mode operation. The refractive index profile consists of a low NA central core region having a diameter of tens of microns with Yb^{3+} ions selectively doped into the central part of the core to give maximum gain to the fundamental mode. The 'dip' of the refractive index profile in the core can encourage the fundamental mode to expand its mode area significantly to occupy the whole area of the core. An outer ring of raised index is designed to reduce the fibre bending loss. Although the core size has been extended beyond the single mode region, LMA fibre can still output diffraction limited beam quality light by managing the fibre launching and bending carefully. With LMA fibre, for the first time, pulse energy exceeding 10 μJ in the ultrashort pulse regime was demonstrated in fibre in 1996 [15]. In addition to reducing the intensity in the fibre for a given power, a larger core also increases the core-clad area ratio, enhancing overlap of pump modes with the core, allowing reduction in fibre length and further suppression of nonlinearities.

Polarization Maintaining Double clad LMA

Compared to most solid state lasers, which use birefringent gain crystals, fibre lasers in general have an obvious drawback in that the output beam polarisation is random. Single polarization output is required for many applications: for example wavelength conversion. Optical fibres always exhibit some degree of birefringence, even if they have a circularly symmetric design, because there is always some amount of mechanical stress or inhomogeneity which breaks the fibre symmetry. In addition, this variation is not uniform along the whole length of fibre. A single mode fibre is not truly single mode because it can support two orthogonally polarized modes which, in the presence of any birefringence, have different wavenumbers [8]. The two orthogonal modes are coupled to each other due to accidental birefringence changes. As a result, the polarization of light propagating in the fibre gradually changes in an uncontrolled manner, which depends on any bending of the fibre and on its temperature. The birefringence of a fibre is defined as $B = \frac{\Delta\beta}{\beta_{av}}$, where β_{av} is the average of the real part of the propagation constant (i.e. the phase delay per unit propagation distance) and $\Delta\beta$ is the difference in β between fast axis and slow axis. Normal single mode fibres always show some degree of birefringence ($B \approx 10^{-6} \sim 10^{-5}$) due to the small defect from cylindrical symmetry.

There are some methods which can alleviate this problem, such as manufacturing very low birefringence fibre ($B \approx 10^{-9} \sim 10^{-7}$) by using a fast rotation technique during the fabrication process [16], or designing and manufacturing absolute single mode fibre which only guides one polarisation mode (Polarisation Extinction Ratio (PER) more than 50 dB) [17]. Due to reasons of cost and practicality, polarization-maintaining (PM) optical fibre is typically the most convenient solution. PM fibre has high birefringence (~10^{-4}), induced by placing two stress rods beside the core [18]. Figure 2.9 shows the structure of one type of PM fibre, the Panda fibre. With increased birefringence, the difference in the propagation constants of the two polarization modes is increased. As a result, the disturbance along the fibre required to effectively couple the two polarization modes is also increased. This makes the signal polarisation less sensitive to bending or heat, as well as to inherent inhomogeneity of the fibre. If light launched into the fibre is aligned with one of the birefringence axes, the input polarization state will be well preserved along the whole fibre length.

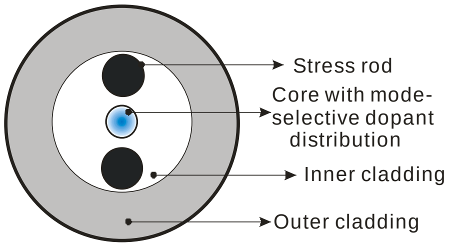

Figure 2.9: High birefringence Panda PM Rare-Earth doped fibre cross section

PM fibre has other advantages. It suppresses nonlinear polarization rotation, where the change in the polarisation state of light in a fibre is dependent on the intensity of the light [8].

Rare-Earth doped Photonic crystal fibre (PCF)

The invention of Photonic crystal fibre (PCF) [19] is the most important breakthrough in fibre optics in recent years. This is because PCF fibres offer many degrees of freedom in their design to achieve a variety of peculiar properties, such as control over dispersion characteristics. PCF is a kind of optical fibre which guides light due to its microstructure, usually consisting of a series of holes running along the length of the fibre. A typical structure of PCF is shown in Figure 2.10. PCFs can have either a ‘solid-core’ or a ‘hollow-core’, with a periodic lattice of hollow channels surrounding round the core which acts as cladding. PCFs can be divided into two main categories according to principle on which the light guides within them. One, usually called Photonic Band-Gap Fibre (PBGF), confines light within a low refractive index ‘hollow-core’ in which light is guided by a photonic bandgap effect [19]. This kind fibre will not be focused on here, as it was not used in the work described in this thesis. The other type of PCF guides light in the solid-core using the same index-guiding principle as conventional optical fibre, where the cladding can be understood as having an “effective index” less than that of the core due to the fraction of its area which is composed of air rather than silica. The material parameters of the cladding are very versatile. The hole diameter *d*, lattice pitch Ë, and the air hole shape in the PCF can be precisely controlled. This allows the refractive index profile to be controlled more broadly and precisely than conventional fibres. Very low index outer claddings can be constructed by having a very high air fraction.

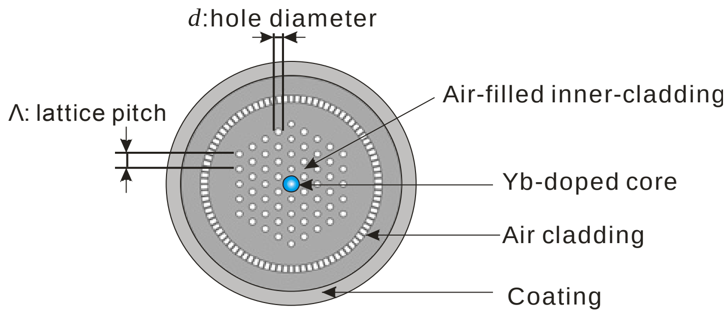

Figure 2.10: A typical design of Yb^{3+}-doped PCF for high power applications [20, 21]

The V-number and the single-mode conditions derived for step-index fibres can still be used in the PCFs by estimating the effective cladding index. This effective cladding index is strongly dependent on λ / Λ [22]. Figure 2.11 shows the single-mode boundary $V = 2.405$ of the normalized wavelength λ / Λ against the relative hole diameter d / Λ [21]. When $d / \Lambda < 0.4$, the PCF becomes single-mode for all the λ / Λ. This region is called the endlessly single-mode region [22]. This feature allows the use of a very large Rare-Earth doped core (>50 μm) while designing amplifiers, in order to scale the pulse energy and peak power. This extremely large core amplifier still outputs near diffraction limited beam quality.

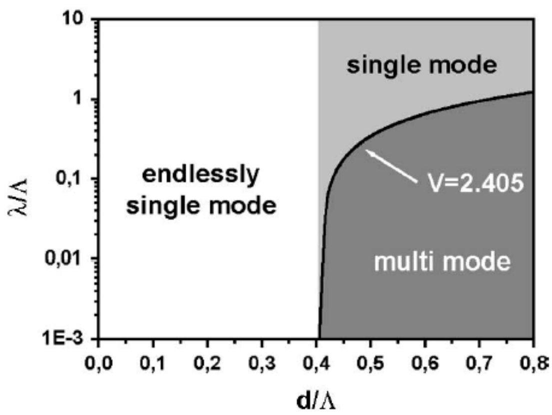

Figure 2.11: Endlessly single-mode region for PCFs [21]

Using micro structuring of the outer cladding can also achieve a very high NA in the inner cladding of the double clad PCF which enables highly efficient pump coupling. The micro-structured air cladding of the fibre can have an effective refractive index similar to air. Due to the very large contrast of refractive index introduced by the air cladding structure, PCFs can have an inner cladding NA of 0.9 or even higher, while normal double clad fibres using low refractive index polymer coating have an inner cladding NA ~0.45. For a given inner cladding dimension a higher NA lowers the requirements for beam quality of the pump source. Alternatively, for the same pump source, the higher NA allows for efficient coupling into a smaller cladding, reducing the cladding to core area ratio and the absorption length.

The scaling of the mode area of PCFs had developed quickly in the last few years. A rod-type PCF with a core diameter of 80 μm (effective mode area of ~4000 μm^2) was reported at Friedrich-Schiller-University, Jena in 2007 [23]. The pump absorption of this fibre was measured to be as high as 30 dB/m at 976 nm, which allowed a length of just a few tens of centimetres to be used in a laser or amplifier setup. The increased effective mode area and reduced fibre length allows for significant pulse peak power and energy scaling, as these changes increase the threshold for nonlinear effects.

The dispersion design of the PCF can be very versatile. Conventional silica fibre has a zero dispersion around 1300 nm. The very useful communication window is in the anomalous dispersion area. This leads to some nonlinear effects like modulation instability which limit the high power amplification in that spectral range. Details of various nonlinearities which are significant in fibre amplifiers will be discussed in section 2.3. Some extremely useful applications such as Supercontinuum Generation, a nonlinear process for strong spectral broadening of light, using PCF results from this versatile dispersion manipulation. Some results achieved using this kind of PCF with an un-doped core are described in this thesis. Details will be given in Chapter 6.

Free space end-pumping & All fiberized pumping

Optical fibres require precise alignment of the signal when it is launched into the core. The traditional way is to launch it in free space. This technique was widely used at the beginning of my work for power scaling because of its simplicity. The multimode pump is also launched into the inner cladding in free space through the fibre ends. Due to the relatively large size of the inner cladding, the pump launch is less critical than the signal launch. The free space end launching setup uses mechanical fibre holders, lenses and dichroic mirrors to launch both signal laser and pump laser to the gain fibre. A typical setup for free space launching into a cladding-pumped fibre is shown as Figure 2.12. This method has some problems, including poor stability and possible coupling to higher order modes in an LMA core.

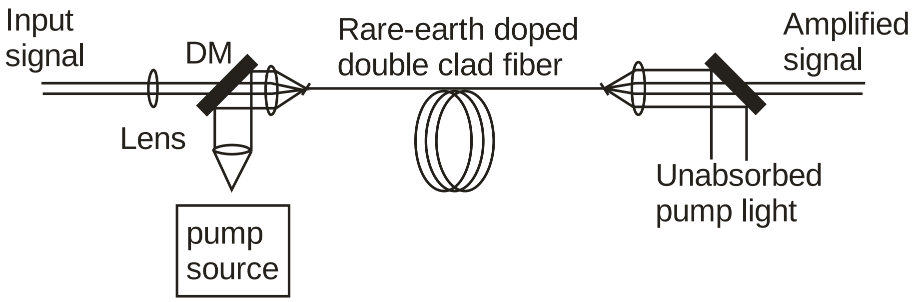

Figure 2.12: Free space end launching

For more reliable laser operation, fully-fiberized methods are needed. Several alternatives exist, for example the GT-Wave design invented by Dr. Anatoly Grudinin and Paul Turner at the ORC, University of Southampton. This structure is shown in Figure 2.13. A fibre with a doped core is held in contact with one or more pure silica dummy fibres, encased together in a low refractive index polymer outer cladding. The insert picture at bottom right shows a real fibre end facet. The fibre pigtailed pump diodes are spliced directly to the dummy fibres and the input signal is spliced to the signal fibre using standard splicers (for example, Fujikura 60S). The pump power is transferred across to the doped fibre and absorbed as the pump light propagates along the GT-Wave fibre. There is almost no loss of the signal and the pump. This method also reduces the possibility of signal laser light being scattered back to the pump laser, and protects the pump from damage by the high peak power signal laser. It can take the fully fiberized system to very high average power (several kilowatts). However, the pump absorption of GT-Wave is relatively low because the effective cladding area is large compared to a standard DCF. Normally a relatively long device length (~10 m) is needed to absorb most of the pump power. The long fibre length limits the output peak power as nonlinearities are proportional to fibre length. An all fiberized 2.5 mJ, 100 W, nanosecond MOPA employing this technique is described in Chapter 3 of this thesis.

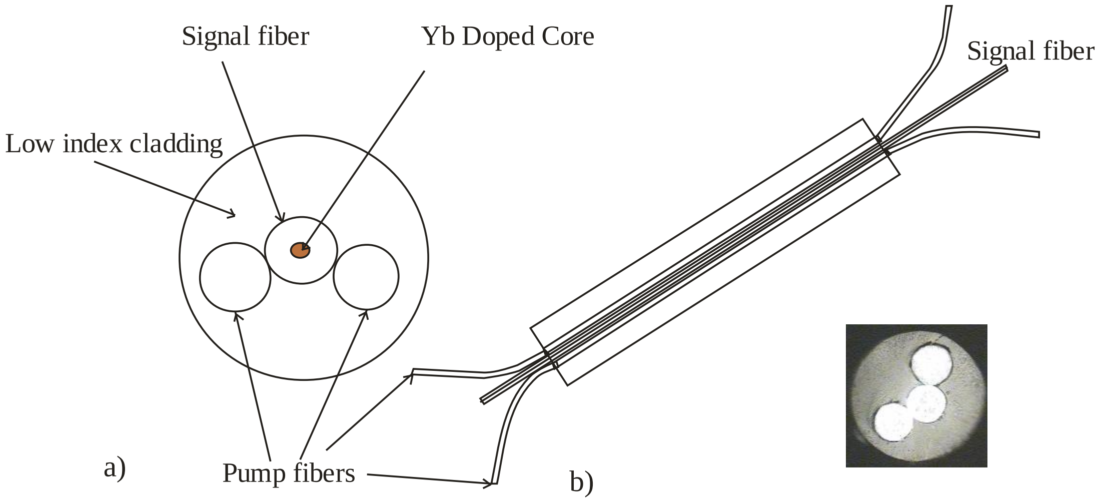

Figure 2.13: (a) GT-Wave configuration at cross section and (b) schematic view and fibre facet image [24]

Another popular pumping scheme is to use a tapered fibre bundle (TFB), combining signal and pump fibres into a single fibre and then splicing this fibre to the gain fibre for amplification. Figure 2.14 shows this all fibre pumping scheme. A single mode fibre is at the centre of the bundle which is spliced to the signal laser. Multiple core-less silica fibres, which are spliced to fibre pigtailed multi-mode laser diodes, surround the single mode fibre. The fibre bundle is tapered to custom designable size and then spliced to a DCF which matches the tapered bundle size [25]. The core of the DCF guides the signal and the inner cladding guides the high power pump light. Both signal laser and pump laser enter the gain fibre through the spliced fibre end.

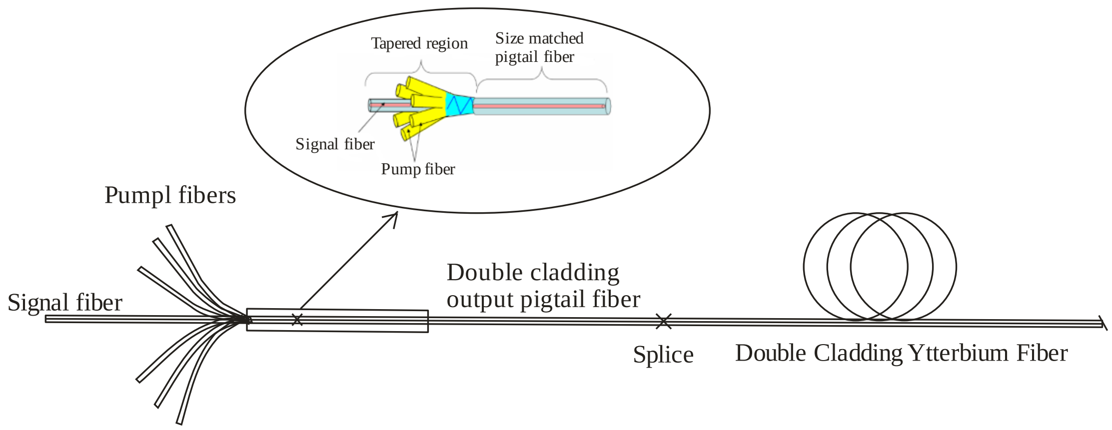

Figure 2.14: TFB pumping scheme

The fibre laser output power can easily be scaled up just by adding more pump diodes to the pump ports. But, the number of pump ports is limited by the brightness acceptance (the inner cladding diameter multiplied by inner cladding NA) of the DCF. Using this technique, fibre lasers can reliably generate hundreds of watts average output power reliably [26]. But some issues like isolation between signal laser and pump laser diode and mode area matching between different fibres need to be carefully considered. We used this technique in pre-amplifiers very often in the work described in this thesis.

2.3 Nonlinearities in fibre

An ideal amplifier is linear; with no distortion to the signal both in the temporal and spectral domain. In reality, when light passes through any dielectric material (for example, a silica optical fibre), nonlinear interactions will occur if the electromagnetic field is sufficiently intense. The total polarization P induced by the electric field satisfies the following nonlinear relation to the electric field **E**.

$$P = \varepsilon_0 \left(\chi^{(1)} \cdot E + \chi^{(2)} : EE + \chi^{(3)} \vdots EEE + \ldots \right) \tag{2.5}$$

where ε_0 is the vacuum permittivity and $\chi^{(j)} (j = 1,2,\ldots)$ is jth order susceptibility. There is no $\chi^{(2)}$ for silica fibre because silica is a glass, and glasses are inherently centro-symmetric. Therefore, the lowest-order nonlinear effects in fibre originate from the third order susceptibility $\chi^{(3)}$, and most of the nonlinear effects arise from nonlinear refraction. The $\chi^{(3)}$ processes can be divided in to two categories: elastic processes and inelastic processes. In an elastic scattering process, the kinetic energy of the incident particles (photons) are conserved, only their direction of propagation is changed, while in an inelastic scattering process the incident particles loose or gain kinetic energy. The Kerr effect, where the refractive index of the medium changes when the electron orbit is deformed by a strong optical field (such as in high peak power pulses) [27] introduces elastic nonlinearities such as self-phase modulation (SPM) and cross phase modulation (XPM). Nonlinearities like Raman and Brillouin scattering are inelastic process, where energy is exchanged with the medium. These nonlinearities normally generate new optical frequencies. However, many elastic processes can also result in the generation of new frequencies. For example, Four Wave Mixing (FWM) generates new frequencies; it is an elastic process since no energy is exchanged between the electromagnetic field (light) and the dielectric medium (silica fibre), i.e. the total energy of the generated photons matches that of the incident photons. Here, only the nonlinearities that are significant for the work described in this thesis will be discussed. More comprehensive explanations can be found in Nonlinear Fibre Optics by G. P. Agrawal [8].

2.3.1 Nonlinear Schrödinger Equation

The propagation equation for broad bandwidth optical pulses propagating in low loss single-mode fibres can be described by the nonlinear Schrödinger equation (NLSE):

$$i\frac{\partial A}{\partial z} = \frac{\beta_2}{2}\frac{\partial^2 A}{\partial t^2} - \gamma |A|^2 A \tag{2.6}$$

where $A(z,t)$ is the normalized amplitude and $|A|^2$ represents the optical power [8]. β_2 is the group velocity dispersion (GVD) per unit length. γ is the nonlinear coefficient, defined as:

$$\gamma = \frac{(n_2 \omega_0)}{(cA_{eff})} \tag{2.7}$$

where n_2 is the nonlinear refractive index, which has a typical value $2.2 \times 10^{-20} m^2 / W$ for silica. A_{eff} is the effective core area which is related to the transverse mode distribution $E(x,y)$ and expressed as:

$$A_{eff} = \frac{\left(\int\int_{-\infty}^{\infty} |E(x,y)|^2 dxdy\right)^2}{\int\int_{-\infty}^{\infty} |E(x,y)|^4 dxdy} \tag{2.8}$$

In solving Equation (2.6), two regimes of propagation can be considered. The first term and the second term on the right hand side govern the effects of dispersion and nonlinearity respectively. The $\frac{\beta_2}{2}\frac{\partial^2 A}{\partial t^2}$ part depends on the pulse duration T_0 and amount of dispersion (assuming the pulse is unchirped). The $-\gamma |A|^2 A$ part depends on the pulse peak power P_0. The dispersion length $L_D = T_0^2 / |\beta_2|$ and the nonlinear length as $L_{NL} = 1/(\gamma P_0)$ define the length scales over which dispersive or nonlinear effects become important for pulse evolution. When $L_D << L_{NL}$, we are in the dispersion dominated regime. Silica fibre normally has a dispersion around a few picosecond per nanometer per kilometer. In our work, the pulse duration is relatively long (between tens of picoseconds and hundreds of nanoseconds) and the fibre is short (a few meters). The effect of dispersion in this case is negligible compared to nonlinearity, $L_D >> L_{NL}$, so we are in the nonlinearity dominated regime. Our lasers normally have a peak power of tens of kilowatts, while the gain fibre in my laser usually has a γ less than $0.1/(W \cdot km)$.

2.3.2 Self Phase Modulation & Cross Phase Modulation

When an optical pulse is transmitted through a gain medium, there is a time-dependent phase shift according to the time-dependent pulse intensity. In this way, an initial unchirped optical pulse becomes a chirped one. The time-dependent phase change caused by self-phase-modulation (SPM) is associated with a modification of the Fourier spectrum. This spectrum modification increases the linewidth of the output beam.

SPM is a consequence of the Kerr effect; the change in refractive index induced by an electric field. The refractive index follows Equation 2.9.

$$\tilde{n}\left(\omega,|E|^2\right) = n(\omega) + n_2|E|^2 \tag{2.9}$$

The phase change of an optical wave is given by,

$$\phi = \tilde{n}k_0 L = \left(n + n_2|E|^2\right)k_0 L \tag{2.10}$$

where $k_0 = 2\pi / \lambda$ and L is the fibre length. The nonlinear phase change can be expressed as:

$$\phi_{NL} = n_2 k_0 L|E|^2 = \gamma A_{eff} L|E|^2 \tag{2.11}$$

As discussed in section 2.3.1, when pulses are in the nonlinearity dominated regime ($L_D >> L_{NL}$) the $\frac{\beta_2}{2}\frac{\partial^2 A}{\partial t^2}$ term can be ignored. Equation (2.6) can be expressed as:

$$i\frac{\partial A}{\partial z} = -\gamma|A|^2 A \tag{2.12}$$

The solution of Equation (2.12) is:

$$A(z,t) = A(0,t)\exp\left[i\phi_{NL}(z,t)\right] \tag{2.13}$$

Where $\phi_{NL}(z,t) = \gamma|A(0,t)|^2 z$.

The frequency chirping resulting from the phase change as:

$$\delta\omega(z,t) = -\frac{\partial \phi_{NL}(z,t)}{\partial t} = -\gamma z \frac{\partial |A(0,t)|^2}{\partial t} \tag{2.14}$$

If we assume the initial pulse is a Gaussian shape with a pulse duration of T_0 and peak power P_0, Equation 2.14 can be re-expressed as:

$$\delta\omega(z,t) = \frac{2\gamma z P_0 t}{T_0^2} \exp\left[-\left(\frac{t}{T_0} \right)^2 \right] \tag{2.15}$$

When $t=T_0/2$, the maximum chirp of the pulse is:

$$\delta\omega(L_{eff}) = \frac{\sqrt{2}\gamma P_0 \ L_{eff}}{T_0} e^{-1/2} \tag{2.16}$$

Where L_{eff} is the effective length of the fibre (taking into account gain in the fibre and that nonlinear evolution will occur primarily where the field is strongest), which is given by $L_{eff} = [1 - \exp(-gL)]/g$, where g is the gain coefficient of the amplifier, assuming gain is constant along the length of the amplifier. It should be noted that in a fibre amplifier pumped from the output end, as in the power amplifiers used in my work, the highest gain will be experienced near the output of the fibre where the intensity is highest. This has the effect of reducing L_{eff}, typically by a factor of two, compared to the value given by the above formula [28].

Cross Phase Modulation (XPM) is the change in the optical phase of a light beam caused by the interaction with another co-propagating beam in a nonlinear medium. This can also be described as a change in the refractive index. XPM is always accompanied by SPM. Compared with the self phase modulation, XPM can be more efficient if the polarisation conditions are well satisfied.

For co-polarised pump and signal:

$$\tilde{n}\left(\omega_s, |E|^2\right) = n(\omega_s) + n_2(|E_s|^2 + 2|E_p|^2) \tag{2.17}$$

For orthogonally polarized pump and signal:

$$\tilde{n}\left(\omega_s, |E|^2\right) = n(\omega_s) + n_2(|E_s|^2 + \frac{2}{3}|E_p|^2) \tag{2.18}$$

Where ω_s is signal angular frequency, E_s, E_p are the electrical field intensity of signal and pump. The second and third terms on the right hand side in Eqns. (2.17) and (2.18) refer to SPM and XPM respectively.

2.3.3 Four Wave Mixing

Four-wave mixing (FWM) involves four optical beams interacting through the electronic response of the third-order susceptibility. When two frequency waves ω_1 and ω_2 with different propagation constants k_1 and k_2 (phase change per unit length for light propagating in the fibre) propagate through an optical fibre, they will interact with each other. Additional light components are generated by transferring part of the optical power from the pump waves into the Stokes wave ω_3 and anti-Stokes wave ω_4 with propagation constants k_3 and k_4. Their frequencies have the relationship $\omega_1+\omega_2=\omega_3+\omega_4$. This process conserves photon energy: two pump photons are annihilated with the simultaneous creation of the new anti-Stokes and Stokes photons with the same total energy. The Stokes wave has a lower frequency than the pump frequencies while the anti-Stokes wave has a higher frequency. FWM is a phase sensitive process. The phase mismatch between the different components is defined as:

$$\Delta k = k_1 + k_2 - k_3 - k_4 \tag{2.19}$$

When high intensity pump waves propagate in a fibre, with the frequencies and propagation constant phase-matched, the Stokes and the anti-Stokes waves are amplified by the parametric FWM process (initially from noise). When considering the phase shift induced by SPM and XPM, the parametric gain can be expressed as Equation 2.20. A detailed derivation can be found on page 394 of Nonlinear Fibre Optics by G. P. Agrawal [8].

$$g = \sqrt{\gamma^2(\sqrt{P_1 P_2})^2 - (\frac{\kappa}{2})^2} \tag{2.20}$$

where P_1 and P_2 are the peak powers of the two frequency wave ω_1 and ω_2, $\kappa = \Delta k + \gamma(P_1 + P_2)$. This is the net phase mismatch between the frequency components when nonlinear phase shifts due to SPM and XPM are incorporated. The maximum gain is reached when κ equals 0, i.e. $\Delta k = -\gamma(P_1 + P_2)$. When $\omega_1 = \omega_2$, the $\Delta k = -2\gamma P_1$. The $g_{\max} = \gamma\sqrt{P_1 P_2}$ shows this process is very efficient. FWM is recognized as an important frequency conversion process as it can not only provide a red shift but also a blue shift.

FWM is observed in this work when we are doing Supercontinuum Generation. As far as we know the FWM is playing an important role in the short wavelength (anti-Stokes) light generation. According to Agrawal [8], the phase matching requirement can be satisfied by several methods: Pumping around zero-dispersion wavelength; In the anomalous dispersion regime, adjusting the pump power; In the normal dispersion regime, mixing waves in orthogonal polarisation. In Chapter 6 of this work, a 1060nm source was used to pump a PCF with a zero-dispersion wavelength of ~1020nm, continuum including bright visible light was generated.

2.3.4 Modulation Instability

MI can be interpreted in terms of a four-wave-mixing process that is phase-matched by SPM. Modulation instability (MI) is one of the main reasons responsible for the degradation of beam quality in high-power laser systems. MI requires anomalous dispersion and manifests itself as a breakup of CW or Quasi-CW radiation into a train of ultrashort pulses [8, 29]. MI transfers the energy into side-bands and limits power amplification to the watt level. In standard silica fibre, the zero dispersion point is around 1.3 µm. The useful window for fibre-optic communications is positioned in the anomalous dispersion regime. MI is a significant limiting factor for pulse energy and peak power scaling. However, it has been found that MI plays an important role in supercontinuum generation in PCF [30]. M. Kumar and J. M. Dudley found that the MI initializes the continuum generation [29, 31]. From NLSE (Equation 2.6), the theoretical MI gain coefficient can be described as Equation 2.21. A detailed derivation can be found at page 138 of Nonlinear Fibre Optics by G. P. Agrawal [8]:

$$g(\omega) = |\beta_2 \omega| \sqrt{\omega_c^2 - \omega^2} \tag{2.21}$$

Where ω_c is the modulation cut off frequency and $\omega_c^2 = \frac{4\gamma P_0}{|\beta_2|} = \frac{4}{\beta_2 L_{NL}}$. Gain occurs only when $\omega \le \omega_c$. The maximum gain occurs when $\omega = \pm \frac{\omega_c}{\sqrt{2}}$, the maximum gain can be expressed as:

$$g_{\max} = \frac{1}{2} |\beta_2| \omega_c^2 = 2\gamma P_0 \tag{2.22}$$

Although Equation 2.21 does not include a loss factor, it provides a simple estimation of MI gain in most cases.

2.3.5 Stimulated Brillouin Scattering & Stimulated Raman Scattering

Another two important nonlinear processes that limit the peak power in Silica fibre are Stimulated Brillouin Scattering (SBS) and Stimulated Raman Scattering (SRS).

SBS originates from scattering of photons by acoustic phonons, resulting in a frequency shift of about 10-20 GHz. The relatively low frequency acoustic noise originates from thermal noise. The weak scattered light interferes with the co-propagating light to create a power induced refractive index modulation in the fibre through the Kerr effect. This refractive index modulation acts as Bragg grating. This grating moves at a speed given by the optical frequency difference between the forward and scattered waves. If this speed is similar to the speed of sound in the fibre at this frequency, an acoustic wave is created. This acoustic wave can enhance the scattering process. SBS has an extremely narrow gain spectrum of only 50-100 MHz. The Stokes beam intensity is found to grow exponentially in the backward direction. The impact of SBS can be estimated by using the concept of critical power. The critical power of SBS is defined as the power where the Stokes wave at the fibre input end becomes equal to the pump power at the fibre output end. The SBS critical power is expressed as:

$$P_{Critical}^{P} = 21\frac{A_{eff}\,\mathrm{K}}{g_B L_{eff}} \tag{2.23}$$

Where K is the polarization factor of the pump (for polarized light, K =1 and for un-polarized light K = 2). A_{eff} is the effective core area which is defined in Equation 2.8. The peak value of g_B is nearly independent of the pump wavelength and it has a typical value $g_B = 5.0\times\frac{10^{-11}m}{W}$ for fused silica. This value is nearly three orders of magnitude larger than the SRS gain coefficient. However, the effect of SBS on a particular amplifier system will be suppressed if the bandwidth of the transmitted light is large; frequency components separated by more than the SBS bandwidth experience SBS independently of each other [8, 32].

SRS originates from the scattering of photons by optical phonons. Frequency down-shifted light is generated in high Raman gain material from high power pump light through Raman scattering. It provides an efficient mechanism for wavelength conversion. Once the peak power of the amplified pulses reaches the critical Raman power (threshold), the generated Stokes wave starts growing rapidly inside the fibre. Most of the pulse energy will transfer into the Stokes component after a short propagation distance.

The Raman gain spectrum in silica fibre is very broad. The total bandwidth is up to 30 THz, as shown in Figure 2.15. The first peak of Stokes light in silica fibre is located at the wavelength ~13 THz from the pump wavelength. The Raman gain peak value is approximately $g_R = 1.0 \times \frac{10^{-13} m}{W}$ when pumping at 1 μm wavelength.

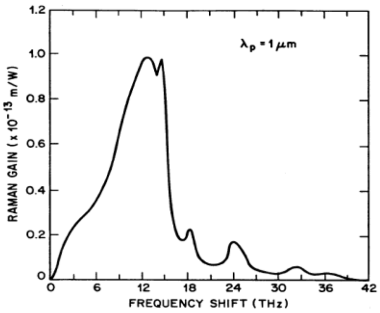

Figure 2.15: Raman gain spectrum for fused silica [8, 33]

The pump light intensity, I_p and Stokes light intensity, I_s, can be described by the following equations

$$\frac{dI_s}{dz} = g_R I_p I_s - \alpha_s I_s \tag{2.24}$$

$$\frac{dI_p}{dz} = -\frac{\omega_p}{\omega_s} g_R I_p I_s - \alpha_p I_p \tag{2.25}$$

where g_R is Raman gain coefficient, and α_s and α_p are the loss due to fibre absorption at the Stokes and pump frequency, respectively.

The critical Raman power is defined as the input pump power when the Stokes power becomes equal to the pump power at the fibre output end, when there is no Stokes light at the fibre input end and stimulated Raman scattering builds up from the spontaneous Raman scattering. From Equation 2.24 and Equation 2.25, the value of the critical Raman power can be estimated from [34]

$$P^P_{Critical} = 16 \frac{A_{eff} \mathrm{K}}{g_R L_{eff}} \tag{2.26}$$

$P^{P}_{Critical}$ corresponds to the maximum peak power of the output pulse at the pump wavelength. For a typical single-mode fibre amplifier at ~1 μm wavelength with Yb^{3+}-doped fibre length of ~3 m, gain of ~20 dB, A_{eff} of ~28 μm^2, the predicted critical Raman power is ~7.8 kW. The critical Raman power increases with an increase in the fibre mode area and a decrease in the effective fibre length. One reason LMA fibre is used in amplifiers is to increase the critical Raman power to avoid SRS. With proper design, LMA fibre can have a critical Raman power over 1 MW [21, 35, 36].

It is possible to utilise Raman Scattering for deliberate frequency conversion. This has been demonstrated with high efficiency in fibres [37].

2.4 Conclusion

This chapter reviewed the history of the development of high power Rare-Earth doped fibre MOPA systems. The Yb^{3+}-doped fibre system was focused on, as the work presented in this thesis is primarily based on this technology. Key technologies developed in this area have been introduced briefly. Nonlinear effects in fibre relevant to the work described in this thesis, either because they limit laser performance or because they allow wavelength conversion, have been described.

More specific background information concerning my experiments will be given in the relevant chapters.

References

[1] E. Snitzer, "Optical Maser Action of Nd in Barium Crown Glass," Physical Review Letters, vol. 7, p. 444, December 15 1961.

[2] C. J. Koester and E. Snitzer, "Amplification in a Fiber Laser," Appl. Opt., vol. 3, pp. 1182-1186, 1964.

[3] H. M. Pask, R. J. Carman, D. C. Hanna, A. C. Tropper, C. J. Mackechnie, P. R. Barber, and J. M. Dawes, "Ytterbium-doped silica fiber lasers: versatile sources for the 1-1.2 µm region," IEEE Journal of Selected Topics in Quantum Electronics, vol. 1, pp. 2-13, 1995/04/ 1995.

[4] R. Paschotta, J. Nilsson, A. C. Tropper, and D. C. Hanna, "Ytterbium-doped fiber amplifiers," IEEE Journal of Quantum Electronics, vol. 33, pp. 1049-1056, 1997.

[5] M. J. F. Digonnet, Ed., Continuous-Wave Silica Fiber Lasers (Rare-Earth-Doped Fiber Lasers and Amplifiers. USA: Marcel Dekker, 2001.

[6] J. K. Sahu, S. Yoo, A. J. Boyland, M. P. Kalita, C. Basu, A. S. Webb, C. L. Sones, J. Nilsson, and D. N. Payne, "488 nm irradiation induced photodarkening study of Yb-doped aluminosilicate and phosphosilicate fibers.," in CLEO/QELS 2008, San Jose, USA, 2008.

[7] G. R. Atkins and A. L. G. Carter, "Photodarkening in Tb3+-doped phosphosilicate and germanosilicate optical fibers," Opt. Lett., vol. 19, pp. 874-876, 1994.

[8] G. P. Agrawal, Nonlinear Fiber Optics, Third ed. USA: Academic Press, 2001.

[9] A. W. Snyder and J. Love, Optical Waveguide Theory: Springer, 1983.

[10] J. Senior, Optical Fiber Communications, 2nd ed. New York Prentice Hall 1992.

[11] D. Marcuse, "Curvature loss formula for optical fibers," J. Opt. Soc. Am., vol. 66, pp. 216-220, 1976.

[12] J. P. Koplow, D. A. V. Kliner, and L. Goldberg, "Single-mode operation of a coiled multimode fiber amplifier," Optics Letters, vol. 25, pp. 442-4, 2000/04/01 2000.

[13] R.J.Mears, L.Reekie, I.M.Jauncey, and D.N.Payne, "Low-noise erbium-doped fibre amplifier operating at 1.54µm," Electronics Letters, vol. 23, pp. 1026-1028, 1987.

[14] J. Kafka, "Laser diode pumped fiber lasers with pump cavity," U.S Patent 4.829.529, 1989.

[15] D. Taverner, A. Galvanauskas, D. Harter, D. J. Richardson, and L. Dong, "Generation of high energy pulses using a large mode area erbium doped fibre amplifier," presented at the CLEO, Anaheim CA, 1996.

[16] Y. Wang, C.-Q. Xu, and V. Izraelian, "Characterization of spun fibers with millimeter spin periods," Opt. Express, vol. 13, pp. 3841-3851, 2005.

[17] K. Okamoto, T. Edahiro, and N. Shibata, "Polarization properties of single-polarization fibers," Opt. Lett., vol. 7, pp. 569-571, 1982.

[18] T. Hosaka, K. Okamoto, T. Miya, Y. Sasaki, and T. Edahiro, "Low-loss single polarisation fibres with asymmetrical strain birefringence," Electron Letters, vol. 17, pp. 530-531, 1981.

[19] P. Russell, "Photonic Crystal Fibers," Science, vol. 299, pp. 358-362, 2003.

[20] K. P. Hansen and J. Broeng, "High-power photonic crystal fiber lasers," Photonics Spectra, vol. 40, p. 82, May 2006.

[21] J. Limpert, F. Roser, T. Schreiber, and A. Tunnermann, "High-power ultrafast fiber laser systems," IEEE Journal of Selected Topics in Quantum Electronics, vol. 12, pp. 233-244, Mar-Apr 2006.

[22] T. A. Birks, J. C. Knight, and P. S. Russell, "Endlessly single-mode photonic crystal fiber," Optics Letters, vol. 22, pp. 961-963, Jul 1997.

[23] F. Röser, D. Schimpf, O. Schmidt, B. Ortac, K. Rademaker, J. Limpert, and A. Tunnermann, "90 W average power 100 uJ energy femtosecond fiber chirped-pulse amplification system," Optics Letters, vol. 32, pp. 2230-2232, Aug 2007.

[24] SPI. http://www.spilasers.com/.

[25] D. J. DiGiovanni, "Tapered fiber bundles for coupling light into and out of cladding-pumped fiber devices " U.S Patent 5864644, 1999.

[26] M. Faucher, E. Villeneuve, B. Sevigny, A. Wetter, R. Perreault, Y. K. Lize, and N. Holehouse, "High power monolithically integrated all-fiber laser design using single-chip multimode pumps for high reliability operation," 2008, p. 68731T.

[27] E. Marcatili, "Improved Coupled-Mode Equations for Dielectric Guides," IEEE Journal of Quantum Electronics, vol. 22, pp. 988-993, Jun 1986.

[28] C. Jauregui, J. Limpert, and A. Tünnermann, "Derivation of Raman threshold formulas for CW double-clad fiber amplifiers," Opt. Express, vol. 17, pp. 8476-8490, 2009.

[29] M. Kumar, C. Xia, X. Ma, V. V. Alexander, M. N. Islam, F. L. Terry, C. C. Aleksoff, A. Klooster, and D. Davidson, "Power adjustable visible supercontinuum generation using amplified nanosecond gains-witched laser diode," Opt. Express, vol. 16, pp. 6194-6201, 2008.

[30] J. K. Ranka, R. S. Windeler, and A. J. Stentz, "Visible continuum generation in air-silica microstructure optical fibers with anomalous dispersion at 800 nm," Opt. Lett., vol. 25, pp. 25-27, 2000.

[31] J. M. Dudley, G. Gentry, and S. Coen, "Supercontinuum generation in photonic crystal fiber," Rev. Mod. Phys, vol. 78, pp. 1135–1184, 2006.

[32] RPphotonics. http://www.rp-photonics.com/encyclopedia.html.

[33] D. Hollenbeck and C. D. Cantrell, "Multiple-vibrational-mode model for fiber-optic Raman gain spectrum and response function," J. Opt. Soc. Amer. B, vol. 19, p. 2886, 2002.

[34] R. G. Smith, "Optical Power Handling Capacity of Low Loss Optical Fibers as Determined by Stimulated Raman and Brillouin-Scattering," Applied Optics, vol. 11, p. 2489, 1972.

[35] A. Galvanauskas, "Mode-scalable fiber-based chirped pulse amplification systems," IEEE Journal of Selected Topics in Quantum Electronics, vol. 7, pp. 504-517, Jul-Aug 2001.

[36] F. Röser, J. Rothhard, B. Ortac, A. Liem, O. Schmidt, T. Schreiber, J. Limpert, and A. Tunnermann, "131 W 220 fs fiber laser system," Optics Letters, vol. 30, pp. 2754-2756, Oct 2005.

[37] A. Malinowski, K. T. Vu, K. K. Chen, P. Horak, and D. J. Richardson, "Selective Generation of Individual Raman Stokes Wavelengths Using Shaped Optical Pulses," 2008, p. OTuB3.

Chapter 3 High power nanosecond Yb^{3+}-doped Fibre MOPA

Overview

This Chapter demonstrates high power nanosecond pulse generation from an externally modulated semiconductor laser incorporating a pulse shaping method using an Electro-Optic Modulator and power amplification through a Yb^{3+}-doped fibre amplifier chain to over 300 W average power. Various custom defined pulse shapes were produced at the final output: Square, step, triangle and even smooth pulse shapes were achieved. This Chapter is organized as follows: 3.1 Introduction to the fibre MOPA; 3.2 Analysis of the gain saturation effect which leads to reshaping of nanosecond pulses; 3.3 The development of shaping techniques and results; 3.4 A brief summary.

3.1 Introduction

Many applications require high peak power pulsed lasers capable of delivering pulses with nanosecond durations. For example; material processing, imaging applications, medical applications and many types of scientific research [1-3]. At present, solid state Q-switched lasers which operate at 1064 nm or its harmonics are the workhorses in this area. Fibre based Master Oscillator Power Amplifier (MOPA) systems incorporating a semiconductor diode as a seed laser and rare-earth doped fibre amplifiers[4, 5] show a lot of attractive features such as good management of thermal effects, good mode quality, great flexibility in pulse duration and peak power, high efficiencies, compactness, low cost of manufacture and ownership. All these advantages have driven progress in pulsed fibre lasers in the last few years. Examples include a nanosecond pulse fibre laser system [6] reported in 2002, and a Q-switched fibre laser system [7] reported in 2004. Fibre lasers have also shown potential for high average powers [8, 9].

To achieve high pulse energies (mJ) and high peak powers (>10 kW) in a fibre MOPA system, typically requires gain of order 40-50 dB. This huge gain will result in gain saturation effects for pulsed systems: significant pulse reshaping over the timescale of the pulse can take place within the amplifier chain due to depletion of the population inversion [10]. This reshaping effect causes a square input pulse to be amplified to a pulse with a very high peak power at the beginning and exponential decrease to a lower power level at the end of the pulse.

There are various reasons for wishing to produce particular pulse shapes from an amplifier. For example, stimulated Raman scattering (SRS) acts as a cap on peak power at the signal wavelength, by efficiently scattering the light to other wavelengths. If the peak power exceeds the threshold for SRS this will limit the pulse energy available at the signal wavelength. Therefore it is desirable to achieve flat-topped pulses, thus maximising pulse power for a given peak power.

One possible way to achieve control of output pulse shape is to actively control the shape of the input pulse so as to pre-compensate for the effects of the gain saturation induced pulse shaping. Our group has demonstrated active shaping of the driving electrical pulses to a laser diode[11]. However, in this case pulse quality was limited by the transient response of the electronics driving the diode, with unwanted oscillations at the leading edge of the pulse. In addition, the practical dynamic range over which the diode power can be controlled is only about 10 dB, which is inadequate for some shaping requirements. Using an Electro-Optic Modulator (EOM), which has a response speed of tens of gigahertz and high extinction ratio, to sample the original pulse has the potential for much better performance. In this chapter, I will discuss the development of such a shaping technique for use within a high power MOPA system. Using active pulse shaping at the amplifier input we show that it is possible to generate a range of user-defined pulse shapes at the output in a very straightforward fashion. As examples, we demonstrate the generation of high energy square optical pulses, as well as the generation of two-step pulses and even smooth shapes pulses. Different optimisation techniques for achieving the best possible pulses are also examined.

3.2 Gain saturation

When an infinitesimally narrow width pulse propagates in a high gain laser medium, which has a constant gain along the laser medium, it experiences an uniform inversion along its pulse width, and the pulse grows exponentially. However, if the width of the pulse is relatively long, say in the nanosecond regime, we must take into account that the pulse front and pulse tail encounter different levels of population inversion. In this case, the amplification process is more complicated and needs to be described by a nonlinear time dependent radiation transfer equation according to Frantz and Siegman's theory [10, 12]. We adopt the following definitions; $N_0 \equiv \int_{z=0}^{z=L} \hat{N}(\hat{z}, \hat{t}_0) d\hat{z}$ - the total initial inversion; $G_0 \equiv e^{\sigma N_0}$ - the initial amplifier gain; $U_{in}(t) \equiv \int_{t_0}^{t} I_{in}(t) dt$ and

$U_{out}(t) \equiv \int_{t_0}^{t} I_{out}(t)dt$ - the input and output pulse energies per unit area from starting time until time t, and $U_{sat} \equiv \frac{\hbar\omega}{2\ \sigma}$ - the saturation energy per unit area. The gain temporal profile can be expressed as [13]:

$$G(t) = 1 + (G_0 - 1)e^{-U_{out}(t)/U_{sat}} \tag{3.1}$$

or equivalently

$$G(t) = 1 + (G_0 - 1)e^{-E_{out}(t)/E_{sat}} \tag{3.2}$$

where $E_{out}(t) = U_{out}(t)A_{eff}$, $E_{sat} = U_{sat}A_{eff}$.

We can see from the above equations that pulse reshaping in an amplifier chain occurs because the leading edge of the pulse depletes the inversion in the amplifier, meaning that subsequent parts of the pulse experience reduced gain. This effect is usually referred to as gain saturation. This is a significant problem in fibre amplifiers due to their fairly low saturation energy. For a given input pulse shape $I_{in}(t)$ it is possible to calculate the output pulse shape $I_{out}(t)$.

$$I_{out}(t) = I_{in}(t)G(t) \tag{3.3}$$

This expression can be inverted in order to establish the input $I_{in}(t)$ required to obtain the desired output $I_{out}(t)$ as a function of G_0, $E_{out}(t)$, and E_{sat}, i.e.

$$I_{in}(t) = \frac{I_{out}(t)}{1 + (G_0 - 1)e^{-E_{out}(t)/E_{sat}}} \tag{3.4}$$

At this point, in order to calculate pulse evolution we need only know G_0 and E_{sat}. Thus, if we can obtain G_0 and E_{sat} experimentally for a given amplifier, we can use the above equation to calculate the input pulse shape required to obtain a desired output pulse shape without any detailed knowledge of the fundamental amplifier characteristics, such as the cross-section, effective area, length or inversion distribution.

3.3 Active shaping with external modulation

3.3.1 MOPA setup

Our MOPA comprises a diode laser and three amplifier stages. A schematic of the set-up is shown in Figure 3.1. The seed is a commercially packaged, fibre-pigtailed diode laser operating at a wavelength of 1061 nm (with a free-running bandwidth ~3 nm). The diode generates pulses with an output peak power of ~700 mW. The broad spectrum is actually composed of several very narrow lines spaced by ~0.2 nm, the mode spacing determined by the length of the diode cavity. A fibre Bragg grating (FBG) is spliced to the diode output at a distance of ~2 m from the fibre facet. By attaching a grating, which has a larger reflectivity (~5%) than the diode front facet, we create a longer cavity with a bandwidth set by the grating reflectivity characteristics, with very many cavity modes within the envelope, creating a smooth spectrum with 0.3 nm width. This yields of order 600 cavity modes (mode separation ~100 MHz) compared to the diode spectrum without the FBG which consists of only a small number of longitudinal modes (~15), and as a result would be expected to be subject to stimulated Brillouin scattering (SBS) at the power levels encountered in this work. Since the SBS bandwidth is ~25 MHz, the individual cavity modes would be expected to generate SBS effectively independently, and the effective SBS threshold will be approximately proportional to the number of modes [14]. The estimated SBS threshold per mode in our power amplifier is ~ 200 W. If we assume ~600 longitudinal modes this gives an effective threshold of order 120 kW. In fact, we observed no evidence of SBS during our experiments with this line-narrowed laser.

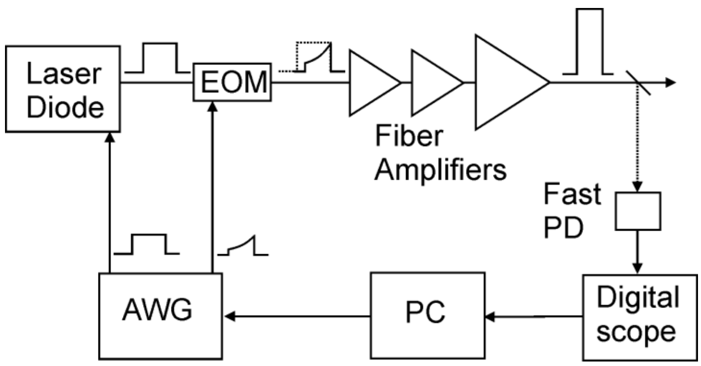

Figure 3.1: Schematic of active pulse shaping system with EOM

This diode was driven at repetition rates of up to several 100 kHz using one channel of a computer controlled Arbitrary Waveform Generator (AWG). The pulse duration set on this pulse generator could be changed from tens of nanoseconds to tens of microseconds as desired. In general, the AWG provided a square pulse with a duration slightly longer than that of the pulse ultimately targeted. Operating the diode in pulsed mode allowed us to utilise larger diode peak powers (up to the full 700 mW) whilst keeping the average power below the 50 mW operating limit of our EOM.

The output from the diode was fed through the EOM, which has a 20 GHz response with 30 dB extinction ratio, and which was synchronously driven from the second channel of the AWG. The EOM was used to carve the required amplifier input pulse forms from the square pulse output from the diode. The first 100 ns of the pulse from the seed laser was eliminated in the carving process, since the diode had a rise time of tens of nanoseconds and it takes several tens of nanoseconds to stabilise the amplitude. Moreover, this represents several round trip times of the external cavity defined by the FBG, so that we can be confident that after this time the diode is emitting with the desired, SBS-safe, densely mode-spaced spectrum.

The AWG has 16-bit amplitude resolution and a time resolution of 4 ns. The optical power transmission of the EOM varies sinusoidally rather than linearly with applied voltage. This is taken into account when calculating the control voltage waveform which is sent to EOM in order to ensure that the desired output optical pulse form is obtained in the carving process. An isolator was spliced between the seed laser and the amplifier chain. Due to losses in the EOM and isolator totalling ~6 dB, the peak seed power to the amplifier system is ~175 mW.

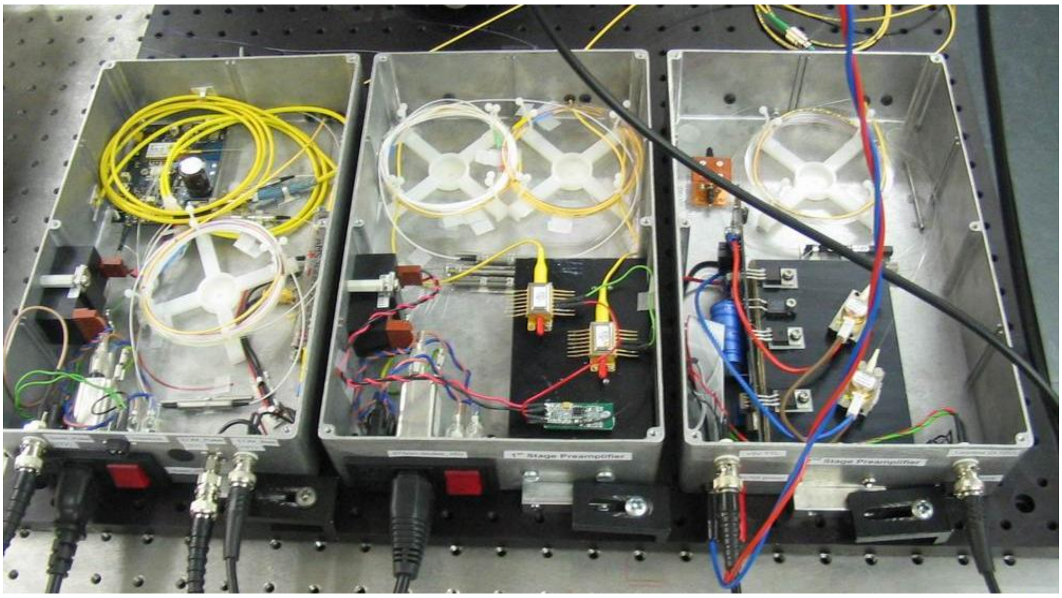

Figure 3.2: Real experiment set-up of (from left to right) seed laser, first stage and second stage amplifier.

The amplifier system comprises three distinct diode-pumped Yb^{3+}-doped amplifier stages. The first two stages are fully fiberized (shown as figure 3.2). A core-pumping scheme incorporating a 4 m length of ytterbium doped single mode fibre is used for the first stage and a 8 m length cladding pumped fibre amplifier with a 10 μm core diameter and 0.07 NA (mode field diameter (MFD)~11 μm) for the second stage. Coupling of the single mode pump radiation (300 mW at 976 nm) into the first stage was performed using a 976 nm/1060 nm WDM coupler. Delivery of the multimode pump radiation (7 W at 915 nm) into the second stage amplifier was performed using a tapered fibre bundle (TFB). The amplifier fibres in both stages are approximately single mode and the output at second stage has an $M^2<1.2$. The maximum saturated average output powers from the two amplifiers were 50 mW and 3 W from stages 1 and 2 respectively. Typically, small signal gains were up to 20 dB in the first stage (depending on duty cycle) and about 20 dB in the second stage, with losses of the order 2 dB between stages, due to the isolator.

The final (third) amplifier stage was end-pumped using a 500 W 975 nm diode stack. The final stage amplifier fibre has a 30 μm core diameter and 0.06 NA (MFD~24 μm) and 400 μm diameter cladding, was 10 m long and was typically operated with a gain around or below 20 dB. The fibre was manufactured in the ORC. The core was theoretically multimode (supporting ~5 modes) but with appropriate (free-space) signal launch was close to single mode in amplified output (M^2~1.5). The peak gain through the whole amplifier chain (including losses due to isolation) was up to ~55 dB. The highest output peak power that we measured was about 35 kW. Based on Equation 2.23 and Equation 2.26 described in Chapter 2, the Stimulated Raman Scattering (SRS) threshold for this amplifier was estimated [15] at 80 kW, well above any instantaneous power obtained in the experiments described, and as mentioned above the estimated SBS threshold was well over 100 kW.

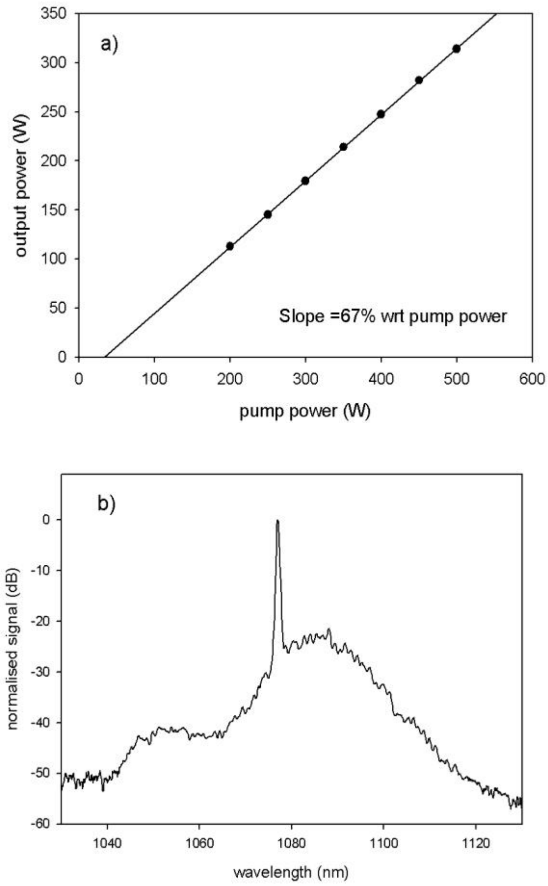

Figure 3.3: (a) MOPA output power curve and (b) output spectrum at 200W and 1% duty cycle

Figure 3.3 (a) shows the average output power of the MOPA plotted against the output of the pump laser. The amplifier efficiency was 67% calculated with respect to the launched pump power. The spectrum, shown in figure 3.3 (b), did not broaden significantly compared to the initial bandwidth of 0.3 nm during amplification.

3.3.2 Pulse shaping method

It is possible to achieve the target output pulse shape by actively controlling the shape of the input pulse so as to pre-compensate for the effects of the gain saturation. This has been demonstrated experimentally using feed-back loops to optimise the pulses [16-18], or by simulating the amplifier performance and calculating the required pulse analytically [19]. The method in this work is to parameterize the pulse shapes. To determine the parameters for the pulse shaping, it is necessary to make a measurement of the output of the MOPA for a test input pulse. Any pulse shape can be chosen for the input pulse; however a square pulse was typically used for convenience. The pulses are sampled and detected by a 1 GHz photodiode which is connected to a 500 MHz oscilloscope under computer control. By comparing the input and output pulses a measurement of the instantaneous gain G(t) at each point in the pulse is obtained. By iteratively fitting this data to Equation 3.2, numerically integrating to obtain $E_{out}(t)$, an estimate of E_{sat} and G_0 are obtained. The fitting process takes just a few seconds. We make no assumptions about the details of the gain distribution within the system, so no simulation or detailed knowledge of the amplifier chain is required.

In this work, three methods for selecting the best input pulse for obtaining desired output pulses were investigated. The first method is simulated annealing [20] based on the results of E_{sat} and G_0 fitting. The input pulse is modeled as one or more segments, and the parameters of the segments are varied whilst the expected output pulse is calculated using our measured values of E_{sat} and G_0. This algorithm (running on a PC) seeks to minimise the fitness factor (difference calculated output pulse and target pulse) until it achieves a specified tolerance (or number of iterations). Simulated annealing is inspired by the annealing method in metallurgy, in which a material is heated up and slowly cooled down to maximize the size of crystals and minimise defects. This process is equivalent to minimizing the energy state of the system. Because of thermal motion of the atoms in the materials, the system which is initially stuck in one state might jump out of that state to a new one. If the new state has lower energy than the initial one, the system stays there, but if the new state has higher energy, there will still be a probability that it will stay at the new state. The system slowly moves to the local minimum of total energy by some random upward jumps to higher energy levels and slow lowering of the temperature. Simulated annealing is found to be an efficient and time-saving method to achieve a best fit input pulse shape for the MOPA in our case.

The second method is simulated annealing based on measured MOPA output. This is an experimental process rather than a simulation. It is identical to the previous method except that the pulse shape is sent to the amplifier chain and we measure the output pulse from the amplifier and compare it with target pulse shape. This was generally used after method one (the optimized pulse shape obtained by method one being used as the initial guess for the pulse shape) in the hope of further improving the output pulse shape.

The third method is to directly calculate the required input pulse from our chosen output pulse shape utilising Equation 3.4 and our measured values of E_{sat} and G_0 (again using numerical integration to give $E_{out}(t)$). After calculating the pre-compensated waveform, the desired pulse shape will be achieved by launching it into the amplifier chain.

3.3.3 Pulse Shaping Results

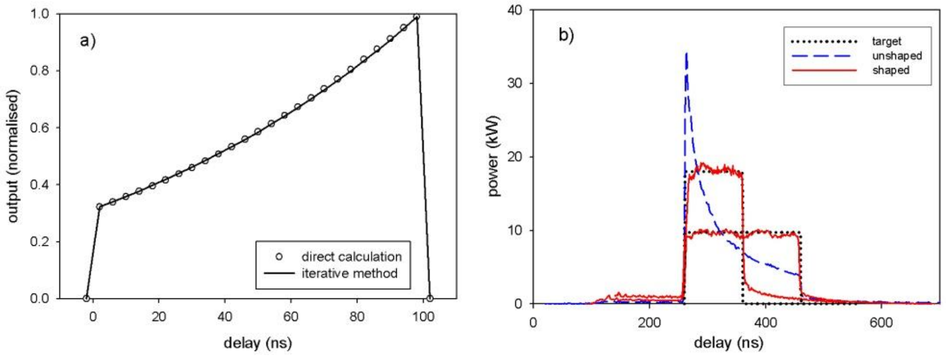

Figure 3.4: (a) Input pulses to generate a square 100 ns output pulse, produced by direct calculation or iterative method, (b) Square output pulses with 100 and 200 ns pulse durations.

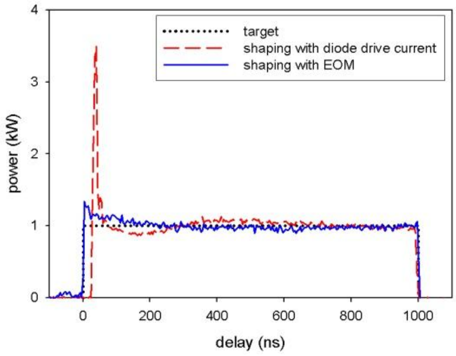

Figure 3.5: Square pulses generated via modulating diode current or modulating EOM

Figure 3.4 (a) shows the optimised input pulse shapes for a targeted 100 ns square pulse produced by the iterative approach using simulated amplifier response and by the direct calculation method. The iterative method uses a pulse modelled as a single curved segment specified by the height of the starting point of the pulse L, an exponential factor (α) and a fixed width T, as described in [11]:

$$y = L + \frac{1-L}{e^{\alpha T}}(e^{\alpha t} - 1) \tag{3.5}$$

In order to get square output pulses in this instance then it was necessary to optimise just two parameters (L and α). Data points are spaced by 4 ns to match the resolution of the AWG. Direct calculation of the required input pulses based on Equation 3.4 produced pulses which were virtually indistinguishable from those obtained using the iterative method in simulation (less than 1% deviation in amplitude across the entire pulse shape between the two methods for all pulse durations considered). Typically of order 20 iterations were required to achieve convergence.

Figure 3.4 (b) shows various pulses produced at a pump power level of 350 W, corresponding to an average MOPA output power of 200 W. Pulse repetition rate was 100 kHz and the pulse energy was 2 mJ. The long-dashed curve is the shape of the output pulse from the amplifier when the seed pulse was a 200 ns duration square pulse. Based on fitting this pulse we obtained a saturation energy for our amplifier of 0.6 mJ, so we are operating ~3-4 times above saturation energy. It can be seen that reshaping is significant, with the leading edge of the pulse having an instantaneous power of 35 kW, which has dropped to ~ 4 kW after 200 ns. The FWHM width of this pulse is only about 20 ns.

When the calculated input pulses were fed into the system, they produced the square pulses shown in figure 3.4 (b). The black lines show the target (square) pulse shape and the red curves show output pulses of varying duration produced by active shaping of the seed pulse. The obtained pulses match the target pulse, with deviations in amplitude from the target not exceeding 10% over the duration of the pulse. Simulated annealing using the actual output of the amplifier yielded no detectable further improvement in pulse shape.

Since both methods produced virtually identical inputs we can state that for square target pulses the direct calculation method produces results indistinguishable from the iterative process, giving great confidence in this simplified approach.

Figure 3.5 compares shaping results (for a 1 μs duration pulse) obtained using the iterative optimisation method but in one case (red), shaping the input pulse using direct modulation of the seed diode current, as in [19, 21] and in the other case (blue), using gating with the EOM to create shaped pulses. It can be seen that there is a large transient on the pulse in the directly modulated case. This was observed on all pulses produced by direct modulation of the diode. We attribute this to changes in the seed spectrum that arise during pulse build up, as described above. Because the gain is wavelength dependent, changing the centre wavelength and bandwidth during the pulse as it develops will change the gain experienced. The pulse shaping methods used, which do not account for such changes, will not correct for this feature. As expected, this only affects the first few 10 s of nanoseconds of the pulse. Using the EOM to shorten and shape the pulses completely removes the issue of diode startup dynamics. It should be noted that this problem could potentially also be addressed in other ways. For example, a diode with an external grating packaged very close to the diode (as are becoming commercially available) might eliminate this problem.

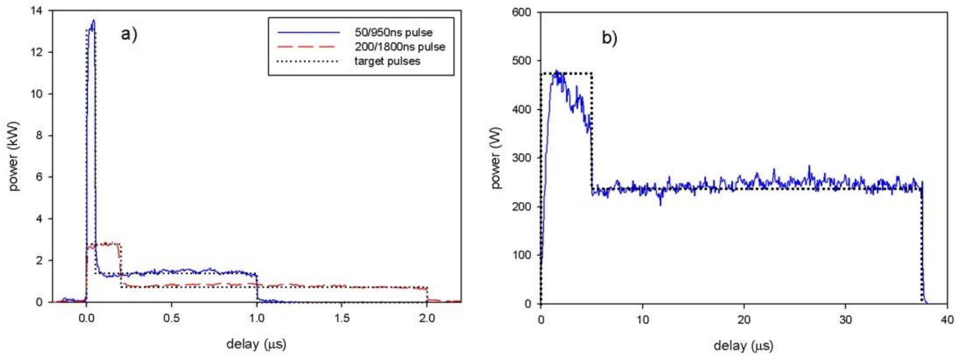

Figure 3.6: Two-step pulse shape with (a) low duty cycle, (b) high duty cycle

We also produced various duration two-step pulses at high average power. In order to produce two-step pulses, as shown in Figure 3.6, using the iterative method, we simply simultaneously optimised two segments with fixed durations and independent starting heights and exponential factors, so that a total of four parameters required optimisation. In simulation, the iterative process converged after ~100 iterations. As observed with the square pulses, iterations based on the real amplifier output did not improve on the results obtained in simulation.

Figures 3.6 (a) show results for relatively low duty cycle 2-step pulses, Figure 3.6 (b) for a high duty cycle pulse. As with the square pulses, in these experiments the average power was 200 W and the repetition rate 100 kHz, giving a pulse energy of 2 mJ. The duty cycles were 20% and 10% for the two pulses shown in Figure 3.6 (a). In both cases deviations in amplitude from the target pulse do not exceed 10%. Figure 3.6 (b) shows a pulse generated for an average power of 200 W and a repetition rate of 20 kHz, giving a pulse energy of 10 mJ. The pulse displayed consists of an initial 5 ms section and a final 32.5 ms (75% duty cycle). The final part of the pulse has a power level close to 200 W (i.e. near the average power) whilst the power level in the initial section is approximately twice this.

In theory, our approach is not expected to be precisely accurate for high duty cycle pulses, since our analysis ignores pumping during the pulse: there is no replenishment of the inversion during the pulse. This is a reasonable approximation for low duty cycle pulses only. However, as we see, this approach is still sufficient to produce fairly good quality pulses even at 75% duty cycle, with deviation from target pulse being less than

30% for ~90% of the duration of the first section of the pulse, and considerably better during the second section.

We also generated smooth output pulse shapes. In generating smooth pulses, the advantages of the direct calculation method over the iterative method become clear. In order to produce smooth pulses shapes, such as Gaussian or parabolic pulses by the simulated annealing method, we used input pulses composed of a number of segments. In order to keep the number of independent parameters being optimised at a manageable number, we used straight line segments of fixed duration, with only the initial height of each segment being varied (i.e. only one parameter per segment).

To get convergence on the target pulse using SA with calculated results and using a pulse composed of 12 segments typically required of order 1000 iterations. With each experimental iteration requiring of order 2 seconds, it was impractical to employ experimental optimisation to further improve the results obtained in simulation, negating the most obvious possible advantage of the SA method; i.e. that it does not necessarily depend on our assumptions about ideal amplifier performance but more on the actual performance of the amplifier chain.

It was also observed that with these pulse shapes, on occasion the solution would get stuck at a local minimum which did not correspond very closely to the desired pulse. Although these could be improved upon by varying the annealing parameters, this further indicated the inconvenience of this method for smooth pulse shapes. In contrast, the direct calculation approach requires no choices to be made about fitting parameters, and requires no more processing time for these pulse shapes than for square pulses.

Figure 3.7 shows results for a targeted parabolic pulse of 1 mJ pulse energy. Figure 3.7 (a) shows various input pulse shapes used and Figure 3.7 (b) shows the corresponding output pulses. It can be seen that a parabolic input pulse (long blue dashes) yields an output pulse which is heavily skewed, as expected. It can be seen that the direct calculation method (solid red line) in this case produces a significantly better approximation of the targeted pulse shape (black dots) than the iterative method (short green dashes), which appeared to get stuck at a local minimum. The output pulse produced by the calculation method differed from the target pulse by less than 10% of the peak power over the full duration of the pulse.

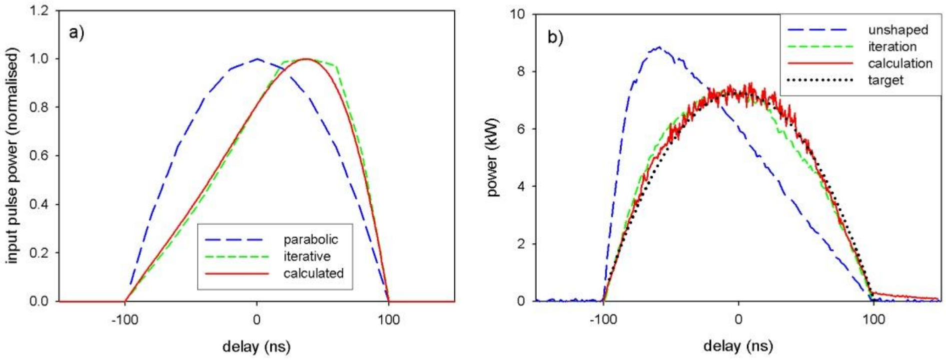

Figure 3.7: Parabolic pulse (a) input pulses (b) output pulses

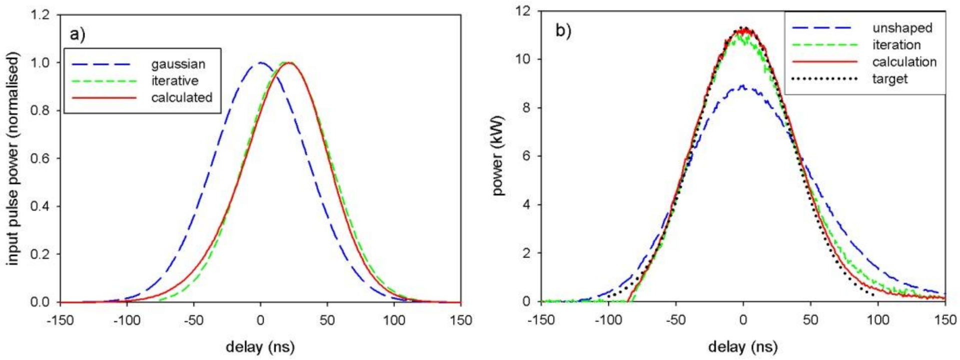

Figure 3.8: Output pulses obtained by various methods with a targeted Gaussian pulse shape

Figure 3.8 shows similar outputs for a targeted Gaussian output pulse of 100 ns duration. Again, the pulse energy is 1 mJ. The targeted pulse shape is shown (black dots). The output pulse obtained for an input Gaussian pulse of the desired output duration is shown by long blue dashes. It can be seen that while the effects of gain reshaping are more subtle than in the case of a square pulse; the pulse increases in duration and becomes slightly asymmetric during amplification. The solid red curve shows the output pulse obtained using direct calculation. The best result obtained by SA using calculated results is shown by the short green dashes. It can be seen, that while both methods produce a result close to the desired pulse shape, direct calculation produced slightly superior results. The deviation from target pulse amplitude is less than 2% of the peak power everywhere within the 10 dB full width of the pulse.

3.4 Fiberized polarisation maintaining nanosecond source

For many industrial applications such as micromachining, a key issue is the strength of absorption of the material at the laser wavelength, and hence it is advantageous if the laser can be frequency converted to provide a range of machining wavelengths. To ensure high efficiency frequency conversion processes (e.g. SHG) it is useful to maintain a narrow line-width and therefore nonlinear spectral broadening in the fibre amplifiers should be avoided. Moreover, it is critical that good polarization purity is maintained, because most wavelength conversion processes are polarization sensitive. Hence, a fiberized, polarisation maintaining source is built to achieve such wavelength conversion ability. A schematic diagram of the all-fibre PM MOPA is shown in Figure 3.9. The seed was still a PM fibre pigtailed Fabry-Perot laser diode chip (Bookham CPE425) working around 1060 nm. The centre wavelength of the seed signal was set to 1060 nm with an external fibre Bragg grating. The corresponding 3 dB bandwidth was 0.3 nm. The optical output of the seed laser was passed through a high extinction ratio (>30dB) lithium niobate EOM, which was used to carve pulses as described in the previous section. The insertion loss of the EOM was 5 dB and the typical duty cycle used in our experiments was 1:100 (e.g. 100 ns pulses at a repetition rate of 100 KHz).

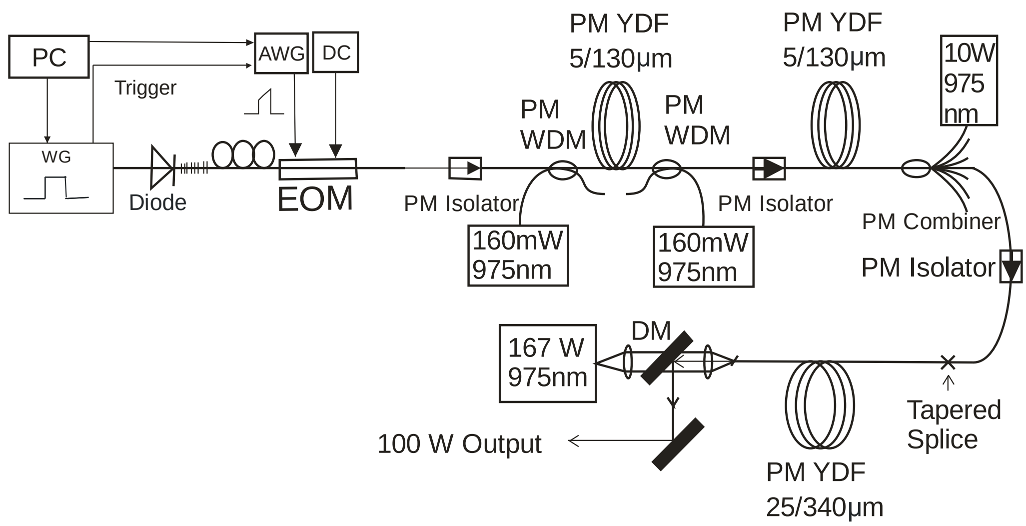

Figure 3.9: Schematic diagram of the Yb^{3+}-doped fibre MOPA

Approximately 0.3 mW of average seed signal power from the EOM was amplified by a three-stage amplifier chain. The first pre-amplifier stage is based on a core pumped, Yb^{3+}-doped active polarisation maintaining fibre with a core diameter and NA of 5 μm and 0.13 respectively. The amplifier was pumped in a co-propagating configuration by a wavelength stabilized 976 nm single-mode laser diode. The measured core absorption of the fibre was ~600 dB/m at 976 nm. The length of the active medium (3 m) was chosen such that the amplifier provides maximum gain around 1060 nm. A maximum saturated output power of over 100 mW was obtained from this stage, corresponding to a signal gain of 25 dB. The output of the first stage amplifier was coupled into the second pre-amplifier stage via a fiberized PM optical isolator. The isolator limits both signal and ASE cross-coupling between the two amplifier stages.

The active medium of the second-stage amplifier used double-clad technology. The fibre was commercial available from Nufern. It was a 7 m long single mode (5 µm core, NA=0.13; 130 µm inner cladding NA=0.46) PM Yb^{3+}-doped fibre with 10 W, 975 nm pumps coupled into the inner cladding using a fibre-pigtailed broad-stripe diode laser through a (6 + 1) fused tapered fibre bundle (TFB) in a backward pumping configuration. The length of the active medium was chosen such that the amplifier provides maximum gain at the signal wavelength with balanced ASE. The maximum saturated output power from this stage was limited to <1 W to extract maximum possible gain from the final-stage amplifier without compromising performance by spectral line width broadening and ASE build-up. This helps in two ways: (i) it reduces the output power required from the 2nd pre-amplifier stage and power handling demands on the in-line optical components and (ii) reduces the effective length of the final-stage amplifier, which depends exponentially on the gain parameter, resulting in clean, high peak power pulse generation from the fibre MOPA.

The linearly polarized optical signal from the two PM pre-amplifier stages was aligned to the slow-axis of an in-line fast axis blocking PM isolator to further purify the polarisation extinction ratio (PER) up to 35 dB. The resulting linearly polarized signal was then coupled into a large mode area (LMA), PM, double-clad, Yb^{3+}-doped active fibre (PLMA-YDF-25/345 from Nufern). The fibre has a core diameter of 25 µm and a core NA of 0.06. The cladding diameter of the polymer coated fibre was 345 µm with an NA of 0.45. The measured cladding absorption of the fibre at the pump wavelength (975 nm) was 2.7 dB/m. The length of the active medium (5.7 m) was chosen such that the amplifier not only provides maximum signal gain but also absorbs most of the launched pump power. Free-space pump coupling through the signal output end was used to pump the active medium. To minimize the splice loss between the passive single-mode PM fibre (SM98-PS-U25A from Fujikura) and LMA active fibre the outer diameter of the LMA fibre was tapered down to 125 µm and a core diameter of 9 µm. The associated V-number was therefore reduced to 1.5 so that only the fundamental mode would be supported. The length of the tapered region was optimised by repeated testing of the output mode quality with different taper lengths. We finally selected a taper length of 80 mm, which was found to be the minimum length that led to robust single-mode output from the amplifier fibre. This helps to reduce the mode field diameter mismatch between the two dissimilar fibres ensuring lower splice loss. The maximum splice loss measured was <1 dB, substantially lower than that obtained without tapering (~2 dB). Moreover, tapering allowed us to obtain robust single mode operation even though the active fibre core can support several transverse modes. To prevent damage to the output, a 2 mm long pure silica mode-expanding end-cap was spliced to the fibre and it was angle polished to avoid power retro-reflected back into the fibre core. The amplifier was end-pumped using a 975 nm diode stack with maximum pump power of 167 W. The diodes were water-cooled to ensure wavelength stability. A simple lens combination was used to achieve ~80% coupling efficiency into the fibre. Signal and pump paths were split by dichroic mirrors.

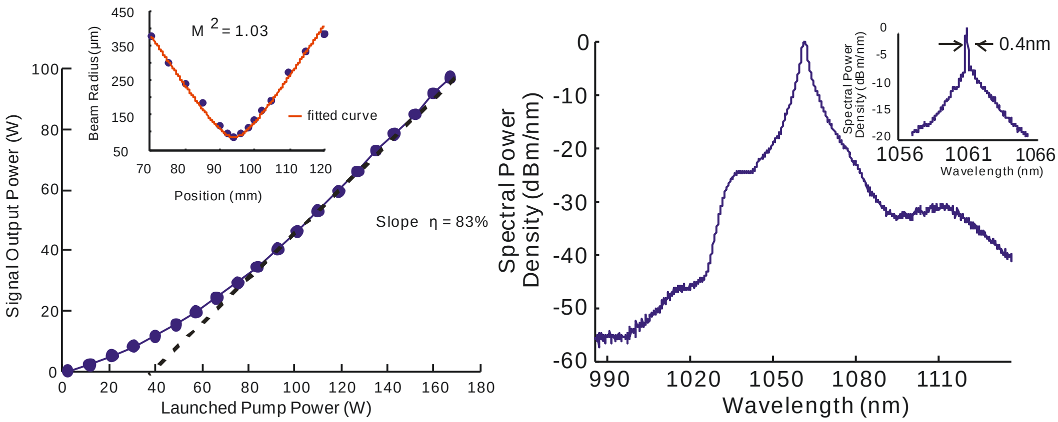

(a) (b)

Figure 3.10: (a) Fibre MOPA output power vs. launched pump power. (b) Spectrum at full power at 2.0 nm OSA resolution; inset shows the output spectra with 0.05 nm OSA resolution.

Figure 3.10 shows the performance of the final amplifier. The slope efficiency was 83% with respect to launched pump power, and the amplifier shows no power roll-off up to 100 W. The beam quality of the amplified signal output was measured to be $M^2 = 1.02$ at a power of 100 W. The maximum extracted pulse energy was 1 mJ, corresponding to a peak power of 10 kW at an average output power of 100 W. The spectral bandwidth of the amplified pulses increased from 0.3 nm to 0.4 nm due to SPM assisted spectral broadening inside the final stage amplifier (Figure 3.10(b)). The amount of ASE is less than 7% according to power intergradations. The measured polarization extinction ratio (PER) was 19 dB under full power operation.

A significant pulse narrowing was observed due to gain depletion on the time scale of the 100 ns when a square input pulse was launched into the amplifier chain as shown in Figure 3.11(a). This was corrected by the method described in the previous section [22]. The corresponding output spectra for both shaped and unshaped input optical pulses to the MOPA chain are shown in Figure 3.11(b).

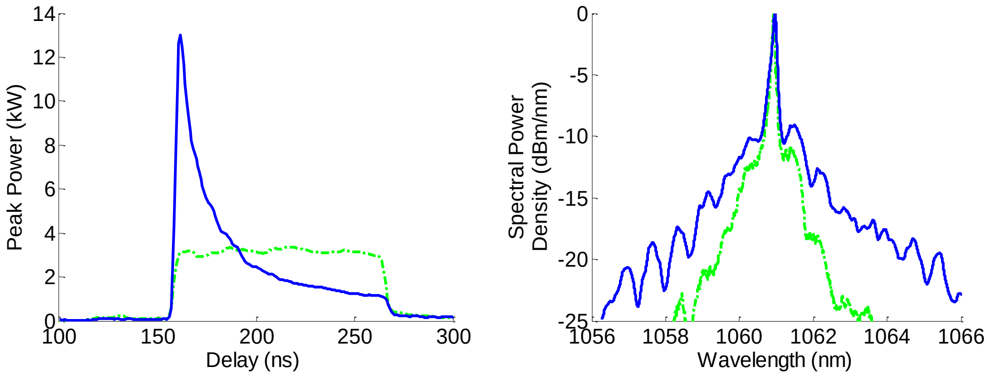

(a) (b)

Figure 3.11 (a) Peak power of shaped (green dash dotted line) and unshaped (solid blue) fundamental pulse at 36 W power level. (b) Spectra of the corresponding shaped (green dash dotted line) and unshaped (solid blue) fundamental pulse at 36 W power level.

These linearly polarized, high spectral integrity, shaped pulses are useful for high efficiency and high quality frequency conversion. Such as second harmonic generation (SHG), optical parametric oscillation (OPO), Raman frequency shift conversion and so on. These frequency conversion experiments will be discussed in Chapter 5.

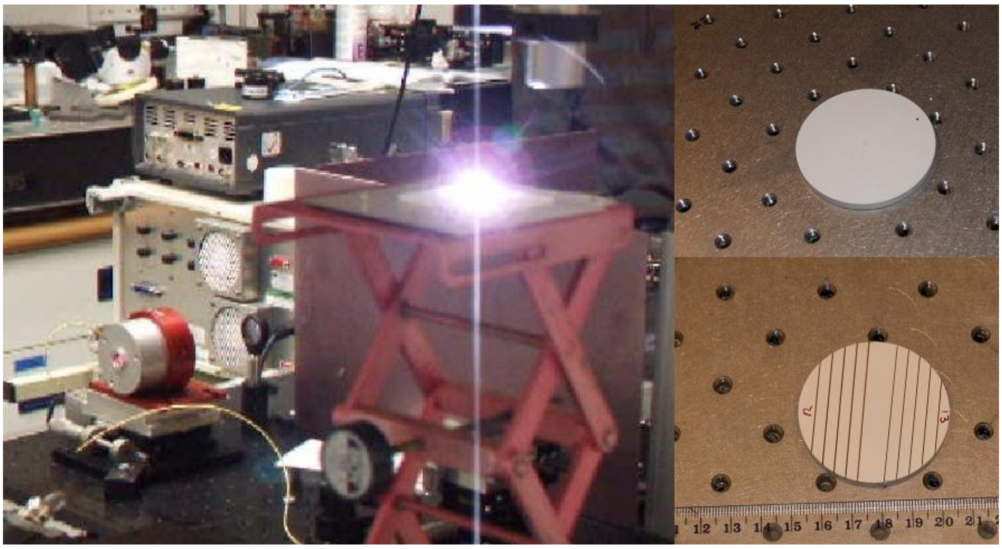

Figure 3.12: A ceramic plate is being cut by the 100 W, 100 ns duration, 100 kHz repetition rate nanosecond pulses; Top right is sample before cutting; Bottom right is sample after cutting.

The output beam directly from the fibre laser was also used to carry out material processing. Metals, ceramics and organic glue bonded material were tested under different pulse shapes and powers. The laser behaved very reliably and no failure or performance degradation was observed during three weeks of use (~100 hours total operating time). A maximum of 3% of average power variation was observed at full operational power. Figure 3.12 shows the cutting process and examples of the preliminary cutting results. Comprehensive analysis of the cutting results is still being carried out by our project partners.

3.5 Conclusion

We have successfully demonstrated a fiberized, diode-seeded, YDFA MOPA system generating linearly polarized, diffraction-limited, nanosecond and longer pulses. Arbitrary pulse shapes including square pulses, 2-step pulses and pulses with smooth profiles can be produced. An average power of up to 300 W was achieved.

By using an EOM to shape our seed pulses, high quality pulses were produced, avoiding any transients introduced by the operation of the diode or its drive electronics and limitations imposed by its available dynamic range. This will also allow shaping of a much wider variety of seed lasers, including those which do not have a short pulse operation mode.

The method of calculating the required input pulse from the measured gain parameters of the amplifiers is rapid and allows optimisation of smooth pulse shapes, where the iterative method based on pulses composed of simple segments becomes unmanageable due to the number of parameters which need to be optimised. The direct calculation method is shown to produce output pulses which match the target pulse shape at least as well, if not better, than the iterative method for all the pulse shapes examined.

Our method is indifferent to the detailed architecture of the amplifier chain; the only parameters required can be obtained via a single experimental measurement. This will allow the approach to be adapted rapidly to a wide variety of amplifier chains. This should be of significant value in enhancing the use of fibre based MOPA systems for a range of industrial and scientific applications.

The same seed laser and shaping method were used to seed a PM fibre amplifier to generate a linearly polarized beam for frequency conversion applications. In addition, material processing experiments using this source were also carried out and long term stable performance verified. The fiberized configuration enhances the robustness of the fibre laser.

References

[1] K. F. Kleine and K. G. Watkins, "Pulse Shaping for Micro Cutting Applications of Metals with Fiber Lasers," in Photonic West, San Jones, 2004.

[2] K. K. Chen, S.-u. Alam, P. Horak, C. A. Codemard, A. Malinowski, and D. J. Richardson, "Excitation of individual Raman Stokes lines in the visible regime using rectangular-shaped nanosecond optical pulses at 530 nm," Opt. Lett., vol. 35, pp. 2433-2435, 2010.

[3] X. D. Wang, X. Yuan, S. L. Wang, J. S. Liu, A. Michalowski, and F. Dausinger, "Efficient Laser Drilling with Double-Pulse Laser Processing," in Advanced Design and Manufacture to Gain a Competitive Edge, X.-T. Yan, et al., Eds., ed: Springer London, 2008, pp. 759-766.

[4] J. Nilsson, J. K. Sahu, Y. Jeong, W. A. Clarkson, R. Selvas, A. B. Grudinin, and S. Alam, "High-power fiber lasers: new developments," in Advances in Fiber Lasers, San Jose, CA, USA, 2003, pp. 50-59.

[5] F. Ghiringhelli, K. Vysniauskas, L. M. B. Hickey, M. N. Zervas, A. Malinowski, and D. J. Richardson, "Pulse shaping in high gain all-fiber pulse MOPA," in CLEO Europe 2005, Munich, 2005.

[6] J. Limpert, S. Hofer, A. Liem, H. Zellmer, A. Tunnermann, S. Knoke, and H. Voelckel, "100-W average-power, high-energy nanosecond fiber amplifier," Applied Physics B (Lasers and Optics), vol. B75, pp. 477-9, 2002/10/ 2002.

[7] A. Piper, A. Malinowski, K. Furusawa, and D. J. Richardson, "High-power, high-brightness, mJ Q-switched ytterbium-doped fibre laser," Electronics Letters, vol. 40, pp. 928-929, 2004.

[8] Y. Jeong, J. K. Sahu, D. N. Payne, and J. Nilsson, "Ytterbium-doped large-core fibre laser with 1 kW of continuous-wave output power," Electronics Letters, vol. 40, pp. 470-472, 2004.

[9] A. Liem, T. Limpert, H. Zellmer, A. Tunnermann, V. Reichel, K. Morl, S. Jetschke, S. Unger, H. P. Muller, J. Kirchhof, T. Sandrock, and A. Harschak, "1.3 kW Yb-doped fiber laser with excellent beam quality," in Lasers and Electro-Optics, 2004. (CLEO). Conference on, 2004, pp. 1067-1068.

[10] L. M. Frantz and J. S. Nodvik, "Theory of Pulse Propagation in a Laser amplifier," Journal of Applied Physics, vol. 34, p. 2346, August 1963 1963.

[11] K. T. Vu, A. Malinowski, D. J. Richardson, F. Ghiringhelli, L. M. B. Hickey, and M. N. Zervas, "Adaptive pulse shape control in a diode-seeded nanosecond fiber MOPA system," Opt. Express, vol. 14, pp. 10996-11001 2006.

[12] A. E. Siegman, Lasers: University Science Books, 1986.

[13] K. T. Vu, "HIGH POWER NANOSECOND PULSED FIBER LASER AMPLIFIERS," Ph.D Thesis, University of Southampton, 2007.

[14] E. Lichtman, Friesem, A.A., Waarts, R.G. and Yaffe, H.H., "Stimulated Brillouin scattering excited by two pump waves in single-mode fibers," J. Opt. Soc. Am. B 4, 1397, 1987.

[15] G. P. Agrawal, Nonlinear Fiber Optics, Third ed. USA: Academic Press, 2001.

[16] W. Williams, C. Orth, R. Sacks, J. Lawson, K. Jancaitis, J. Trenholme, S. Haney, J. Auerbach, M. Henesian, and P. Renard, "NIF Design Optimization," in Inertial Confinement Fusion Annual Report, (Lawrence Livermore National Laboratory, 1996) p. 184.

[17] M. Shaw, W. Williams, R. House, and C. Haynam, "Laser Performance Operations Model (LPOM)," in InertialConfinement Fusion Semiannual Report (Lawrence Livermore National Laboratory, 2004).

[18] W. Shaikh, I. O. Musgrave, A. S. Bhamra, and C. Hernandez-Gomez, "Development of an amplified variable shaped long pulse system for Vulcan," in Central Laser Facility Annual Report (CCLRC Rutherford Appleton Laboratory, 2005/2006) p. 199.

[19] D. N. Schimpf, C. Ruchert, D. Nodop, J. Limpert, A. Tünnermann, and F. Salin, "Compensation of pulse-distortion in saturated laser amplifiers," Opt. Express, vol. 16, pp. 17637-17646, 2008.

[20] S. Kirkpatrick, C. D. Gelatt, and M. P. Vecchi, "Optimization by Simulated Annealing," Science, vol. 220, p. 671, 1983 1983.

[21] R. Paschotta, J. Nilsson, A. C. Tropper, and D. C. Hanna, "Ytterbium-doped fiber amplifiers," IEEE Journal of Quantum Electronics, vol. 33, pp. 1049-1056, 1997.

[22] A. Malinowski, K. T. Vu, K. K. Chen, J. Nilsson, Y. Jeong, S. Alam, D. Lin, and D. J. Richardson, "High power pulsed fiber MOPA system incorporating electro-optic modulator based adaptive pulse shaping," Opt. Express, vol. 17, pp. 20927-20937, 2009.

Chapter4 High power picosecond Yb^{3+}-doped fibre MOPA

Overview

This Chapter demonstrates picosecond pulse generation from a self-seeded gain switched laser diode and power amplification using polarisation maintaining Yb^{3+}-doped fibre amplifier chain to 100 W average power. This Chapter is organized as follows: section 4.1 introduces the state of the art picosecond fibre system; 4.2 describes the self-seeded gain switched seed laser; 4.3 details the performance of the diffraction limited, polarization maintaining high power Yb^{3+}-doped fibre amplifier chain; 4.4 describes the nonlinear pulse compression of the MOPA output using diffractive gratings; 4.5 describes the subsequent SHG experiment with compressed pulses; finally a brief summary of the chapter is given in section 4.6.

4.1 Introduction

High average power laser sources operating in the picosecond regime are useful for a wide range of applications including materials processing, frequency-doubling and broadband wavelength tuning by means of OPOs. Over recent years, fibre amplifiers have become a key enabling technology in many of these areas. In particular, Yb^{3+}-doped fibre amplifiers (YDFA) have high single-pass gain, low quantum defect and optical-to-optical efficiencies above 80%. The resulting low thermal load and inherently favorable geometry minimize thermal effects to enable continuous-wave powers of 6 kW in a diffraction-limited beam [1].

However, picosecond pulsed fibre MOPA operated at repetition rates below ~100 MHz, nonlinear effects such as self-phase-modulation (SPM) and stimulated Raman scattering (SRS) arising in the core of the fibre have restricted the power scaling. Since the high peak power is the key factor, nonlinearity management techniques such as chirping the input pulses and using microstructured fibre to achieve extremely large mode areas are commonly applied in femtosecond systems [2, 3]. The disadvantages of such techniques are that the dispersion management components increase the complexity of the system, and that the novel fibre architectures have not yet been thoroughly field tested [4, 5].

An attractive route to achieve high average powers with short pulse sources without problematic nonlinear effects is to reduce the energy per pulse by dramatically increasing the repetition rate. There has been progress with fibre oscillators, VECSEL sources [6-8] and gain-switched laser diodes for generating high repetition rate picosecond pulses. Output powers in excess of 300 W have previously been demonstrated from a YDFA system using a 1060 nm gain-switched Fabry–Pérot (FP) laser diode delivering 20 ps pulses at GHz repetition rates as a seed laser [9-11]. However, the sub-microJoule pulse energies from those systems were far from ideal for material processing whilst free space pump and signal coupling greatly compromised the practicality of the systems. Moreover, the output was not robustly single-transverse-moded and the amplifiers were not all polarization-maintaining (PM), thus limiting the environmental stability and the utility of the system for many frequency conversion applications.

4.2 Gain switched seed laser

Picosecond pulses are typically generated by mode-lock techniques such as mode-locked fibre lasers [12, 13] and external cavity mode-locked semiconductor lasers [14, 15]. The disadvantages of cavity mode-locked lasers are the requirements of complex setup whilst the cavity length defines the pulse repetition rate. Gain switching of semiconductor diode laser to generate picosecond pulses has many attentions because of its simplicity and convenience in terms of continuously variable repetition rate, output power etc.

The experimental setup of the gain-switched seed source is shown in Figure 4.1. A 1060 nm FP laser diode in a fibre-pigtailed package was gain-switched using a pulsed drive current with an associated DC bias. Stable pulse-to-pulse operation was obtained by reflecting a fraction of each optical pulse back into the diode using a fibre-Bragg-grating (FBG). The fibre length between the diode and the FBG was chosen to be approximately 3.5 m. The reflected pulses were carefully synchronized with the following optical pulse by adjusting the repetition rate to fine-tune the pulse-to-pulse delay. The 3 dB bandwidth of the self-seeding grating was 0.15 nm with a reflectivity of 99%. A 10 dB tap was used in between the diode and the FBG so that only ~1% of the output power was coupled back into the diode. This method of self-seeding ensures single longitudinal mode operation with a side-mode-suppression-ratio of over 40 dB. This technique provides considerable advantages in terms of simplicity and reduced cost compared to using an external narrow-linewidth laser to stabilize the wavelength [16]. Measured amplitude jitter was ~2% and the timing jitter was ~3 ps (dominated by jitter from the drive electronics) [17].

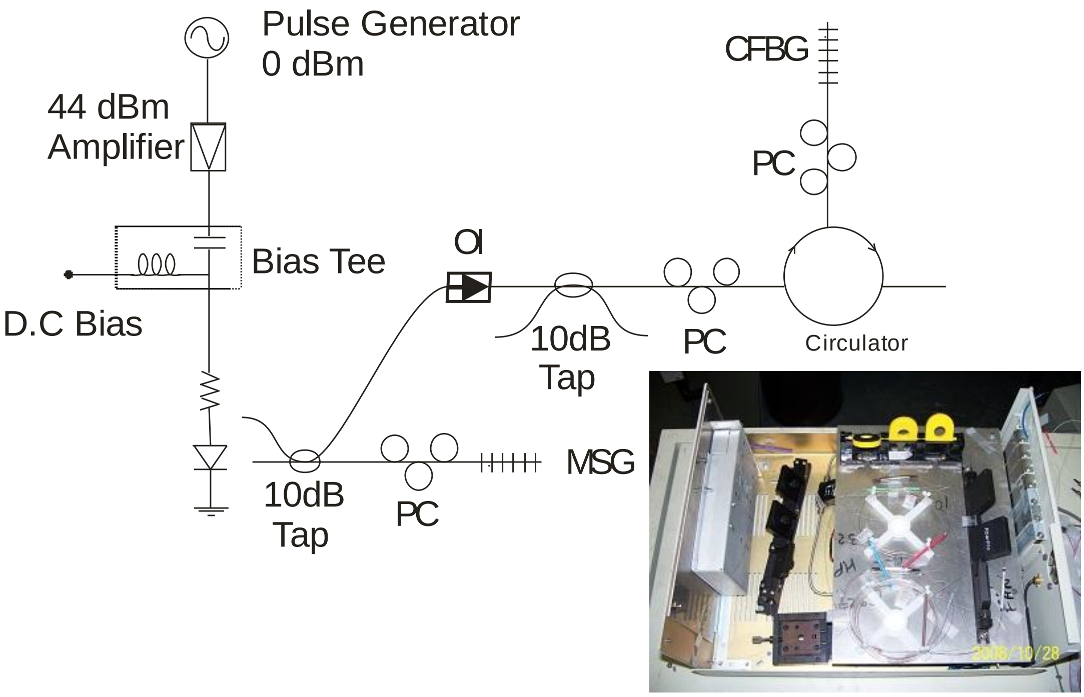

Figure 4.1: Schematic diagram of the gain switched diode with mode selection grating and compression grating (bottom right insert shows the setup photo)

Since pulses from GS diodes are inherently chirped [18], a chirped fibre Bragg grating (CFBG), fabricated in house, was used to compensate the chirp as reported in ref. [19]. The central wavelength of the self-seeding FBG was tuned to match that of the CFBG by compression of the grating [20, 21]. It is to be noted here that the CFBG can also be compression-tuned. This allows me to find a point where the mechanical compression of both the CFBG and FBG were minimized. I observed that once set at the lowest compression point, the tension of either of the gratings did not require adjustment for several weeks when in the laboratory environment.

Compressed pulses after the CFBG were characterised using a linear FROG technique [19]. The gate width of the EOM-based FROG was set to ~200 ps, an order of magnitude longer than the expected pulse length, so that complete pulse information can be retrieved. The pulses measured after the CFBG compressor had a duration of ~21 ps with an average output power of 1.3 mW at a repetition rate of 910 MHz. The temporal profile of the pulse and the associated residual chirp are shown in Figure 4.2(a). The pulse spectrum is shown in Figure 4.2(b), with 3 dB bandwidth of 0.15 nm corresponding to a time-bandwidth product ($\Delta\nu\Delta t$) of ~0.8.

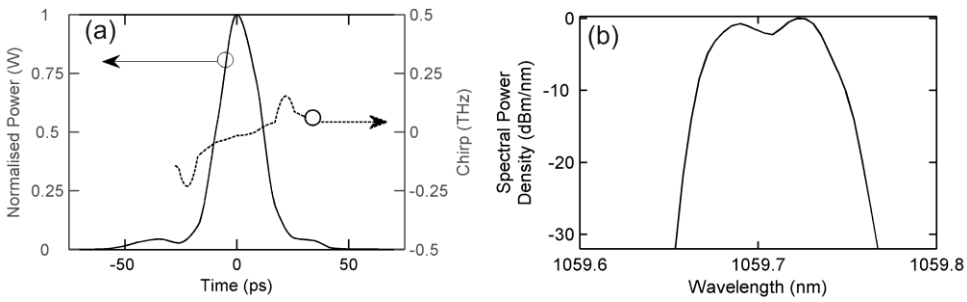

(a) (b)

Figure 4.2: (a) Seed pulse temporal profile and chirp; and (b) Spectrum of the seed pulse. The temporal and spectral data have been normalized with respect to the peak power or peak spectral density respectively.

4.3 Fibre amplifier

The experimental setup is shown in Figure 4.3. The gain-switched seed laser described in 4.2 was spliced to a fibre pigtailed EOM which was used as a pulse picker to reduce the repetition rate. This allows me to optimize the seed in terms of side-mode-suppression-ratio and chirp, while maintaining repetition rate flexibility. I also found this easier to operate in terms of maintaining optimum pulse quality compared with changing the diode modulation frequency directly as we had reported earlier [22].

The MOPA chain consisted of three-stage YDFA. Fiberized optical isolators were used to prevent ASE leakage between the amplifier stages. The first stage was a 3 m long core pumped YDFA based on single mode (5 µm core, NA=0.13;130 µm cladding), PM, Yb^{3+}-doped fibre and was bi-directionally pumped using 160 mW, 975 nm telecommunication-grade diodes. The second stage YDFA was a 7 m long cladding pumped single mode (5 µm core, NA=0.13; 130 µm inner cladding, NA=0.46) PM Yb^{3+}-doped fibre pumped by a 10 W, 975 nm multimode diode in backward pumping configuration through a (6+1)x1 fiberized PM pump-signal combiner. The 1060 nm wavelength was chosen in order to optimise the performance of the cladding-pumped power amplifier. However this required careful choice of the preamplifier fibre lengths in order to balance the conflicting requirements of nonlinearity management and short-wavelength ASE suppression. The pigtail fibre of the final isolator was kept as short as possible to minimize SPM induced linewidth broadening.

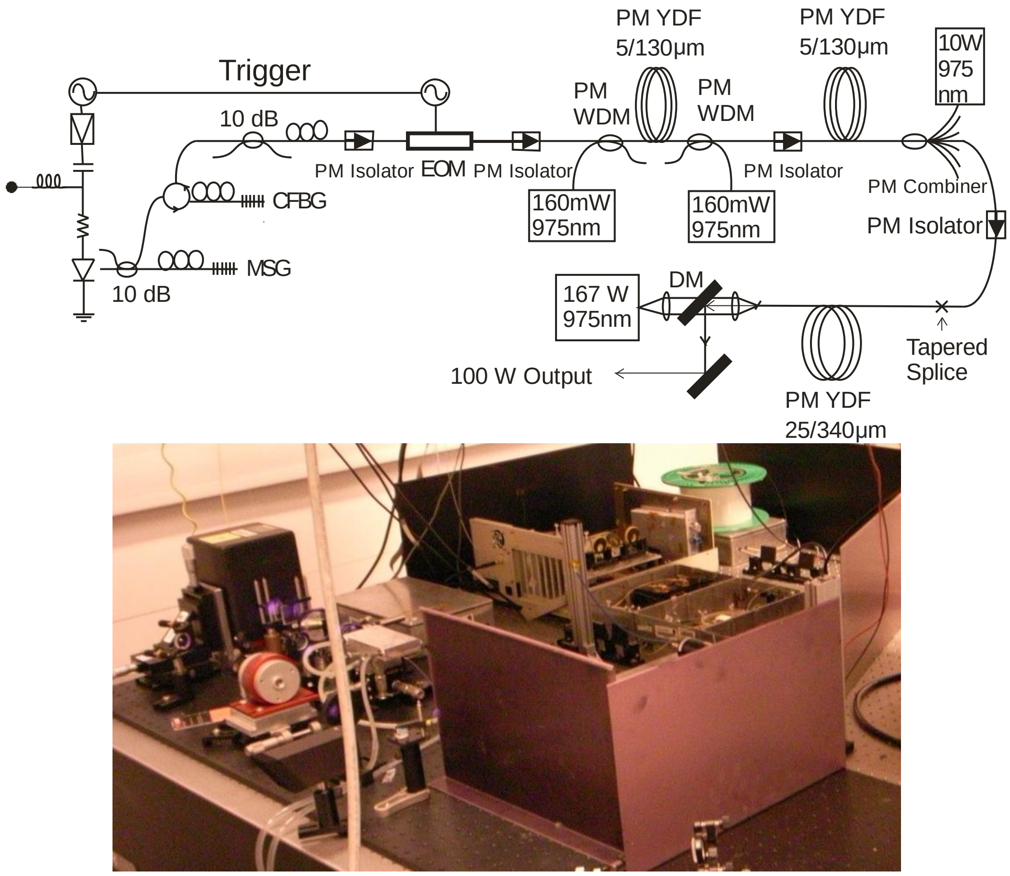

Figure 4.3:Top: Schematic diagram of the Yb^{3+}-doped fibre MOPA，MSG – mode selective grating; CFBG – chirped fibre-Bragg-grating. Bottom insert shows the photo of actual setup

The power amplifier was a 5.7 m long, PM fibre with an inner cladding diameter of 340 µm with an NA of 0.46 and a core diameter of 25 µm with an NA of 0.055 (Nufern). The V number of the core was 4.07 and had the ability to support approximately 7 transverse modes. The fibre was tapered down to 125 µm outer diameter such that the core diameter was reduced to 9.2 µm. Consequently the V number of the core became 1.5 which meant that the core can support only the fundamental mode. The tapered fibre was spliced to a 15 cm long passive PM 980 fibre (Corning). The uncoated tapered region and the splice point were protected with a high index UV cured coating and the entire section was mounted on an aluminium plate in order to dissipate heat due to unabsorbed pump light. The splice loss from the taper to the PM 980 fibre was measured to be less than 1 dB. A taper length of 80 mm was selected, which was found to be the minimum that led to single mode output from the LMA fibre. The M^2 was measured to be ~1.02 when the LMA fibre operated at the maximum 100 W output power. Compared to a free space launch where coupling variations lead to mode variations, this fiberized approach greatly improves the mode stability. To prevent damage to the output, a 2 mm long pure silica mode-expanding end-cap was spliced to the fibre and was angle polished to avoid backward-reflected power from coupling back into the fibre core. The amplifier was end-pumped using a commercially available 975 nm diode stack with a maximum pump power of 167 W. The diodes were water-cooled to ensure wavelength stability. A simple lens combination was used to achieve ~83% coupling efficiency into the fibre. The signal and pump paths were split by dichroic mirrors. Since the fibre had a absorption of ~2.7 dB/m at 975 nm, there was only a low level (~5 W maximum) of unabsorbed pump at the tapered splice section. This residual pump light was stripped by the high index UV cured coating and the heat generated in the process was removed using a heatsink.

The system was characterized at an average output power of 200 mW after the pre-amplifiers, and 100 W after the MOPA chain. Due to the pulse energy and peak-power requirements of our intended applications, we operated the system at repetition rates of 227 MHz and 56 MHz. As shown in Figure 4.4, a reasonable output OSNR was maintained as the repetition rate was reduced – the signal was 30 dB (227 MHz) or 25 dB (56 MHz) above the ASE level. Numerical integration indicated that the corresponding signal was 98 % or 96 % of the total measured power at 227 MHz and 56 MHz respectively. Therefore the maximum extracted pulse energy was 1.71 µJ at a repetition rate of 56 MHz with a corresponding peak power of 85 kW at an average output power of 100 W. Figure 4.4 shows the onset of SRS approximately 30 dB below the signal at a wavelength of ~1115 nm for the 56 MHz case. The SRS peak power threshold of the final amplifier, calculated assuming 27 dB gain and constant gain per unit length, was ~89 kW, which is similar to the experimentally measured power [23, 24].

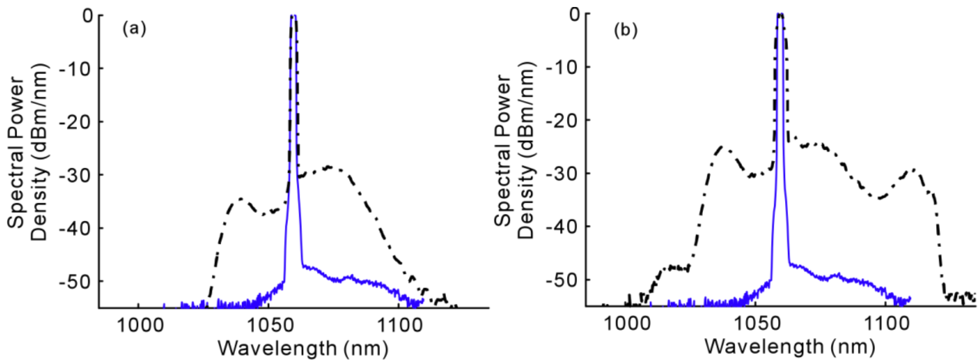

Figure 4.4: Spectra of seed-diode (blue solid line) and final 100 W output (black dash line). (a) Pulse repetition rate 227 MHz; and (b) Pulse repetition rate 56 MHz. The spectra were measured with an ANDO (AQ6317B) spectrum analyser using 2.0 nm resolution.

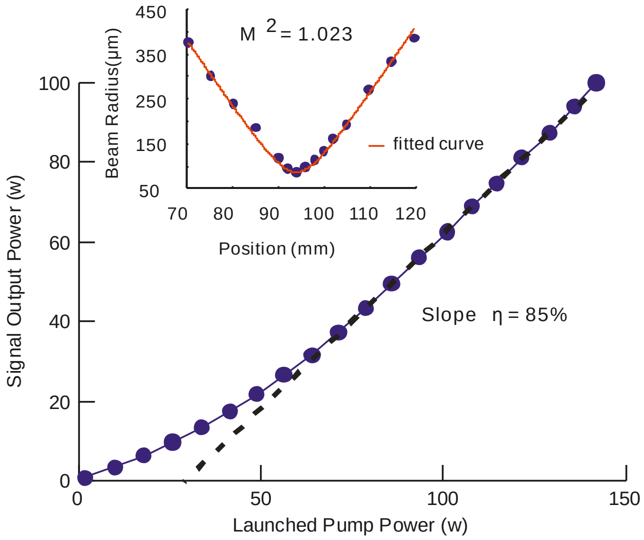

Figure 4.5: Output power from the final stage amplifier vs. launched pump power. Inset: Mode quality measurements data. (Beam diameter vs. distance from a f=100 mm focal length lens.)

Figure 4.5 shows the performance of the final amplifier. The slope efficiency was 85% with respect to launched pump power, and the amplifier shows no power roll-off at the 100 W level. The beam quality of the amplified signal output was measured to be $M^2 = 1.02$ at a power of 100 W as shown by the inset. The measured polarization extinction ratio (PER) was 19 dB under full power operation.

The spectra in Figure 4.6(a) are shown at the sub-harmonics of the diode repetition rate. There was minimal nonlinear evolution at a repetition rate of 908 MHz but as the repetition rate was reduced the pulse peak power increased and the spectra were broadened due to SPM. The degree of spectral broadening observed is relatively modest in absolute terms – just a few nm at the lowest repetition rates (highest peak powers) investigated, although this corresponds to relative broadening by factors of up to 20. The spectral broadening at a given repetition rate can obviously be eliminated by reducing the average output power (and corresponding peak power), however for many applications the spectral properties are not of great importance and it is the peak power and pulse duration that matter. In this regard the spectral broadening can in fact be beneficial as we shall see in section4.4 where it has been exploited to allow pulse compression and peak power enhancement, thus greatly extending the operational parameter space of the source. In the time domain the pulse shape was measured using a 32 GHz photodiode and sampling oscilloscope providing ~30 ps overall time resolution. The traces in Figure 4.6(b) show that the seed and final output pulses were both within the resolution limit and thus that there is minimal temporal broadening. (Note that the extended tail was an artifact of the diode/scope system since it was also seen in an impulse response measurement using clean 200 fs pulses.)

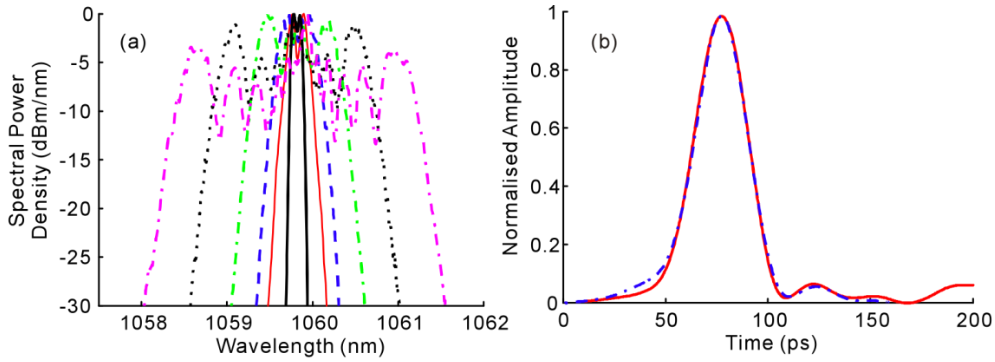

Figure 4.6:(a) Spectra of seed (black solid line) and final output at a power of 100 W at repetition rates of 908 MHz (red solid line), 454 MHz (blue dashed line), 227 MHz (green dash dotted line), 113 MHz (black dotted line) and 56 MHz (pink dash dotted line); and (b) photo diode trace of seed pulse (red solid line) and final output (blue dash dotted line) measured at an average power of 100 W and repetition rate of 56 MHz.

The maximum average power at the system output was limited by the available pump power. The saturation energy, E_{sat}, was calculated to be 50 μJ and hence it is not a constraint to pulse energy in our system [25] and since neither SRS nor SPM were constraints at the 100 W power level, significant further average power scaling should be possible by using a pump source having higher output power than currently available in our laboratory. Suitable pump sources capable of delivering output powers of ~800 W that can be focused into the 330 μm spot size required for the final amplifier fibre are commercially available [26]. Neither SRS nor SPM are critically limiting the performance of the system even at the lowest 56 MHz repetition rate so the main considerations would be maintaining a good OSNR and managing the thermal load. We consider that it is quite reasonable to expect output powers in the region of 500 W would be achievable at repetition rates of 227 MHz and above. To avoid OSNR degradation of the amplified signal the output power of the 2nd pre-amplifier could be increased from 0.2 W to 1.0 W (increasing the gain from ~9 dB to 16 dB) so as to maintain the same maximum gain required from the final stage amplifier.

The MOPA output was also used for material processing. Same material samples processed using nanosecond pulses were also tested under picosecond pulses for comparison. Again, the laser behaved very reliably and no failure or performance degradation was observed during the process trials. Figure 4.7 shows the live process and the processed sample photos. Comprehensive analysis of the cutting results is still being carried out by our project partners.

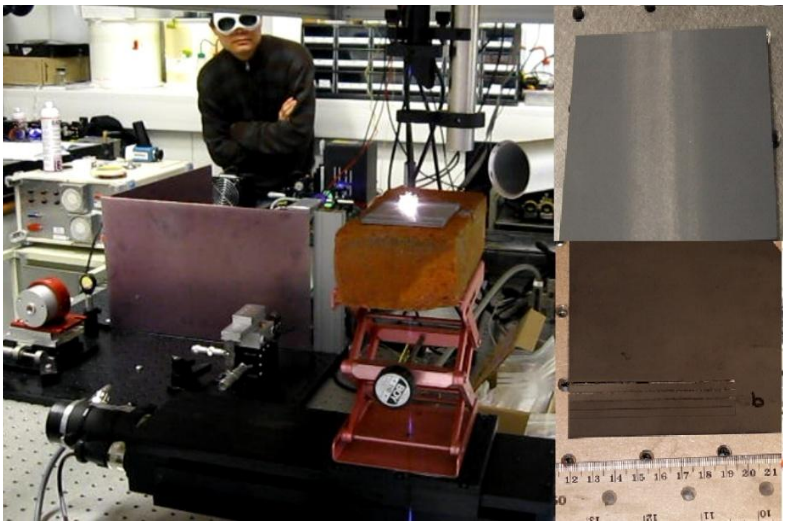

Figure 4.7: A sample was being cut by the 100 W,118 MHz repetition rate, picosecond pulses; Top right is sample before cutting; Bottom right is sample after cutting.

4.4 Pulse compression

In this part I will demonstrate pulse compression that enables the MOPA system to address applications that require increased peak power and improved time resolution. The use of SPM in a nonlinear element to obtain pulse compression is a well established technique [27, 28] and either an external length of fibre can be used for spectral generation, or the spectral broadening can occur in the amplifier chain (as in parabolic pulse generation [29]). In the system pulses emerge from the GS diode were with a negative chirp but after the CFBG they became close to transform limited. SPM in the amplifier chain then broadens the bandwidth without changing the pulse duration. Hence, at the output of the system the pulses are chirped due to the SPM. Adding a diffraction grating compressor at the output of the system eliminates that chirp [28]. To complement the experimental work, a member of my group performed numerical modelling using a standard split-step code to numerically solve the nonlinear Schrödinger equation (NLSE) with gain[28]. The amplifier fibre lengths, core diameters and gain in the simulations were set to match the experimentally measured values for each amplifier stage. A numerically optimized compressor was implemented to maximize the peak power by applying second and third order dispersion. The numerical model was used to calculate the B-integral and the quality of the recompressed simulation pulses was assessed by numerically integrating the power in the main peak (without pre- or post-pulses). The B-integral refers to the accumulated nonlinear phase at the pulse centre. The B-integral in a fibre amplifier can be written as $B = \frac{n_2 \omega_0}{c A_{eff}} P_0 L_{eff}$ [30]. The compressor transmission efficiency of 65% was assumed in order to match the experimentally observed efficiency for the dielectric grating compressor described below.

The highest levels of SPM and hence the maximum degree of pulse compression were obtained at the lowest repetition rate of 56 MHz. Modelling showed that with the compressor in place, an acceptable fraction of the energy remained in the main peak (excluding pre or post-pulses) at average powers of up to 70 W and this was confirmed experimentally by observing the increase in the pedestal level on the autocorrelation measurements.

For the experimental results a 1500 gr/mm gold coated grating was initially used, and passed only a fraction of the output power through the compressor to avoid thermal distortions arising from the heat load on the grating surface. Figure 4.8(a) shows the uncompressed-pulse autocorrelations and demonstrates that the pulses were very similar in duration at both 35 W and 70 W output powers. The red dotted line is the autocorrelation of the seed pulse before the amplifiers, which confirms that there is no significant temporal broadening due to the pulse evolution through the system. The clipping seen at the left edge of the trace is due to the limited span of the instrument. The compressed pulse autocorrelation data is shown in Figure 4.8(b). The grating separation at each power level was adjusted to minimize the autocorrelation width observed on an oscilloscope. The autocorrelation FWHM was 2.7 ps at the 35 W output power level and 1.8 ps at the 70 W output power level. The quality of the compressed pulses is high. The spectra shown in Figure 4.8(c) have the characteristic modulation associated with SPM and the 3 dB bandwidth (measured at the widest edges of the spectrum) was 1.1 nm at 35 W, and 2.3 nm at 70 W output power. When compared with the seed pulse bandwidth of 0.15 nm, the data clearly shows substantial nonlinear broadening.

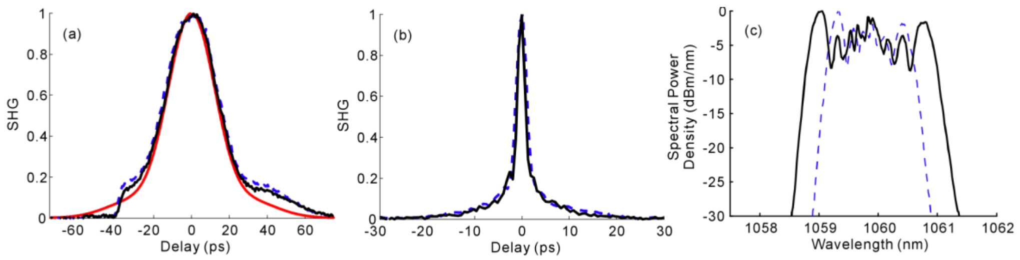

Figure 4.8: (a) Autocorrelations of uncompressed pulses; (b) Autocorrelations compressed pulses; and (c) Spectra of the final output pulses at 56 MHz. Data shown at a power of 35 W (blue dashed lines) and at 70 W (black solid line). The autocorrelation of the seed pulse before the amplifier chain is shown in red on (a). The spectra in (c) were measured with 0.01 nm resolution, and have been normalized with respect to the peak.

The modelled autocorrelation predictions (data not shown in the interests of brevity) were in good agreement with the experimental results with gold coated gratings. For the 70 W simulations at 56 MHz the estimated B-integral was ~27 radians, the estimated pulse duration was ~1.1 ps and the compressed peak power was ~431 kW. Numerical integration indicated that the main peak (without pre- or post-pulses) contained 57 % of the total energy. Recently, compressor efficiencies in excess of 90% have been demonstrated using suitably designed dielectric gratings which would enable an increase in output power of 38 % compared to the results here [5] giving a maximum possible peak power of ~595 kW.

4.5 SHG using compressed pulses

A consideration for industrial applications such as micromachining is that many materials have larger absorbance in the green compared to the near IR. Using green laser sources also enables a smaller spot size to be used than is achievable using near-IR wavelengths. Hence it is advantageous if the Yb-laser output at ~1.06 μm can be frequency doubled which requires that the output has good polarization purity and narrow linewidth (without excessive nonlinear spectral broadening).

In order for the output bandwidth to be suitable for SHG with a LBO crystal having an acceptance bandwidth of 0.7 nm a repetition-rate of 227 MHz was then selected and the maximum power was kept about 83 W while keeping the spectral broadening within the crystal acceptance bandwidth. Using a dielectric grating with 1740 lines per mm in the compressor we passed the full power from the system through the compressor and the measured throughput efficiency was 65% (~ 54 W output from the compressor). Figure 4.9 shows the results with the grating separation fixed at the optimum position for pulse compression at the 83 W power level. The compressed pulse autocorrelation widths decreased from 8.2 ps to 6.0 ps as the MOPA system power increased from 30 W to 83 W. The pulse peak power output from the compressor was ~40 kW. Figure 4.9(b) shows the spectra at full power at the input and output of the compressor which confirms the full bandwidth was transmitted by the compressor. The 3 dB bandwidth measured at the widest edges of the spectrum was 0.6 nm at 83 W output power. For the 83 W simulations at 227 MHz the estimated B-integral was ~6 radians, the pulse duration was ~4.2 ps and the peak power was ~46 kW. Numerical integration indicated that the main peak (without pre- or post-pulses) contained 77 % of the total energy. An increase in the maximum peak power to ~63 kW would be possible using state-of-the-art gratings in the compressor.

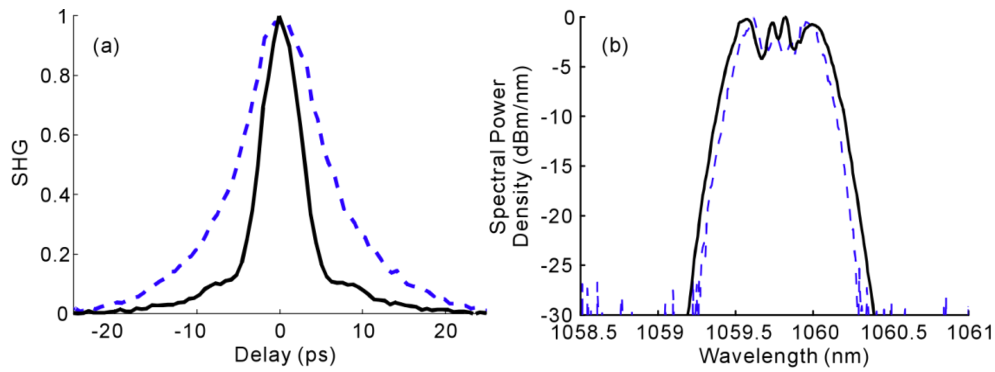

Figure 4.9:(a) Compressed pulse autocorrelations at 227 MHz with final amplifier powers of 30 W (blue dash line) and 83 W (black solid line); (b) Spectra of 83W average power level at the compressor input (black solid line) and compressor output (blue dash line).

The experimental setup for SHG using the compressed pulses is shown in Figure 4.9(a). The 15 mm long LBO crystal was cut for noncritical phase matching at an operating wavelength of 1060 nm. The LBO crystal was chosen because of its high damage threshold relative to other potential crystal choices such as periodically poled lithium niobate (PPLN) or Potassium Titanyl Phosphate (KTP). The beam size at the waist position was 43 µm ($1/e^2$intensity diameter) with corresponding Rayleigh range of 1.4 mm. (The beam waist was measured in air prior to inserting the crystal and the Rayleigh range also corresponds the value in air.) A half-wave plate placed immediately before the focusing lens was used to rotate the polarization of the fundamental light to maximize the second harmonic signal. Figure 4.9(b) shows the average output power of the compressed pulses and of the second harmonic signal as a function of the power from the MOPA. The LBO crystal was kept at a constant temperature of 152 ^{0}C for maximum conversion efficiency. A maximum of 52 W of power was produced from the compressor which produced 26 W of power at 530 nm corresponding to an optical conversion efficiency of 50%. The insets to Figure 4.9(b) show that the spectrum of the 530 nm pulses had a FWHM of 0.2 nm and that the M-squared measurement of the SHG beam gave a value of 1.08, which was very close to that of the MOPA pump beam.

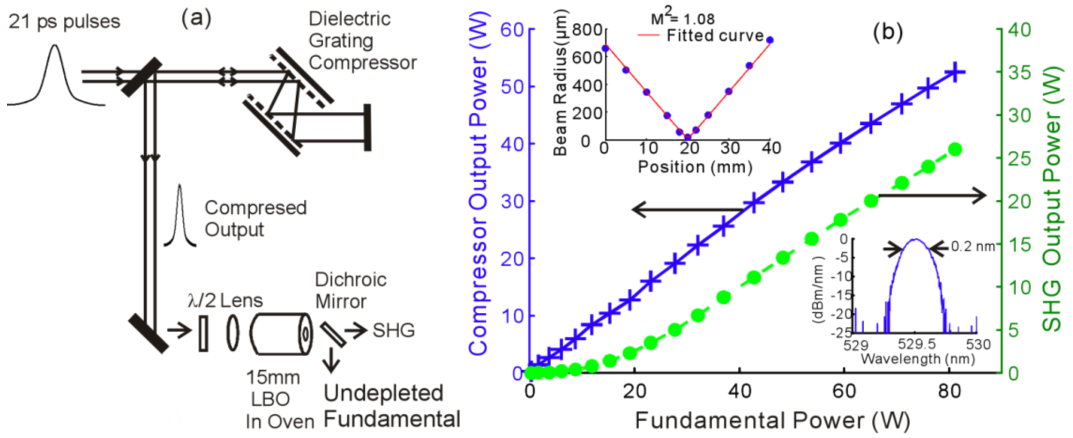

Figure 4.10: (a) Schematic setup of SHG using compressed pulses at 227 MHz; (b) Compressor output power and SHG Output Power vs. Fundamental power from fibre MOPA; Top left insert shows beam quality of SHG; Bottom right insert shows the spectrum of SHG at 26 W.

4.6 Conclusion

In this chapter, a fiberized, diode-seeded, YDFA MOPA system generating linearly polarized, diffraction-limited, 21 ps pulses at repetition rates ranging from 56 MHz to 908 MHz and at an average output power of 100 W was demonstrated. The polarization stability is ensured by using PM amplifier fibres and the stability of the mode quality is ensured by using a tapered splice to the final amplifier. Compared to our previous work [31], the incorporation of a robustly single mode, PM amplifiers directly spliced together has considerably improved the modal and polarization stability. At the lowest repetition rate of 56 MHz the 21 ps pulses from our system have a maximum energy of 1.7 µJ, and peak power of 85 kW. This system represents a considerable improvement in practicality and performance relative to previous high power, fibre-based picosecond pulse sources [32]. This high power picosecond source was used in the industrial material processing experiments, during which it showed high reliability and good performance. In short, the system demonstrated an attractive combination of controllable repetition-rate gain-switched diode seed and high-power single-mode PM-fibre amplifiers for a wide variety of applications.

The system has proven to be very reliable in the laboratory and it was recently used to pump an OPO [33] and for frequency doubling of the output with a Lithium Triborate (LBO) crystal which provided >56% SHG efficiency to create a 56 W visible source of 20 ps pulses [34]. Generation of 39 W supercontinuum was also demonstrated using the picosecond source as pump [35]. These wavelength conversion experiments will be discussed in Chapter 6.

In addition, compression of the pulses to as short as 1.1 ps was demonstrated by exploiting the SPM induced spectral broadening (observed at the highest pulse energies) and adding a grating-based compressor at the output. A maximum compression factor of 17 was achieved using gold coated grating and a corresponding enhancement in peak power to ~590 kW would be possible with the use of optimized compressor gratings. The compressed 4.2 ps pulses at a repetition rate of 227 MHz and average (compressed with dielectric grating) output power of 52 W was used to frequency double to 26 W of visible laser power corresponding to 50% SHG efficiency.

References

[1] V. Gapontsev, "IPG Photonics 6 kW CW singlemode ytterbium fiber laser in all-fiber format," in Solid State Diode Laser Technol. Rev., Albuquerque, NM, 2008.

[2] J. Limpert, F. Roser, D. N. Schimpf, E. Seise, T. Eidam, S. Hadrich, J. Rothhardt, C. J. Misas, and A. Tunnermann, "High Repetition Rate Gigawatt Peak Power Fiber Laser-Systems: Challenges, Design, and Experiment," IEEE Journal of Selected Topics in Quantum Electronics, vol. 15, pp. 159-169, 2009.

[3] M. E. Fermann and I. Hartl, "Ultrafast Fiber Laser Technology," IEEE Journal of Selected Topics in Quantum Electronics, vol. 15, pp. 191-206, Jan-Feb 2009.

[4] N. G. R. Broderick, D. J. Richardson, D. Taverner, J. E. Caplen, L. Dong, and M. Ibsen, "High-power chirped-pulse all-fiber amplification system based on large-mode-area fiber gratings," Optics Letters, vol. 24, pp. 566-568, Apr 15 1999.

[5] T. Eidam, S. Hanf, E. Seise, T. V. Andersen, T. Gabler, C. Wirth, T. Schreiber, J. Limpert, and A. Tünnermann, "Femtosecond fiber CPA system emitting 830 W average output power," Opt. Lett., vol. 35, pp. 94-96, 2010.

[6] S.-P. Chen, H.-W. Chen, J. Hou, and Z.-J. Liu, "100 W all fiber picosecond MOPA laser," Optics Express, vol. 17, pp. 24008-24012, 2009.

[7] L. Orsila, R. Herda, and O. G. Okhotnikov, "High repetition rate mode-locked ytterbium fiber laser using dichroic fiber mirrors and photonic bandgap fiber technology," in Fiber Lasers V: Technology, Systems, and Applications, 2008, pp. U318-U325.

[8] P. Dupriez, C. Finot, A. Malinowski, J. K. Sahu, J. Nilsson, D. J. Richardson, K. G. Wilcox, H. D. Foreman, and A. C. Tropper, "High-power, high repetition rate picosecond and femtosecond sources based on Yb-doped fiber amplification of VECSELs," Optics Express, vol. 14, pp. 9611-9616, 2006.

[9] P. Dupriez, A. Piper, A. Malinowski, J. K. Sahu, M. Ibsen, Y. Jeong, L. M. B. Hickey, M. N. Zervas, J. Nilsson, and D. J. Richardson, "321 W average power, 1 GHz, 20 ps, 1060 nm pulsed fiber MOPA source," Optical Fiber Communications Conference, Post deadline Paper PDP3, 2005.

[10] P. Dupriez, A. Piper, A. Malinowski, J. K. Sahu, M. Ibsen, B. C. Thomsen, Y. Jeong, L. M. B. Hickey, M. N. Zervas, J. Nilsson, and D. J. Richardson, "High average power, high repetition rate, picosecond pulsed fiber master oscillator power amplifier source seeded by a gain-switched laser diode at 1060 nm," IEEE Photonics Technology Letters, vol. 18, pp. 1013-1015, 2006.

[11] P. Dupriez, A. Malinowski, J. K. Sahu, Y. Jeong, D. J. Richardson, and J. Nilsson, "80 W green laser based on frequency-doubled picosecond, single-mode, linearly-polarised fiber laser " in Conference on Lasers and Electro Optics (CLEO), paper CThJ1, Long Beach, CA, 2006.

[12] M. E. Fermann, M. Hofer, F. Haberl, A. J. Schmidt, and L. Turi, "Additive-pulse compression mode locking of a neodymium fiber laser," Optics Letters, vol. 16, pp. 244-6, 1991.

[13] F. O. Ilday, J. Buckley, L. Kuznetsova, and F. W. Wise, "Generation of 36-femtosecond pulses from a ytterbium fiber laser," Optics Express, vol. 11, 2003.

[14] D. J. Derickson, R. J. Helkey, A. Mar, J. R. Karin, J. G. Wasserbauer, and J. E. Bowers, "Short pulse generation using multisegment mode-locked semiconductor lasers," IEEE Journal of Quantum Electronics, vol. 28, pp. 2186-202, 1992.

[15] K. Yvind, P. M. W. Skovgaard, J. Mork, J. Hanberg, and M. Kroh, "Performance of external cavity mode-locked semiconductor lasers employing reverse biased saturable absorbers," Physica Scripta Volume T, vol. T101, pp. 129-32, 2002.

[16] K. T. Vu, A. Malinowski, M. A. F. Roelens, and D. J. Richardson, "Detailed comparison of injection-seeded and self-seeded performance of a 1060-nm gain-switched Fabry-Perot laser diode," IEEE J. Quantum Electron, vol. 44, pp. 645-651 2008.

[17] K. T. Vu, A. Malinowski, M. A. F. Roelens, M. Ibsen, and D. J. Richardson, "Detailed comparison of injection-seeded and self-seeded performance of a gain-switched laser diode," presented at the Conference on Lasers and Electro-Optics (CLEO), 2007.

[18] R. A. Linke, "Modulation Induced Transient Chirping In Single Frequency Lasers," IEEE Journal of Quantum Electronics, vol. 21, pp. 593-597, 1985.

[19] K. T. Vu, A. Malinowski, M. A. F. Roelens, M. Ibsen, P. Petropoulos, and D. J. Richardson, "Full characterization of low-power picosecond pulses from a gain-switched diode laser using electrooptic modulation-based linear FROG," IEEE Photonics Technology Letters, vol. 20, pp. 505-507, 2008.

[20] A. Iocco, H. G. Limberger, R. P. Salathe, L. A. Everall, K. E. Chisholm, J. A. R. Williams, and I. Bennion, "Bragg grating fast tunable filter for wavelength division multiplexing," Journal of Lightwave Technology, vol. 17, pp. 1217-1221, 1999.

[21] G. A. Ball and W. W. Morey, "Compression-tuned single-frequency Bragg grating fiber laser," Opt. Lett., vol. 19, pp. 1979-1981, 1994.

[22] K. K. Chen, S.-U. Alam, D. Lin, A. Malinowski, and D. J. Richardson, "100W fiberised linearly-polarized picosecond Ytterbium doped fiber MOPA " in Conference on Lasers and Electro Optics (CLEO), paper CWK2, Baltimore, USA, 2009.

[23] A. Galvanauskas, "Mode-scalable fiber-based chirped pulse amplification systems," IEEE Journal of Selected Topics in Quantum Electronics, vol. 7, pp. 504-517, Jul-Aug 2001.

[24] R. G. Smith, "Optical power handling capacity of low loss optical fibers as determined by stimulated Raman and Brillouin scattering," Applied Optics, vol. 11, pp. 2489 - 2494, 1972.

[25] C. C. Renaud, H. L. Offerhaus, J. A. Alvarez-Chavez, J. Nilsson, W. A. Clarkson, P. W. Turner, D. J. Richardson, and A. B. Grudinin, "Characteristics of Q-switched cladding-pumped ytterbium-doped fiber lasers with different high-energy fiber designs," IEEE Journal of Quantum Electronics, vol. 37, pp. 199-206, Feb 2001.

[26] www.laserline.de e.g. the LDF series.

[27] T. Sudmeyer, F. Brunner, E. Innerhofer, R. Paschotta, K. Furusawa, J. C. Baggett, T. M. Monro, D. J. Richardson, and U. Keller, "Nonlinear femtosecond pulse compression at high average power levels by use of a large-mode-area holey fiber," Optics Letters, vol. 28, pp. 1951-1953, Oct 2003.

[28] G. P. Agrawal, Nonlinear Fiber Optics, 2nd ed. San Diego: Academic Press, 1995.

[29] M. E. Fermann, V. I. Kruglov, B. C. Thomsen, J. M. Dudley, and J. D. Harvey, "Self-similar propagation and amplification of parabolic pulses in optical fibers," Physical Review Letters, vol. 84, pp. 6010-6013, Jun 26 2000.

[30] G. P. Agrawal, Nonlinear Fiber Optics, Third ed. USA: Academic Press, 2001.

[31] P. Dupriez, A. Piper, A. Malinowski, J. K. Sahu, M. Ibsen, Y. Jeong, L. M. B. Hickey, M. N. Zervas, J. Nilsson, and D. J. Richardson, "321 W average power, 1 GHz, 20 ps, 1060 nm pulsed fiber MOPA source," Anaheim, CA, USA, 2005, p. 3 pp. Vol. 5.

[32] J. Limpert, A. Liem, T. Gabler, H. Zellmer, A. Tunnermann, S. Unger, S. Jetschke, and H. R. Muller, "High-average-power picosecond Yb-doped fiber amplifier," Optics Letters, vol. 26, pp. 1849-1851, 2001.

[33] F. Kienle, K. K. Chen, S.-u. Alam, C. B. E. Gawith, J. I. Mackenzie, D. C. Hanna, D. J. Richardson, and D. P. Shepherd, "High-power, variable repetition rate, picosecond optical parametric oscillator pumped by an amplified gain-switched diode," Optics Express, vol. 18, pp. 7602-7610, 2010.

[34] K. K. Chen, S.-u. Alam, J. R. Hayes, H. Baker, D. Hall, R. Bride, J. H. V. Price, D. Lin, A. Malinowski, and D. J. Richardson, "56W Frequency Doubled Source at 530 nm Pumped by a Single-Mode, Single-Polarization, Picosecond, Yb^{3+}-Doped Fiber MOPA," Photonics Technology Letters, IEEE, vol. 99, published online April 2010.

[35] K. K. Chen, S.-u. Alam, J. H. V. Price, J. R. Hayes, D. Lin, A. Malinowski, C. Codemard, D. Ghosh, M. Pal, S. K. Bhadra, and D. J. Richardson, "Picosecond fiber MOPA pumped supercontinuum source with 39 W output power," Opt. Express, vol. 18, pp. 5426-5432, 2010.

Chapter 5 Frequency conversions based on nanosecond source

Overview

This Chapter demonstrates the potential for frequency conversion of the nanosecond source described in Chapter 3. This Chapter is organized as follows: an introduction to frequency conversions based on nanosecond pulse lasers is given in section 5.1; section 5.2 details the experimental results for an Optical Parametric Oscillator; 5.3 detailed experimental results of Second Harmonic Generation; 5.4 presented the experimental results of order selectable Raman Conversion; Finally a brief conclusion is given in section 5.5.

5.1 Introduction

The high brightness of single-mode pulsed fibre sources lends itself to a number of industrial and research applications in the remote sensing field, micromachining, especially when combined with extended wavelength coverage via nonlinear wavelength conversion. LIDAR for vegetation monitoring requires pulsed output in the visible and near-IR regions of the spectrum; the obstacle avoidance and clear air turbulence detection applications can be supported by a pulsed source operating in the mid-IR. Countermeasures applications also require outputs in these wavebands. A laser with a wavelength of ~1 μm can potentially act as a common pump source using frequency upconversion to access visible, UV and frequency downconversion to shift the output to the mid-IR. The gap in between can be covered using Raman frequency shift of the 1 μm or the visible light.

Periodically poled-magnesium oxide doped lithium niobate (PPMgLN) based OPOs represent a particularly attractive approach due to high optical nonlinearity, excellent power handling characteristics and wide transparency range of PPMgLN crystals. Such sources have been widely investigated over the last decade and have been shown to be capable of both high-power and highly-efficient operation when pumped with a variety of bulk solid state pump sources [1-3]. Given the rapid recent developments in high power fibre laser technology [4, 5] considerable interest in fibre laser pumped, PPMgLN-based OPOs has developed over recent years. The excellent heat dissipation characteristics of the fibre environment is particularly advantageous for OPO pumping since excellent beam quality, an indispensable requirement to achieve high parametric conversion efficiency, can readily be maintained without recourse to complex thermal management schemes in single-mode (SM) fibres, or effectively single mode (ESM) fibres operating at high average output powers. Fibre laser pumped PPMgLN based OPOs thus promise a route to a new generation of compact, tunable, high power parametric devices [6, 7].

There have been numerous reports on high power fibre laser pumped PPMgLN based OPOs over the years [6-8]. High average power parametric output in excess of 10 W at 2.94 μm was reported from a PPMgLN-based OPO pumped by a 50 W continuous wave (CW) Yb^{3+}-doped fibre laser [7]. However, in the case of pulsed operation, where the peak power is typically much higher than in the CW mode, the maximum average output power for parametric conversion in the 3-4 micron range so far reported has been limited to around the one watt level [8]. A primary reason for this limitation is the difficulty to manage the deleterious nonlinear effects in fibre at the peak power/pulse energy levels (~10 kW/1 mJ regime) that typically entails within the pump laser. Nonlinear Raman and Brillouin scattering can be particularly problematic and can either compromise the overall OPO efficiency, or under certain circumstances, lead to instabilities that have the potential to cause catastrophic damage to the fibre. These problems can be further exacerbated by pulse shaping effects due to dynamic gain depletion on the timescale of the pulse which results in pulse narrowing within the fibre laser, and thus higher peak powers for a given output pulse energy than optimal. For most parametric processes a pulse with a uniform intensity (i.e. a rectangular pulse shape) is desirable since, ignoring transient effects, high uniform conversion efficiency can then be achieved across the full pulse form and better overall efficiency achieved. Using adaptive pulse shaping of the seed laser (using an external modulator) we demonstrate a reduction in the impact of dynamic gain saturation and optical Kerr/Raman nonlinearities within the fibre MOPA, obtaining shaped signal and idler pulses at the OPO output and reduced spectral bandwidths. The maximum average output power from the MOPA at 1062 nm was limited to~26.5 W due to the pump diode. An output power as high as 11W from the OPO at an overall slope efficiency of 67% was achieved, with 2.7 W of output power obtained at a wavelength of 3.5 μm. Experimental results presented in section 5.2 were pump-power limited and considerable scope remains for further power-scaling of such OPOs using this approach. Some applications need visible and mid-IR output at the same time. Pumping by the nanosecond fibre MOPA, a set-up incorporating a mid-IR optical parametric oscillator (OPO) leg based on periodically poled lithium niobate (PPLN) and a frequency doubling leg incorporating a lithium triborate (LBO) crystal was built to generate visible and mid-IR output simultaneously via nonlinear wavelength conversion. Details of the OPO and the frequency doubler performances will be described in section 5.3.

Raman scattering in optical fibre [9] provides a convenient and practical mechanism for wavelength conversion, allowing the creation of high power fibre sources at wavelengths which cannot be generated directly by rare-earth doped fibre lasers. Whilst this has been applied with considerable success for CW sources [10, 11], allowing the development of fibre Raman lasers, progress in the pulsed regime has received far less attention [12]. This is largely due to the fact that Raman scattering is dependent on the instantaneous power of the pump beam. In general, a pulse propagating in an optical fibre will generate several Stokes wavelengths since parts of the pulse with different instantaneous power undergo different amounts of Raman scattering compromising the quality and efficiency of the frequency conversion process. In principle, this problem can be overcome by working with shaped flat-topped rectangular pulses, since in this case all points across the pulse experience identical Raman gain. As a result it is possible for a pulse to cycle all of its energy through sequential frequency shifts to successive order Stokes components. For specific powers, all of the pulse energy can in theory be shifted to a given Raman order, allowing for very efficient wavelength conversion. I have demonstrated selective excitation of individual Stokes wavelengths with high conversion efficiency by using actively shaped flat-topped pulses directly generated using a fibre MOPA system [13].

I have also managed to excite individual Raman Stokes lines of up-to 9th order with relatively high extinction ratio pumped by frequency doubled rectangular shaped optical pulses at 530 nm of 100 ns duration. Detailed experimental results will be provided in section 5.4.

Use of active pulse shaping is important as it allows application of the techniques for fibre laser systems operating at pulse energies well in excess of the saturation energy, thereby permitting mJ level operation [14]. In addition, active pulse shaping technique enable more efficient nonlinear conversion which has a limited acceptance bandwidth such as SHG because the output peak powers are not as high as for unshaped optical pulses resulting in less SPM induced spectral broadening.

5.2PPMgLN based high power nanosecond optical parametric oscillator

5.2.1 MOPA performances

In this section, I will present the experimental results on fibre MOPA pumped PPMgLN based OPO. The experimental configuration is similar to the MOPA described in section 3.4 of chapter 3 except the final stage amplifier. Due to the unavailability of a 975 nm pump source at the time of the experiment, the length of the final stage gain medium, which is similar to that used in the final stage amplifier in section 3.4, was chosen to be ~8 m suitable for 915 nm pumping wavelength.

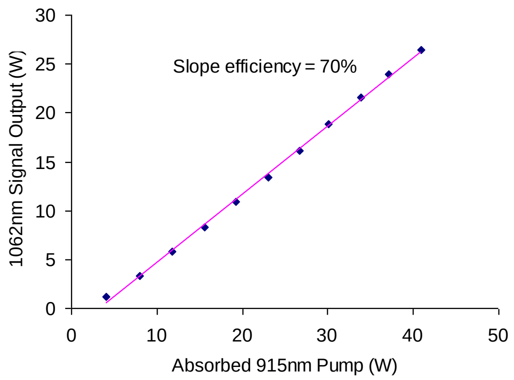

Figure 5.1: Amplified output powers of the 1062 nm signal as a function of 915 nm absorbed pump powers.

A maximum output power of 26.5 W was obtained at an absorbed pump power of 41 W corresponding to a slope efficiency of 70% as shown in Figure 5.1. The output pulse shapes for different output powers are plotted in Figure 5.2. The inset shows the square input pulse launched into the fibre amplifier chain. In all instances significant pulse narrowing was observed due to gain depletion on the timescale of the pulse, as shown in Figure 5.2 for pulse parameters relevant to our actual OPO experiments.

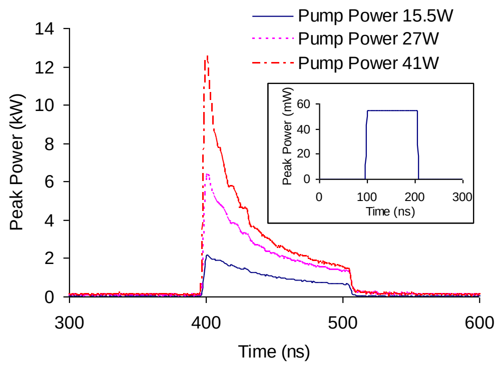

Figure 5.2: Output pulse profiles of unshaped (square) input pulses for different amplified output powers.

A rectangular pulse form is desirable at the system output in order to reduce the peak powers for a given pulse energy and to ensure more uniform frequency conversion. The adaptive shaping technique as described in Chapter 3 was used to realize rectangular shaped pulses. The input pulses with an appropriately (exponentially) increasing rising edge as shown in Figure 5.3(a) were used to obtain rectangular shaped output pulses (Figure 5.3(b)) for different output powers.

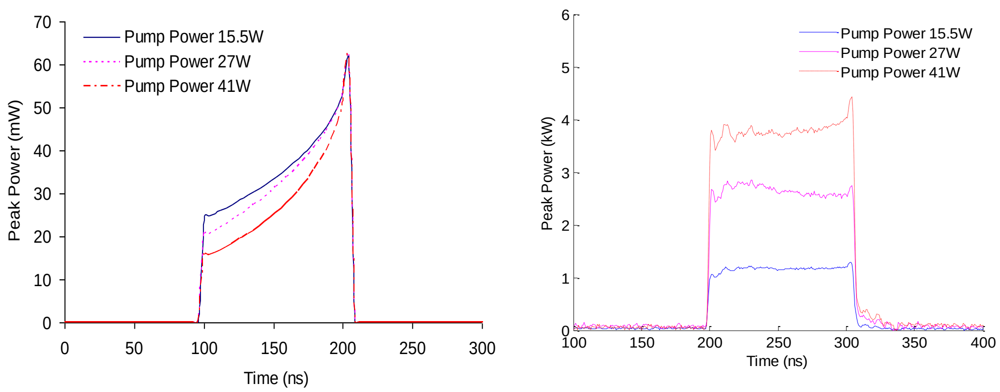

(a) (b)

Figure 5.3: (a) Temporal profiles of the input pulses to obtain square pulses at the output of the MOPA and (b) corresponding output pulse profiles.

The measured polarization extinction ratio (PER) was 19 dB. The spatial beam characteristic of the amplified signal output was also measured using a beam-profiler. The beam quality (M^2) of the MOPA output was estimated to be ~1.1.

The spectra of the MOPA output were measured using an optical spectrum analyzer (Agilent HP 86142) and are displayed in Figure 5.4(a).The resolution of the spectrum analyzer was set at 0.1 nm. It was found that at the highest pulse energies used in the OPO experiments the spectrum of the laser output broadened slightly from 0.2 nm to 0.5 nm for shaped input pulses due to the nonlinear Kerr effect within the amplifier chain. However, the spectral broadening was significantly larger (~1.0 nm) for unshaped (square) input pulses (Figure 5.4(b)) due to the gain saturation effect leading to higher peak power pulses. This highlights the advantages of using shaped input pulses to preserve the spectral integrity at high pulse energies. No evidence of stimulated Raman (or Brillouin) scattering was observed in either case. However the rapid rise in pulse peak power and the associated spectral broadening due to self phase modulation (SPM) experienced by the unshaped pulses inside the fibre amplifiers chain limits the performance of such sources in terms of obtaining clean and efficient parametric conversion of the fundamental signal, as illustrated in the next section.

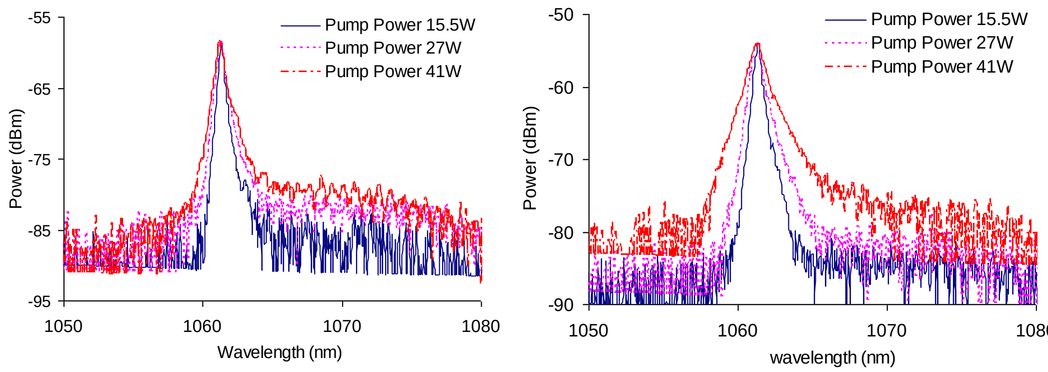

Figure 5.4: Spectra of the amplified 1062 nm signal light for various output powers, (a) shaped and (b) unshaped input optical pulses to the fibre MOPA chain.

5.2.2 Pulsed fibre MOPA pumped OPO

The fibre MOPA described in the previous section was used to pump a PPMgLN based OPO. A double pump pass singly resonant OPO configuration was used to ensure high conversion efficiency. A schematic of the experimental set-up is illustrated in Figure 5.5. The polarization of the amplified signal from the final-stage amplifier was first cleaned up with the help of a polarization beam splitter (PBS). A half wave plate (HWP) prior to the PBS allowed us to rotate the nearly signal polarization output beam of the MOPA to obtain maximum transmission through the PBS. A bulk isolator was used to safeguard the fibre amplifier chain from any unwanted feedback. Introduction of the PBS and the isolator resulted in a 20% loss in output power from the final-stage amplifier. The output from the isolator was directed through a converging lens with a focal length of 300 mm to pump the OPO. The corresponding waist diameter was measured to be 210 μm. The

OPO was configured as a simple linear plane:plane mirror cavity. The input mirror was anti-reflection coated across the 1060 nm band and had a high reflectivity spanning from 1400 nm to 1600 nm as well as from 3.5 µm to 4.0 µm. By contrast the output coupler had a high reflectivity coating across the 1060nm band and exhibited high transmission between 3.5 µm to 4.0 µm. The reflectivity of the output coupler at 1520 nm was 70%. The PPMgLN crystal used in the experiment was fabricated by a collaborative group in China and comprised of a wafer (50 x 10 x 1 mm) patterned with multiple channels with uniform homogeneous domain reverse periods ranging between 27.8 µm to 31 µm for different channels [15]. Both ends of the PPMgLN crystal were finely polished and anti-reflection coated for wavelengths of 1060 nm, 1400 nm to 1600 nm and 3500 nm to 4000 nm. The overall OPO cavity length was about 65 mm.

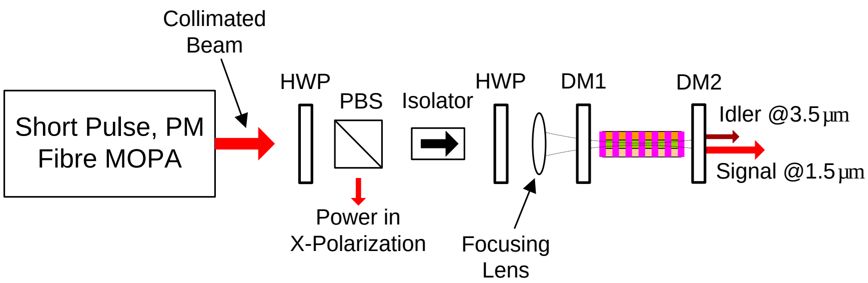

Figure 5.5: A schematic diagram of the fibre laser pumped, PPMgLN based OPO system. HWP: Half Wave Plate, PBS: Polarization Beam Splitter, DM: Dichroic Mirror.

OPO operation was investigated on one specific PPMgLN channel with a domain reversed grating period of 30.0 µm which gave OPO operation at signal wavelength of 1518 nm and corresponding idler wavelength of 3535 nm. The detailed output power dependence of the parametric oscillator on pump power from the fibre laser is illustrated in Figure 5.6(a) and 5.6(b) which show the OPO output as a function of pump power for shaped and unshaped input optical pulses respectively. A total parametric output power as high as 11 W was obtained (with 2.7 W of power at 3.5 µm) for 21 W of incident pump power at 1062 nm. This corresponds to an overall conversion efficiency of 52%. The slope efficiency of the OPO was estimated to be 67%. Note that no evidence of output power saturation with increasing pump power was observed within these experiments – the output power achieved being limited by the available pump power.

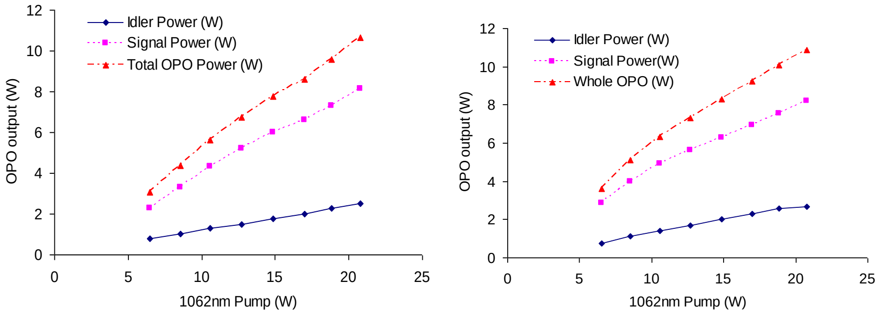

(a) (b)

Figure 5.6: Output power dependence of the OPO on 1062 nm pump power coupled into the 30.0 μm period grating of the MgO:PPLN crystal for (a) shaped and (b) unshaped optical pulses.

Further investigations were carried out to understand the OPO build-up time, energy transfer efficiency etc. as a function of pump pulse peak power and shape. Figure 5.8 shows the pulse characteristics both at 1062 nm and 1518 nm measured both before and after the OPO cavity at different pump pulse peak powers. By comparing the pulse profiles of the combined 1062 nm pump & 1518 nm signal and that of the 1518 nm signal after the OPO cavity it is possible to study the dynamic aspects of the OPO performance e.g. the OPO build-up time and extent of the depletion across the pump pulse.

In Figure 5.7 the shape of various pump and signal pulses of the OPO for both shaped and unshaped pulses for two different power levels are plotted. The onset of parametric oscillation is readily observable with a very strong correlation in timing in terms of increase in output power and the onset of pump depletion. The OPO build-up time (i.e. time between the leading edge of the pulse and the onset of lasing) was found to decrease with increasing pump pulse peak power, resulting in improved energy transfer from the pump pulse to the signal and idler pulses (i.e. since the cavity is above threshold for a greater proportion of the pump pulse duration).

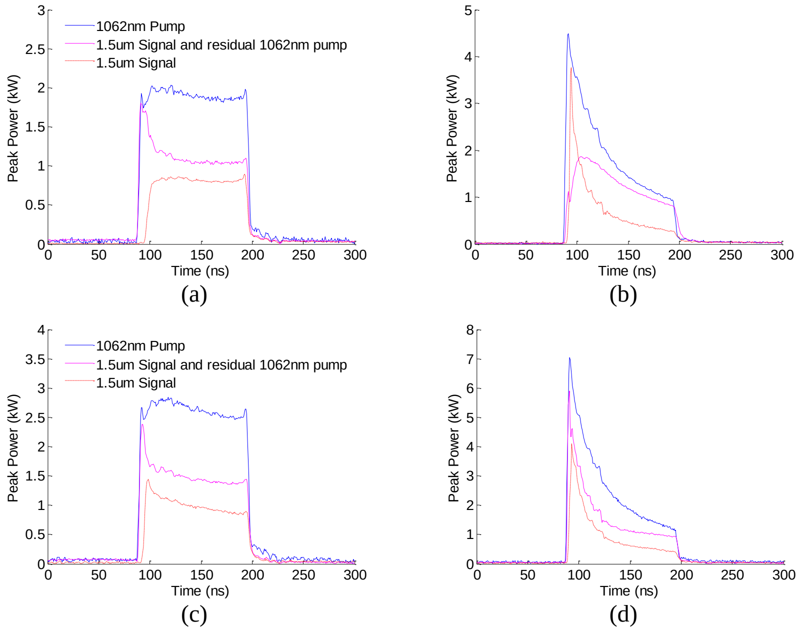

Figure 5.7: Temporal evolution of 1062 nm pump and parametrically converted signal pulses for (a) shaped, (b) unshaped and (c) shaped, (d) unshaped pulses at 23 W and 30 W of 915 nm pump power respectively.

The OPO build-up time as a function of pump pulse peak power is shown in Figure 5.8. The measured experimental points agree well with an exponential fit. The trend is similar to that observed by Alam et.al. [16] With regards to frequency shifted feedback picosecond fibre laser.

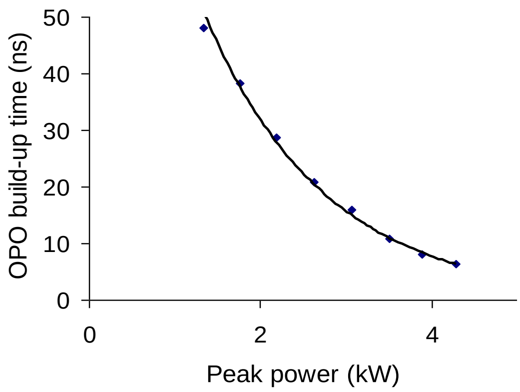

Figure 5.8: OPO build-up time as a function of pump pulse peak power.

Figure 5.9 plots both shaped and unshaped output optical pulses at 1062 nm exhibiting similar leading edge peak powers (the leading edge of the pump pulse plays the dominant role in initiating the parametric conversion process). The corresponding average powers coupled into the crystal for the shaped and unshaped optical pulses were

20.8 W and 10.6 W respectively. Thus the shaped optical pulses can extract around twice as much energy for a given peak power as compared to the unshaped optical pulses even for moderate output peak powers. The extracted energy ratio will be even higher for higher energy (peak power) pulses which experience an even greater amount of gain saturation within the MOPA.

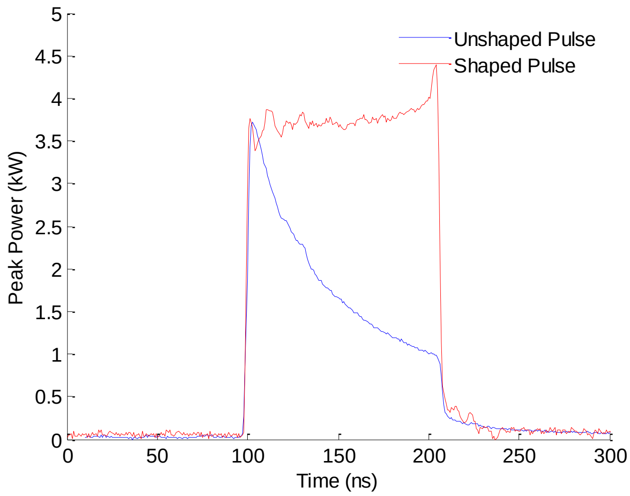

Figure 5.9: Temporal plots of the shaped and unshaped optical pulses at 1062 nm for similar leading edge peak power.

Spectral plots of the 1518 nm signal for both shaped and unshaped input pulses to the amplifier chain are illustrated in Figure 5.10. Once again the resolution of the spectrum analyzer was set at 0.1 nm to enhance the fine structure of the output spectra. For unshaped pulses, the time average central spectral peak of the 1518 nm signal breaks into two reasonably defined peaks for the maximum available pump pulse peak power as shown in Figure 5.10(b). We attribute this to instabilities associated with multi-mode operation at the high peak pump powers due to high parametric gains and the excessively broadened pump spectra. Similar spectral broadening has previously been reported by Myers et al in 1995 who also observed that use of a long stable pulse pump generally resulted in a narrower parametric signal spectrum [17]. Note that the peak central wavelength moves to longer wavelengths with increasing pump power. This can be attributed to internal heating within the PPMgLN crystal due to the relatively high absorption of PPMgLN within the idler wavelength band. The shift in wavelength is observed to be greatest for unshaped optical pulses relative to shaped pulses at the same average pump power – implying that the internal heating of the crystal is peak power dependent and may be associated with the higher idler intensity and the corresponding idler loss. It is possible to estimate the rise in internal temperature of the PPMgLN crystal from the observed wavelength shift. Our calculations indicate that the internal temperatures rose by about 16 °C for the unshaped optical pulses but only by about 6 °C in the case of shaped pulses as the average pump power at 1062 nm increased from 6.5 W to 21 W.

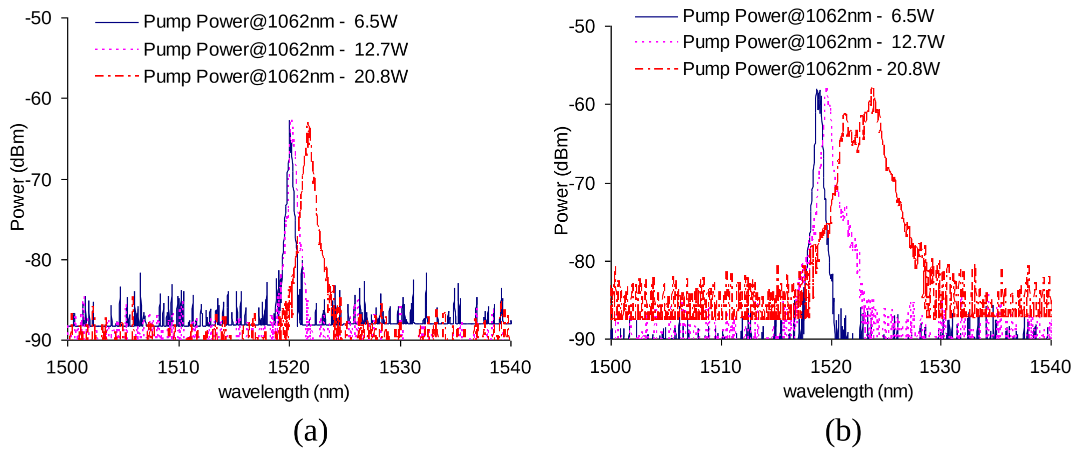

Figure 5.10: Spectra of parametrically converted signal pulses at 1518 nm for various output powers, (a) shaped and (b) unshaped

5.3 Frequency doubling and wavelength doubling

The fiberized MOPA described in Chapter 3 was used to pump a LBO crystal and a PPLN crystal simultaneously for frequency doubling and wavelength doubling the output beam. The average output power was limited to approximately 50 W to avoid damage to the PPLN crystal. The repetition rate was kept fixed at 100 kHz while the pulse duration was maintained at 100 ns throughout the experiment. Once again pulse shaping technique was used to investigate the performances of the frequency doubler and the wavelength doubler. The output of the fibre MOPA has a beam quality of ~1.1.

5.3.1 Wavelength conversion setup

A schematic of the optical set-up is shown in Figure 5.11. Separate legs for pumping an OPO and a frequency doubling crystal with the fibre MOPA output were constructed on a single optical breadboard. An optical isolator was used to protect the pump source from back reflections. This isolator introduced some thermally-induced depolarisation into the pump beam (polarisation contrast ratio reduced to 4:1). Therefore, to produce linearly polarised light for frequency conversion a polarising cube beam splitter was introduced after the isolator. A half-wave plate in combination with a second polarising cube beam splitter allowed control of the pump power into each leg. The losses in this optics train resulted in a maximum available pump power of 38.4 W, with a measured long-term power stability of 0.4 W (1% of the average value). No degradation in beam quality was observed due to the introduction of these optics.

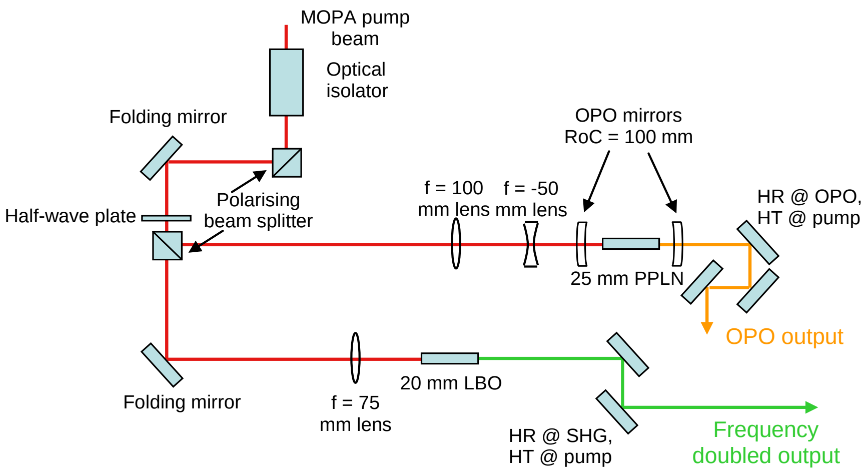

Figure 5.11: Schematic of optical breadboard incorporating the OPO and frequency doubling stages.

5.3.2 Performance of the degenerate PPLN OPO

The degenerate PPLN OPO leg of the optical breadboard is detailed in Figure 5.12. A lens pair was used to focus the pump beam down to a 0.25 mm diameter at the centre of the PPLN crystal. The maximum pump power was 35 W corresponding to energy density of ≤1.5 J.cm^{-2}, which is below the lithium niobate damage threshold of 2 J.cm^{-2}. A 25 mm length of congruently grown PPLN with a poling period of 31.9 μm was used as the gain medium. The nonlinear crystal was AR coated on both ends for the pump and OPO wavelengths, with a worst case reflectivity per surface of 1% at these wavelengths. The PPLN crystal was housed in an oven to allow operation at temperatures in excess of 100 ℃ in order to minimise the deleterious effects of photo refraction.

The OPO resonator consisted of a pair of 100 mm radius of curvature concave mirrors arranged symmetrically around the PPLN crystal, with the shortest resonator length of 70 mm used to minimise the build-up time contribution to the OPO threshold (the minimum length was constrained by the physical size of the PPLN oven). A single-pass pump geometry was used, with both the input and output mirrors measured to have 95% transmission at the pump wavelength. Output mirrors with reflectivities in the range 20% to 90% were available for testing. A series of dichroic mirrors was used to separate the OPO output beam from the depleted pump beam.

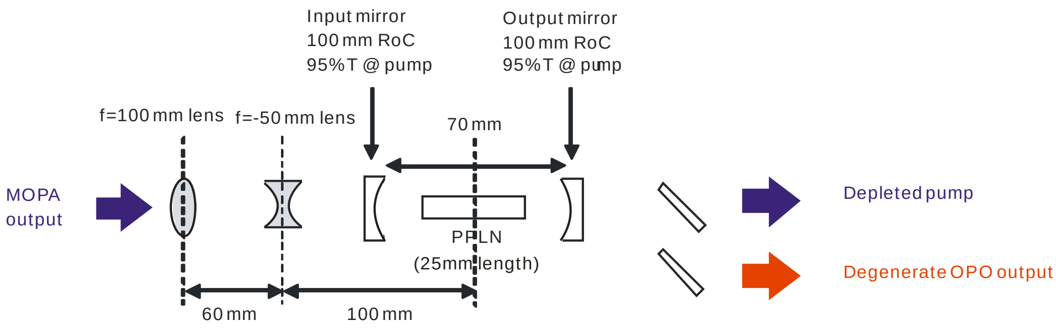

Figure 5.12: Set-up of degenerate PPLN OPO.

The highest output power performance was achieved with a 77% reflectivity output mirror; the generated output power and conversion efficiency data is plotted in Figure 5.13. Note that the incident pump power is used, taking into account the losses of the optics prior to the PPLN crystal. Optimum performance was achieved with a PPLN oven temperature in the range 120 ℃-125 ℃.

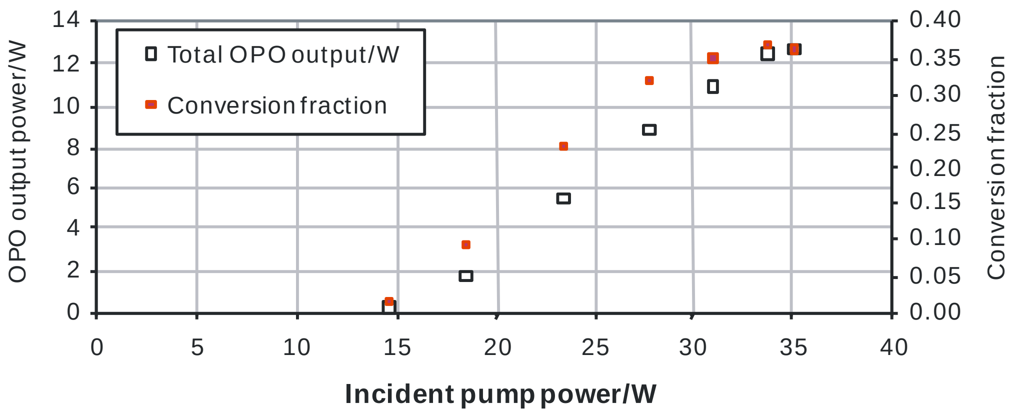

Figure 5.13: Power curve and conversion efficiency trend of the OPO using a 77%R output mirror.

As can be seen in Figure 5.13, the maximum effective output power achieved was 12.7 W at a conversion efficiency of 36%. During these experiments the input mirror, nominally a high reflector at the OPO degenerate wavelength of 2126 nm, was measured to be only 88% reflective, hence the data recorded in Figure 5.13 is for the sum of the OPO power exiting the input and output mirrors.

The threshold pump power was 15 W, with an OPO slope efficiency of 65%. The standard deviation of output power variation with time was 4% of the average power, recorded at the maximum pump power.

A beam profiling system to allow full characterisation of the OPO output beam behaviour was not available during these experiments. Figure 5.14 is a digital camera image of the OPO far-field output beam captured by an infrared camera (SpiriconPyrocam I) and displayed directly on a monitor.

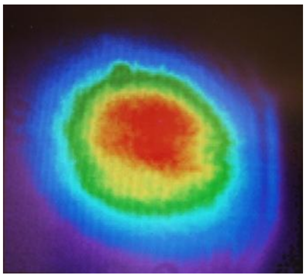

Figure 5.14: Far-field beam profile of OPO output (77% reflectivity output mirror).

There was some evidence of a change in beam shape with output mirror indicating that thermal lensing is present in the PPLN crystal. This was attributed principally to absorption at the OPO wavelengths as the beam distortion increased with increasing output mirror reflectivity i.e. increasing intracavity OPO power. The observed change in beam profile with increasing pump power (independent of mirror reflectivity) was taken as further evidence of the presence of thermal lensing.

Broadband output was expected from the type I degenerate PPLN OPO. A typical output spectrum of the OPO operating at maximum output power is shown in Figure 5.15(a). A centre wavelength of 2125.5 nm was measured at a PPLN oven temperature of 120 ℃ using a Jarrell Ash Monospec 27 monochromator (calibrated to have a wavelength accuracy of ±1 nm), with a full width half maximum linewidth in excess of 170 nm. Small variations in temperature altered the detailed spectral lineshape but not the overall spectral width

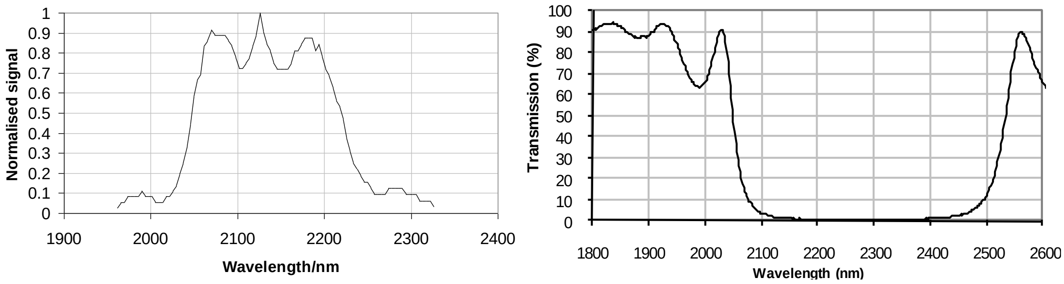

(a) (b)

Figure 5.15: (a) OPO output wavelength spectrum and (b) the spectral performance of the input mirror.

Figure 5.15(b) displays the measured spectral performance of the OPO input mirror. While it is a high reflector (>99.5% reflectivity) at 2126 nm the reflectivity drops for the shorter wavelength component of the OPO output. Based on the data plotted the average reflectivity of this mirror over the FWHM of the OPO output is 88%, in exact agreement with the experimental measurement of the mirror reflectivity.

The recorded temporal pulse behaviour of the pump beam and the OPO output is shown in Figure 5.16. Measurement of the depleted pump pulse shape with respect to the input pump pulse indicates a pump depletion of 34%, in reasonable agreement with the measured OPO efficiency of 36%. The OPO pulse in Figure 5.16(b) was measured using an extended wavelength InGaAs photodiode. The slower decay of the OPO pulse relative to the pump pulse is thought to result from the lower reverse bias voltage of the long wavelength diode, making a comparison of the pulse shapes difficult. The delay between the peak of the pump pulse and the peak of the OPO pulse is 4 ns, based on the data captured, with the OPO pulse displaying a leading edge rise time of 6 ns.

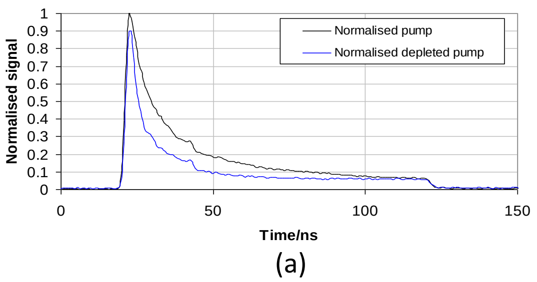

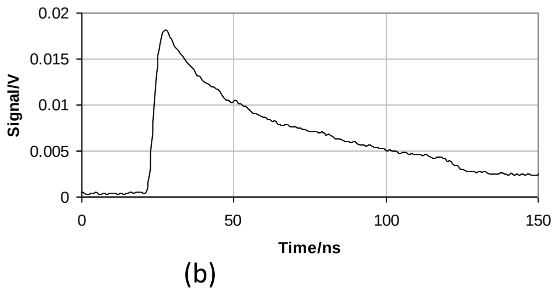

Figure 5.16: (a) Normalised pump pulse and (b) OPO output pulse temporal profiles.

5.3.3 Performance of the frequency doubled output

The experimental set-up for the second harmonic generation (SHG) leg of the optical breadboard is detailed in Figure 5.17: The nonlinear crystal used for frequency doubling was a 20 mm length of LBO used in the type I non-critically phase-matched geometry. The LBO crystal was housed in an oven, with a set point temperature of 162 °C in order to maximise the SHG conversion. The coated ends of the LBO crystal were measured to be 2.5% reflective at the pump wavelength and 4% reflective at the SHG wavelength.

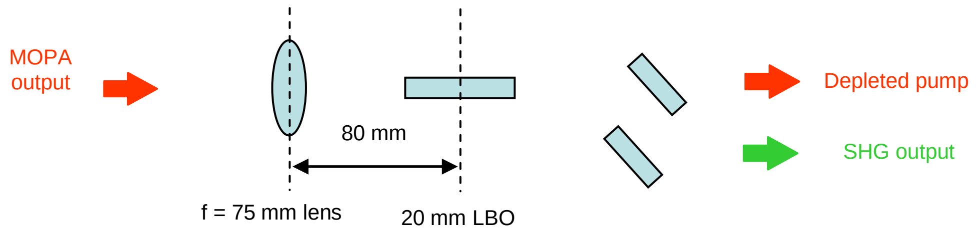

Figure 5.17: Set-up of the LBO frequency doubling stage.

A single lens was used to focus the pump beam to a diameter of 86 μm in the centre of the LBO crystal, resulting in a maximum pump energy density of 12.4 J.cm^{-2}.

The measured SHG power performance is plotted in Figure 5.18. A maximum power in the green of 9.8 W was recorded, which equates to a conversion efficiency of 27% when the pump power incident at the LBO crystal is considered.

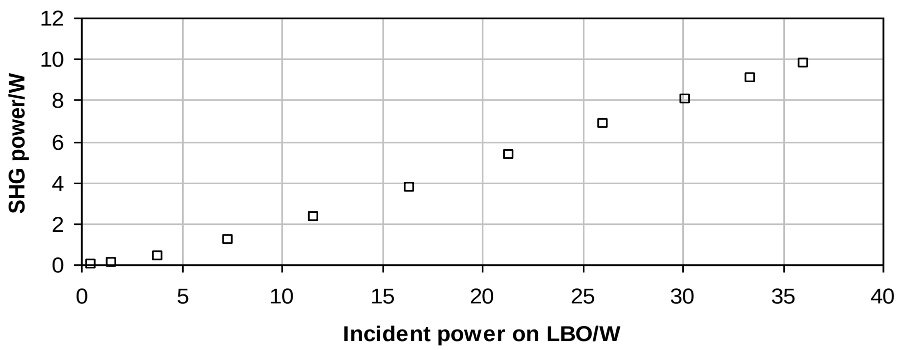

Figure 5.18: SHG output power curve.

The SHG far-field beam profile was recorded at the focal plane of a lens and is shown in Figure 5.19. The centroid jitter was measured to be <2% of the beam divergence. Beam quality factor M^2 values of 1.16 and 1.24 in the horizontal and vertical directions respectively were derived from beam diameter measurements around the beam waist location. Therefore the beam quality has only slightly deteriorated from the pump pulse.

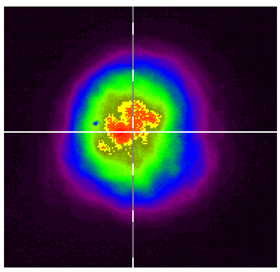

Figure 5.19: SHG output beam profile in the far field.

Temporal pulse-shaping of the MOPA output was briefly investigated. An electro-optic modulator pulse carver is used to control the seed pulse shape entering the amplifier chain. By creating a seed pulse with an exponentially rising leading edge a near flat-top output pulse from the MOPA was generated, as shown in Figure 5.20. The more uniform pump beam intensity in principal allows higher nonlinear conversion efficiencies for a given peak pump power. Figure 5.20(b) highlights the correspondence in pulse shape between the pump pulse and the SHG output pulse when the shaped seed pulse is used. Here the repetition rate and average power were both fixed, hence the unshaped seed pulse configuration generated higher peak power pulses.

The shaped seed pulse however produced lower extraction efficiency from the amplifier chain, resulting in enhanced ASE between seed pulses. Therefore the average output power of the MOPA was restricted to 30 W in order to carry out the assessment. At this power level 33% SHG conversion efficiency was recorded using shaped seed pulses, with a corresponding conversion efficiency of 30% using unshaped seed pulses, a small but measurable enhancement to the SHG conversion efficiency. Note that the conversion efficiency with the unshaped seed pulse at lower pump power is higher than the 27% conversion efficiency recorded at maximum pump power. This is a possible indication of thermal dephasing in the LBO crystal at higher pump powers.

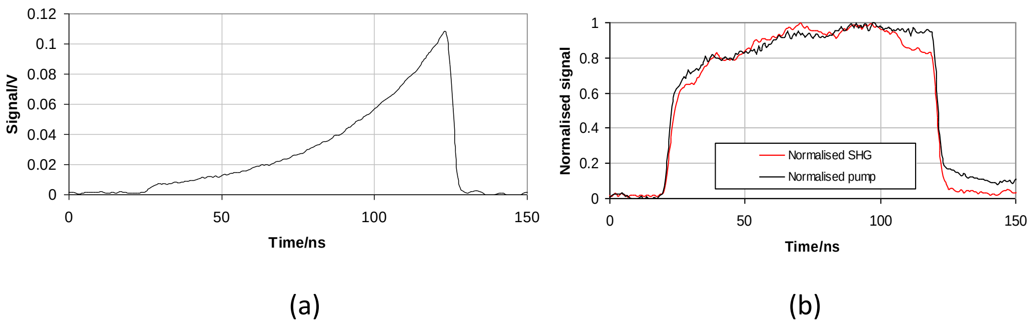

Figure 5.20: (a) Normalised shaped seed pulse shape and (b) resulting output pulse shape with corresponding SHG output pulse shape.

5.4 Raman frequency shift conversion

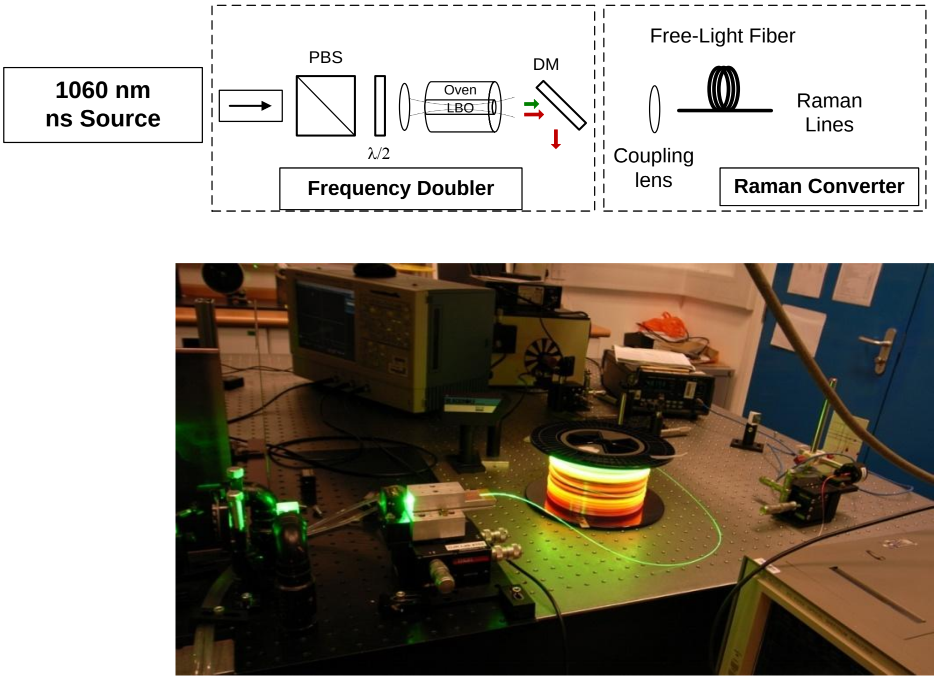

Figure 5.21: Schematic of the frequency-doubler and the Raman-converter pumped by the 1060 nm nanosecond source. Bottom insert shows the setup in working status.

The experimental set-up is shown in Figure 5.21 comprising a 1060 nm fibre MOPA capable of generating rectangular shaped optical pulses, an SHG crystal and a length of fibre for Raman conversion.

The output pulses of the MOPA were first frequency doubled using a 15 mm long LBO crystal as shown in Figure 5.21. The diameter of the focused beam at the waist position was 70 μm through the use of a 100 mm focal length lens, corresponding to a Rayleigh range of 12 mm. The crystal was cut for noncritical phase matching at an operating wavelength of 1060 nm. A free-space isolator was used to protect the MOPA chain from any unwanted feedback. Note that this particular isolator was found to slightly degrade the beam polarization (and indeed also the beam quality) at incident powers above 20 W due to thermal effects, and so I introduced a polarization beam splitter (PBS) to clean-up the output polarization before the SHG crystal. A half-wave plate placed immediately before the focusing lens was used to rotate the polarization of the fundamental light to maximize the second harmonic signal. The crystal was kept at a constant temperature of 155 ^{o}C for maximum frequency conversion.

The second harmonic power was found to increase quadratically at pump powers up to 20 W. Beyond which a roll-over was observed, which is believe to be due to the mode-quality degradation of the fundamental signal in the isolator that we previously noted. A maximum second harmonic power of 10 W was obtained at a fundamental power of 36 W, (corresponding to an overall optical conversion efficiency of 27%), which was more than adequate for our needs. The far-field beam profile (M^2) of the frequency doubled signal was measured to be 1.16 and 1.24 in the horizontal and vertical directions respectively at the 10 W level, which is slightly worse than that of the pump beam. The -3 dB spectral bandwidth of the frequency doubled signal at full power was of the order of 0.1 nm, and the temporal pulse shapes, shown in Figure 5.22, were very similar to that of the pump pulses.

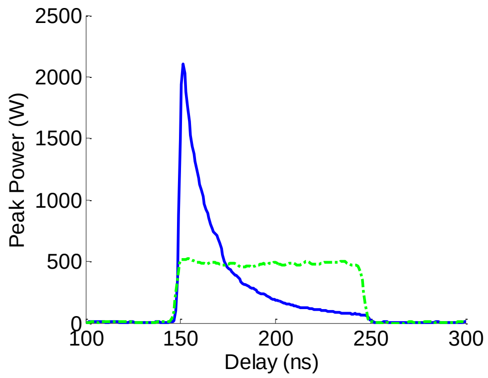

Figure 5.22: Peak power of shaped (green dash dotted line) and unshaped (solid blue) SHG pulses at 5 W power level.

As a Raman gain medium we used a 1 km long Pirelli Freelight fibre (~5 mol% germanium-doped silica core) with a second mode cut-off wavelength of 1450 nm and an estimated propagation loss of ~25 dB/km at 530 nm. The Raman gain peak for germanosilicate fibre lies around 440 cm^{-1}[18], corresponding to a 13.2 THz frequency shift.

In order to confirm what to expect when using this fibre and to establish the pulse power levels required to excite specific Raman orders we developed a model of the Raman excitation process in the fibre. The model is based on a rate equation describing the transfer of pulse energy between different frequency components of a given input pulse during propagation along the fibre [19],

$$\frac{dI(\omega)}{dz} = -\alpha I(\omega) + \int_0^\infty d\Delta\, g_R(\Delta)\left\{ I(\omega+\Delta)\left[I(\omega)+N(\omega)\right] - \frac{\omega}{\omega-\Delta}\left[I(\omega-\Delta)+N(\omega-\Delta)\right]I(\omega)\right\} \tag{5.1}$$

The first term describes propagation losses with a loss coefficient α, which for the sake of the results presented here is set to 25 dB/km at 530 nm. The terms under the integral describe Raman gain: the first term corresponds to gain at frequency ω due to stimulated Raman scattering (SRS) from higher frequency components, while the second term describes the corresponding losses at lower frequency components. Spontaneous Raman scattering is included via N(ω) which is set to an intensity of one photon per mode. Note that the simple model of Equation 5.1 ignores all dispersion effects and Kerr nonlinearities, and assumes idealized pulse shapes.

Numerical modelling was carried out to verify the theory discussed above. The simulation results are presented in Figure 5.23. Figure 5.23(a) shows output spectra for two different peak powers with unshaped input pulses. The spectra exhibit a nearly flat distribution across all Raman orders, while the maximum Stokes order generated depends on the peak power of the pulse. By contrast, Figure 5.23(b) shows the selective generation of Raman Stokes orders with square input pulses. When the unshaped output pulses at 530 nm were launched into the 1 km long Raman gain medium, simultaneous excitation of Raman lines (up to 16 orders) was observed, as plotted in Figure 5.24. The results are just as expected theoretically other than that the Raman linewidths broaden with increasing stokes order. This is entirely to be expected since our calculations do not include any nonlinear effects other than Raman scattering (e.g. SPM and four-wave mixing are ignored).

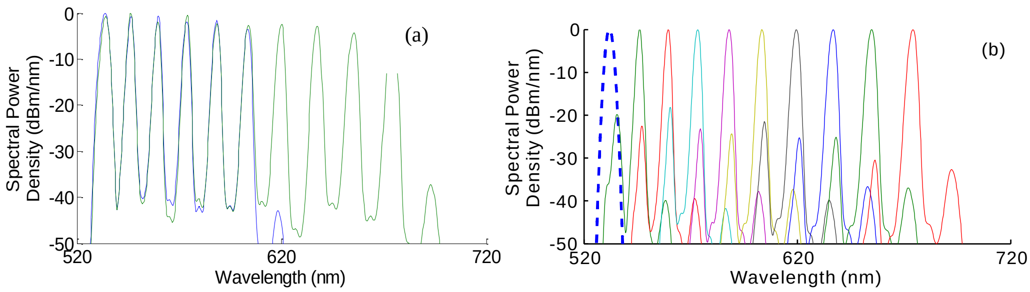

Figure 5.23: (a) Simulated Raman shifted output spectra for unshaped input pulses with 198 W and 400 W peak powers, (b) Simulated Raman shifted output spectra for square input pulses. Dashed line: input spectrum; solid lines: output spectra for incident pulse peak powers (from left to right) of 46 W, 80 W, 115 W, 155 W, 198 W, 240 W, 290 W, 340 W, 400 W.

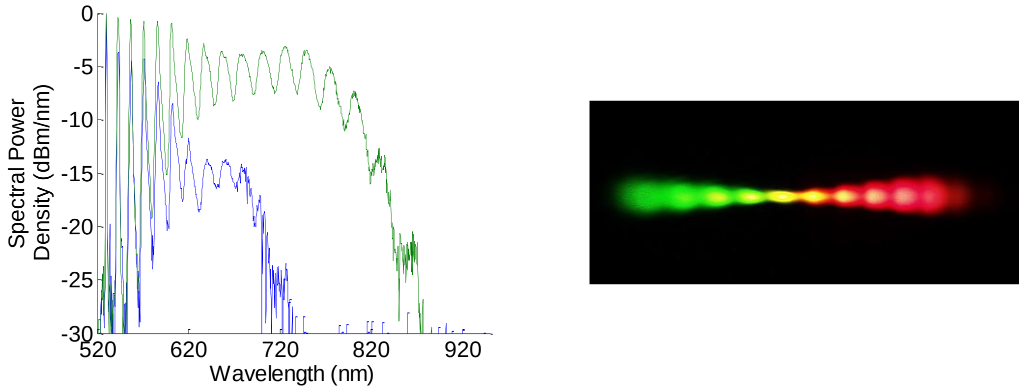

Figure 5.24: Spectra at peak powers of 2000 W (green line) and 1100 W (blue line) pumped with unshaped pulses. Right picture shows the prism separated stokes image up to the 11 th order.

To demonstrate the selective excitation of single Raman orders we then launched rectangular shaped optical pulses at 530 nm into the Raman gain fibre. Figure 5.25 shows the spectra obtained with square shaped optical pulses at different peak power levels. The theoretical prediction of sequential wavelength shifting is well borne out. For an input peak power of 15 W, a significant fraction (95%) of the pump power is transferred to the 1st order Stokes line with no generation of higher order Stokes peaks as expected. The pump depletion was ~15 dB. Similarly we have managed to individually excite the 2nd, 3rd, 4th, 5th, 6th, 7th, 8th and 9thorder Raman stokes lines albeit with decreasing suppression ratios and with broader linewidths than predicted by the simple theory which assumes perfectly rectangular pulses (we clearly have deviations from perfect flatness and finite rise and fall times on our pulses). Nevertheless the principle and effectiveness of using shaped pulses is clearly demonstrated. The frequency separation between the subsequent Raman lines was measured to be ~13.2 THz. The width of the Raman shifted pulses was measured to be slightly larger than the pump pulses due to the walk-off effect between pump and signal pulses, estimated to be ~6 ns in our 1 km long Raman gain medium.

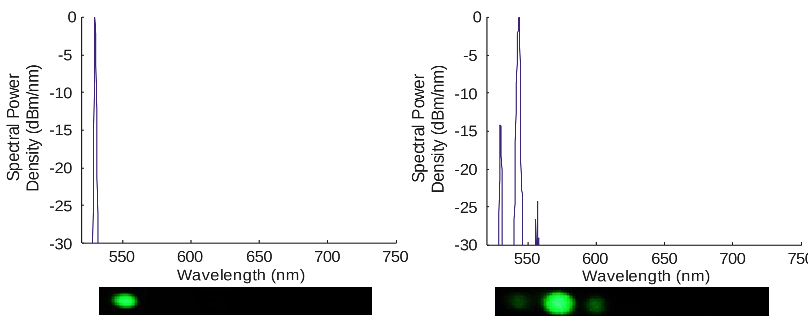

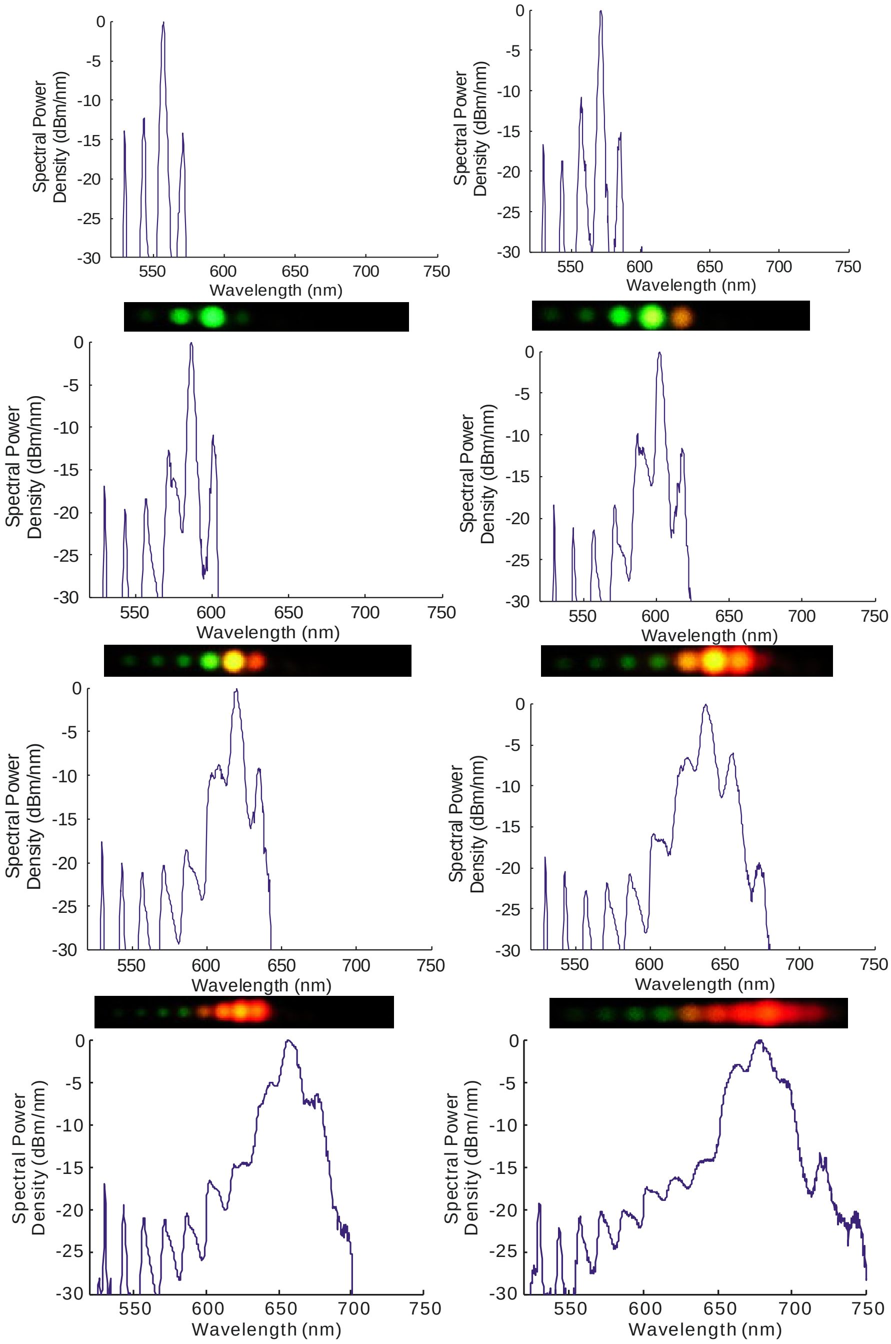

Figure 5.25: Spectra of the output pulses after propagating through 1 km long Pirelli Freelight fibre at an incident pulse peak power of 15 W, 52 W, 81 W, 133 W, 199 W, 280 W, 353 W, 397 W, 441 W and 500 W;) the corresponding prism-separated Stokes images up to 7 orders shown on the bottom of related spectrum .

Note that we find that higher Raman orders are observed at slightly higher peak powers than predicted by our simple model which may be due to the deterioration of the pump beam at higher pump powers due to the isolator, which leads to excitation of higher order fibre modes and a corresponding reduction in the Raman gain, or the assumption of a uniform 25 dB/km loss across the spectral bandwidth involved. A maximum peak power of 8 W was measured for the 9th order Raman line whereas it was only about 0.45 W for the 1st order Raman line due to higher transmission loss of the short wavelength light inside the Raman gain medium. The peak powers for the 2nd, 3rd, 4th, 5th, 6th, 7th, 8th and 9thorder Raman lines were measured to be 0.65 W, 0.95 W, 1.6 W, 2.4 W, 3.4 W, 4 W, 6 W and 8 W respectively.

Finally, just to highlight the importance of operating in the normal dispersion regime, we removed the SHG element and launched the 1060 nm shaped pulses into the Raman fibre. A side mode suppression of better than 10 dB was achieved at low Raman orders as shown in Figure 5.26. However, the number of Stokes orders was limited to 4, beyond which a continuum starts to develop due to the overlap of the Stokes line with the anomalous dispersion regime of the Raman gain medium.

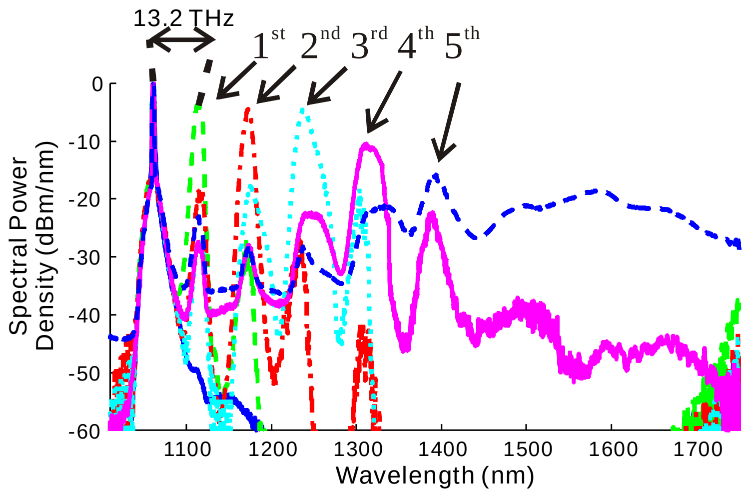

Figure 5.26: Spectra of the Raman converted output pulses after propagating through 1 km long Pirelli Freelight fibre pumped with shaped pulses at 1060 nm.

5.5 Conclusion

In summary, using the high power linearly polarized nanosecond fibre MOPA, a high power PPMgLN -based OPO was demonstrated. More than 9 W of average output power was obtained with over 2.4 W at 3.5 micron. Benefiting from the pulse shaping technique applied in the fibre MOPA, better OPO performance scan be anticipated.

In addition, 12.7 W mid-IR output from a degenerate PPLN OPO and 9.8 W visible output powers from a LBO crystal were achieved. Conversion efficiencies at maximum pump power of 36% for the 2 μm mid-IR output and 27% for the visible output were achieved. The broadband output of the OPO had a FWHM spectral bandwidth in excess of 170 nm. The visible output was measured to have an M^2 of 1.2. An enhancement of SHG conversion efficiency from 30% to 33% was observed for flat top output pulses.

SRS induced wavelength shift to individual orders with good adjacent order suppression ratios through pulse shape control implemented in the fibre MOPA was also demonstrated. Controlling the pump power allowed us to observe individual Stokes lines up to the 9^{th} order. Using this concept with optimized fibre designs and lengths as well as other Raman gain media (e.g. glasses, liquids, gases) [20] it is possible to envisage a host of tunable lasers operating at discrete wavelengths in the visible/near IR. Note that the rapid Raman response time should allow for very rapid wavelength tuning through pulse shape control and may find a number of interesting bio-medical applications.

References

[1] W. R. Bosenberg, A. Drobshoff, J. I. Alexander, L. E. Myers, and R. L. Byer, "93% pump depletion, 3.5-W continuous-wave, singly resonant optical parametric oscillator," Opt. Lett., vol. 21, pp. 1336-1338, 1996.

[2] L. E. Myers and W. R. Bosenberg, "Periodically poled lithium niobate and quasi-phase-matched optical parametric oscillators," IEEE J. Quantum Electron, vol. 33, pp. 1663-1671 1997.

[3] M. Nakamura, S. Higuchi, S. Takekawa, K. Terabe, Y. Furukawa, and K. Kitamura, "Optical damage resistance and refractive indices in near-stoichiometric MgO-doped LiNbO3," Jpn. J. Appl. Phys., vol. 41, pp. L49-L51, 2002.

[4] A. Piper, A. Malinowski, K. Furusawa, and D. J. Richardson, "High-power, high-brightness, mJ Q-switched ytterbium-doped fibre laser," Electronics Letters, vol. 40, pp. 928-929, 2004.

[5] K. T. Vu, A. Malinowski, D. J. Richardson, F. Ghiringhelli, L. M. B. Hickey, and M. N. Zervas, "Adaptive pulse shape control in a diode-seeded nanosecond fiber MOPA system," Optics Express, vol. 14, pp. 10996-11001, 2006.

[6] P. E. Britton, D. Taverner, K. Puech, D. J. Richardson, P. G. R. Smith, G. W. Ross, and D. C. Hanna, "Optical parametric oscillation in periodically poled lithium niobate driven by a diode-pumped Q-switched erbium fiber laser," Opt. Lett., vol. 23, pp. 582-584, 1998.

[7] D.-W. Chen and S. R. Todd, "Low Noise 10-W CW OPO Generation near 3 μm with MgO Doped PPLN," in Conference on Lasers and Electro-Optics (CLEO) 1-3, 2005, pp. 1829-1831

[8] C. H. Avila, R. L. Burnham, Y. Chen, W. Torruellas, H. R. Verdun, and R. A. Utano, "Polarization-maintaining master oscillator fiber amplifier (MOFA) for high-repetition-rate applications," Proceedings of the SPIE - The International Society for Optical Engineering, Fiber Lasers: Technology, Systems, and Applications, 26-28 Jan. 2004, vol. 5335, pp. 24-32, 2004// 2004.

[9] G. P. Agrawal, Nonlinear Fiber Optics, Third ed. USA: Academic Press, 2001.

[10] J. L. Archambault and S. G. Grubb, "Fiber gratings in lasers and amplifiers," J. Lightwave Technol, vol. 15, pp. 1378-1390, August (1997).

[11] C. A. Codemard, P. Dupriez, Y. Jeong, J. K. Sahu, M. Ibsen, and J. Nilsson, "High-power continuous-wave cladding-pumped Raman fiber laser," Opt. Lett., vol. 31, pp. 2290-2292, 2006.

[12] P. Dupriez, C. Farrell, M. Ibsen, J. K. Sahu, J. Kim, C. Codemard, Y. Jeong, D. J. Richardson, and J. Nilsson, "1 W average power at 589 nm from a frequency doubled pulsed Raman fiber MOPA system," in Photonics West, San Jose, CA, USA, 2006, pp. 61021G-6.

[13] A. Malinowski, K.T.Vu, K.K.Chen, P.Horak, and D.J.Richardson, "Selective generation of individual Raman Stokes wavelengths using shaped optical pulses," presented at the OFC, San Diego, 2008.

[14] A.Malinowski, K.T.Vu, K.K.Chen, V.K.Geddes, J.C. Flanagan, and D.J.Richardson, "High Power Pulsed Fiber MOPA System Incorporating Electro-Optic Modulator Based Adaptive Pulse Shaping," JSTQE, 2009.

[15] B. Wu, Y. Shen, and S. Cai, "Widely tunable high power OPO based on a periodically poled MgO doped lithium niobate crystal," Optics & Laser Technology, vol. 39, pp. 1115-1119, 2007.

[16] S. U. Alam and A. B. Grudinin, "Tunable picosecond frequency-shifted feedback fiber laser at 1550 nm," IEEE Photonics Technology Letters, vol. 16, pp. 2012-2014 (2004).

[17] L. E. Myers, R. C. Eckardt, M. M. Fejer, R. L. Byer, W. R. Bosenberg, and J. W. Pierce, "Quasi-phase-matched optical parametric oscillators in bulk periodically poled LiNbO3," J. Opt. Soc. Am. B, vol. 12, pp. 2102-2116, 1995.

[18] N. Shibata, M. Horigudhi, and T. Edahiro, "Raman spectra of binary high-silica glasses and fibers containing GeO2, P2O5 and B2O3," Journal of Non-Crystalline Solids, vol. 45, pp. 115-126, 1981.

[19] K. K. Chen, S.-u. Alam, P. Horak, C. A. Codemard, A. Malinowski, and D. J. Richardson, "Excitation of individual Raman Stokes lines in the visible regime using rectangular-shaped nanosecond optical pulses at 530 nm," Opt. Lett., vol. 35, pp. 2433-2435, 2010.

[20] G. Rivoire and R. Chevalier, "Production of multiple frequencies by stimulated Raman wave coupling in cyclohexane," Optics Communications, vol. 88, pp. 551-558, 1992.

Chapter 6 Frequency conversion based on picosecond source

Overview

This Chapter demonstrates high power and high efficiency Second Harmonic Generation (SHG), Optical Parametric Oscillators and Supercontinuum Generation sources pumped by the picosecond source I have described in Chapter 4. This Chapter is organized as follows: 6.1 provides an introduction to picosecond pulse pumped SHG, OPO and SCG; experimental results on SHG are given in section 6.2; 6.3 details the experimental realisation of a synchronously pumped Optical Parametric Oscillator (OPO); detailed experimental results on SCG in a microstructured optical fibre are presented in section 6.4; and a brief conclusion is given in 6.5.

6.1 Introduction

6.1.1 Picosecond pulse pumped Second Harmonic Generation

High average power laser sources at 530 nm with good beam quality are of great interest for a number of important applications including material processing [1], medical treatments [2], the pumping of visible OPOs [3] and laser displays [4] to name but a few. In material processing green laser sources have been shown to perform better than their counterpart IR sources in a variety of applications such as marking, precision microfabrication and laser trimming to name but a few. The advantages include a smaller spot size limit and a far larger absorbance for many materials of interest. Although femotsecond lasers have conventionally been used extensively for high precision material processing applications these lasers are generally complex in nature, expensive and high maintenance making them unattractive for industrial use. Recently it has been realized that picosecond lasers offer most of the advantages of fs systems e.g. precision, low thermal damage etc. in addition to high material removal rates thanks to the relatively high repetition rates which essentially come as standard with these laser sources.

In this work, using the high power, PM, SM, picosecond source described in Chapter 4, I generated up to 56 W of green light at a repetition rate of 227 MHz and at an overall conversion efficiency of 56%. The diode-to-green optical power conversion efficiency was an impressive 37%.

6.1.2 Synchronously pumped Optical Parametric Oscillator

Synchronously pumped optical parametric oscillators (SPOPOs) are of great interest as source of broadly wavelength tunable picosecond and femtosecond pulses. Such systems are normally pumped by mode-locked bulk solid-state laser systems with typical fixed pulse repetition rates of ~100 MHz. However, the emergence of new sources of ultrashort pulses has led to various demonstrations of SPOPOs with repetition rates up to 39 GHz [5], and combined signal and idler average powers up to ~27 W [6]. The pump sources have also become more compact, allowing SPOPOs based on amplified mode-locked diode sources [7], fibre lasers [8], and passively mode-locked miniature bulk lasers [5, 9]. High-repetition rate ultra-short pulse sources are of interest for a range of applications including telecommunications [5] and non-invasive nonlinear microscopy [10, 11], and SPOPOs in particular are well-suited to CARS microscopy as they deliver synchronized pulses at two different wavelengths [12].

This work was carried out in conjunction with another group in ORC who have studied OPOs for many years and previously successfully demonstrated SPOPO experimentally [13, 14]. The picosecond pulse system described in Chapter 4 was used to build the SPOPO. The pump itself benefits from a highly compact and simple design with a minimum of free-space components and a user-controlled repetition rate up to the GHz regime. At an average pump power of 24 W, up to 7.3 W at 1.54 μm and 3.1 W at 3.4 μm were obtained. I was responsible for customising the pump source for these experiments and participated in all of the OPO construction and testing experiments alongside Mr Florian Kienle who designed and implemented the OPO as part of his PhD work.

6.1.3 Picosecond pulse pumped Supercontinuum Generation in PCF

Supercontinuum generation (SCG) has been an exciting research field over the past few years with new advances being reported on all aspects of the technology [11, 15, 16]. The invention of Photonic crystal fibre (PCF) with high non-linearities and tailored dispersion profiles first enabled SCG pumped by a femtosecond laser oscillator without complex amplification systems, and led to supercontinuum sources becoming a widely used laboratory tool [17-19]. The initial work on visible SCG used Ti:Sapphire lasers, but the high maintenance costs and limited average power led to the development of alternative pump lasers. In particular, fibre lasers have become the standard source in commercial SCG products (e.g. Fianium, Koheras).

Where applications require high average power SC sources with useful power levels available after spectral slicing further source developments are still required. High average power SCG has been reported by Travers et al. [20]. They demonstrated a visible SC source pumped by a 400 W CW laser at 1.07 µm with either 50 W average output power in the region of 1.05 – 2.2 µm or 28 W covering 0.6 – 1.9 µm spectral region with power densities varying between 2 mW/nm in the visible and ~30 mW/nm in the infrared. While CW pump sources are simpler than pulsed sources, they do have some disadvantages such as the long lengths of PCF required for the continuum to form and because a splice with just a few percent loss implies several Watts of heat load due to the high average power of the pumps. As has been demonstrated by Stone and Knight [21], a pulsed source enables higher peak power, visible SCG can be produced at a relatively low average pump power and the pulsed driving format also enables synchronization to a lock-in detection circuit. However, pulse-pumped visible SCG sources that have been reported have lower average power compared to CW sources [21-24].

In this chapter, I will also present our picosecond fibre MOPA pumped SC source with a high optical-to-optical conversion efficiency of up to 74%, covering a spectral range of 0.4-2.25 µm. The maximum average output power was 39 W at an incident pump power of 57 W and repetition rate of 114.8 MHz. The spectral power density of more than 30 mW/nm was relatively uniform across the visible region. At a reduced repetition rate of 28 MHz, we obtained higher peak spectral densities of 26.9 W/nm at visible wavelengths but with a slightly lower average power of 20 W. Following Stone and Knight's demonstration that a high air-fill-fraction PCF design with core diameter of 4.2 µm–4.7 µm range produced more continuum in the 400-450 nm wavelength range than low air-fill designs such as endlessly single mode fibres, we chose a 4.4 µm core diameter, high-delta PCF for the continuum generation [21]. The large core diameter led to a coupling efficiency of up to 80% and an increased optical-to-optical conversion efficiency when compared to CW pumped sources [20]. The large core also provided a higher damage threshold than smaller core fibres and the dispersion profile led to rapid generation of visible continuum and enabled the use of only 2 m fibre length. Detail results will be presented in section 6.4. Note that this work was performed in collaboration with colleagues at the CGCRI in Kolkata India who designed and fabricated the fibres.

6.2 High efficiency Second Harmonic Generation

In this section I will present a frequency doubled green source at 530nm pumped by the picosecond MOPA system.

Figure 6.1 shows the experimental setup. For simplicity, the seed and the pre-amps are shown as boxes. A more detailed schematic can be found in Figure 4.3 of Chapter 4. The single polarization output of the final stage was launched into a 15 mm long LBO crystal (Figure 6.1). The diameter of the focused beam at the waist position was 70 µm corresponding to a Rayleigh range of 12 mm. The crystal was cut for noncritical phase matching at an operating wavelength of 1060 nm. A half-wave plate placed immediately before the focusing lens was used to rotate the polarization of the fundamental light to maximize the second harmonic signal. The crystal was kept at a constant temperature of 155 ^{o}C for maximum frequency conversion. A 530 nm/1060 nm dichroic mirror was used to separate the SHG and fundamental beams.

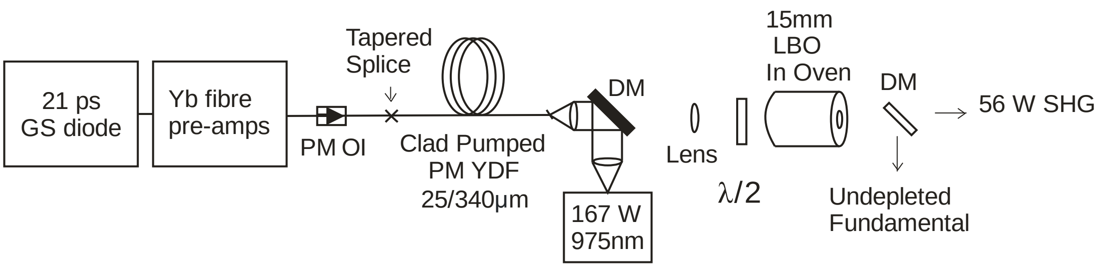

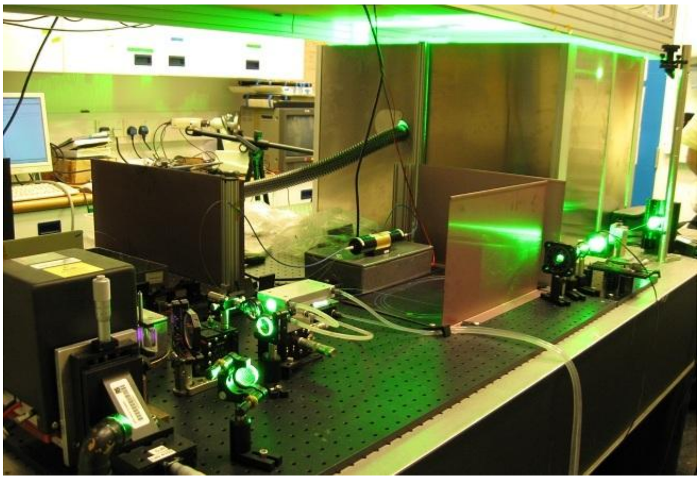

Figure 6.1: Schematic diagram of the Yb^{3+}-doped fibre MOPA pumped SHG; Bottom insert shows the system is working at full power and doing material processing in my lab

The spectra as measured with an ANDO (AQ6315B) spectrum analyzer at a repetition rate of 908 MHz has a signal level about 37 dB above the ASE (OSNR) after the second stage amplifier, and which was maintained at the system output at the 100 W power level as shown in Figure 6.2. The pulse energy and peak-power requirements of our intended applications dictated that we operated the system at a repetition rate of 227 MHz to get the best performance. As shown in Figure 6.2, a good OSNR was maintained as the repetition rate was reduced with an OSNR of 23 dB at the output at 227 MHz with 97 % of the total power in the signal band. Therefore the maximum extracted pulse energy was 0.43 μJ corresponding to a peak power of 21 kW at an average output power of 100 W. The spectral bandwidth of the amplified pulses increased from 0.3 nm to 0.9 nm due to self-phase modulation (SPM) assisted spectral broadening inside the final stage amplifier at this repetition rate. The measured PER was 19 dB under full power operation.

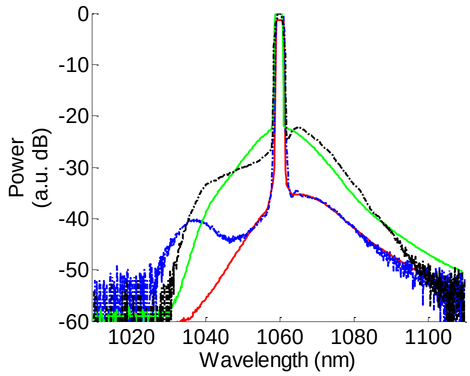

Figure 6.2: Spectral plot of the 2nd stage amplifier output (solid red line), and final output (dashdot blue line) for pulses at repetition rate of 908 MHz and a spectral plots of the 2nd stage amplifier output (solid green line), and final output (dash-dot black line) for pulses at repetition rate of 227 MHz. The spectra were measured with an ANDO (AQ6317B) spectrum analyser using 2.0 nm resolution.

The pulse width of the seed source was measured using the frequency resolved optical gating (FROG) technique and was found to be ~21 ps as shown in Figure 6.3(a). An intensity autocorrelator was used to measure the pulse widths at different average output power levels and are illustrated in Figure 6.3(b). The plots show that no significant temporal distortion occurs during amplification.

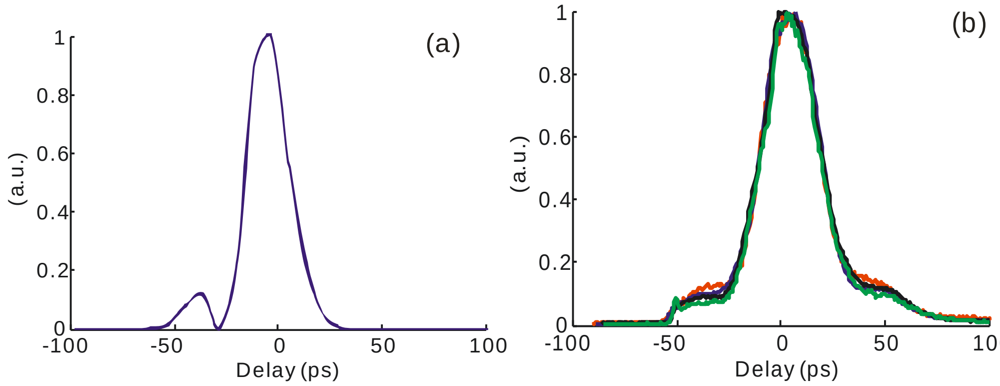

Figure 6.3: (a) FROG trace of seed pulse (b) Autocorrelation traces at 12 W (red), 36 W (blue), 70 W (black) and 100 W (green).

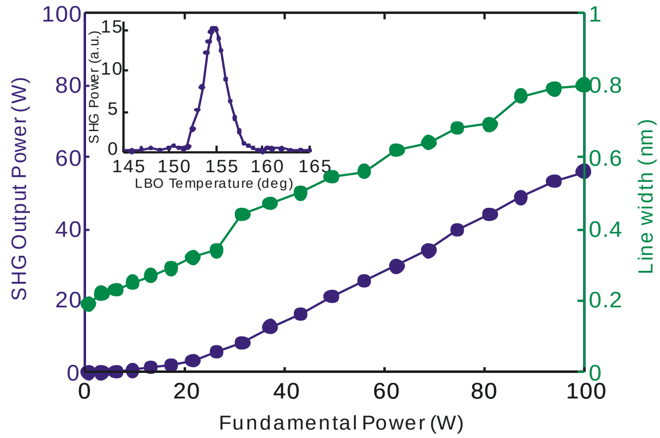

Figure 6.4: Dependence of the second harmonic power at 530 nm on the fundamental signal (circle) and the corresponding spectral bandwidth of the fundamental light (square). The inset shows the temperature tuning curve of the LBO crystal.

Figure 6.4 shows the average output power of the second harmonic signal as a function of the fundamental power. The temperature tuning curve of the crystal is shown in the inset of Figure 6.4 and has a full-width at half-maximum (FWHM) of 3^{o}C. It also shows that the spectral bandwidth of the fundamental signal increases linearly with output power due to SPM inside the power amplifier. A maximum second harmonic power of 56 W was obtained at a fundamental power of 100 W corresponding to an overall optical conversion efficiency of 56%. The observed roll-over in second harmonic generation (SHG) power was believed to be due to the SPM in the final amplifier which broadened the spectrum of the fundamental light beyond the acceptance bandwidth of the SHG crystal for MOPA powers above 80 W. A repetition rate of 227 MHz was found to provide the best combination of induced SPM and conversion efficiency although the MOPA itself can provide far higher pulse peak powers at lower repetition rates. It should be possible to improve the SHG conversion efficiency by carefully designing the final stage amplifier to better maintain the spectral integrity of the seed laser. Nevertheless, we have still managed to achieve an overall diode-to-green optical conversion efficiency of 37%. The 3 dB spectral bandwidth of the frequency doubled signal at full power was measured to be 0.4 nm as shown in Figure 6.5. The M^2 of the frequency doubled light was also measured to be <1.05.

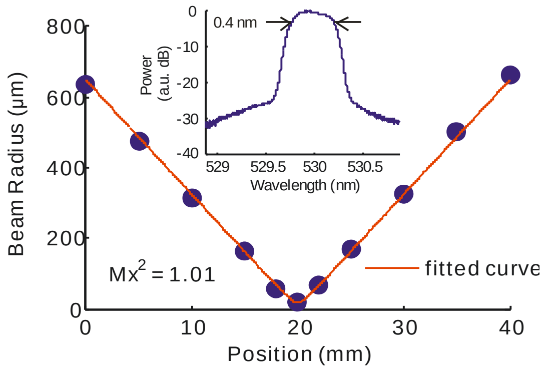

Figure 6.5 SHG M^2 measurement at power of 30 W and in insert: spectrum of the SHG light at a power of 56 W.

6.3 Synchronously Pumped Optical Parametric Oscillator

The setup of synchronously pumped optical parametric oscillator is shown in Figure 6.6. The detailed schematic of the pump source can be found in Figure 5.3 in Chapter 5. Although the polarization extinction ratio (PER) of the output of the MOPA was 19 dB this was degraded somewhat further at the OPO input due to the introduction of an optical isolator to protect the system from spurious feedback. Since a linearly polarized pump beam is required for an efficient parametric interaction in the SPOPO, a $\lambda/2$ waveplate and a polarizing beamsplitter (PER>23 dB) were used to restore the linear polarization. A two-lens telescope and a final focusing lens were used after the polarizing beamsplitter to obtain the required pump waist size.

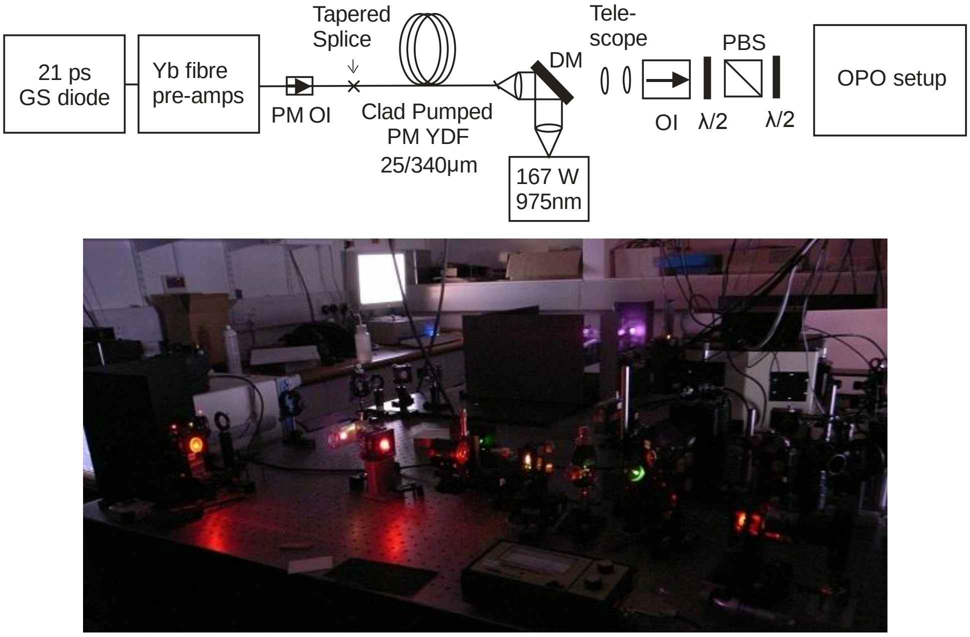

Figure 6.6: Schematic diagram of the pump setup. PBS = Polarizing beamsplitter. Bottom insert shows the SPOPO in working status.

The SPOPO used a periodically poled 5% MgO-doped congruent LiNbO3 (MgO:PPLN) crystal for the nonlinear gain medium. The MgO-doping helps to reduce photorefractive beam distortion and green-induced infrared absorption [25], as well as extending the mid-infrared transparency to ~5 µm [26]. The crystal, provided by Covesion Ltd., was 40 mm long, 10 mm wide and 0.5 mm thick with eleven 0.5 mm wide poled gratings with periods from 26.5 µm to 31.5 µm. It was held in an oven at 150^{o}C to eliminate any residual photorefraction and to provide effective heat sinking. A length of 4 cm was chosen taking into account the size of the beams that can pass through the 0.5 mm by 0.5 mm aperture without clipping and the desire for high nonlinear conversion. The differences in the group velocities of the interacting waves for a 1.06 µm pump, a 1.4 - 1.7 µm signal, and 3 – 4 µm idler are small enough to give a pump acceptance bandwidth that copes with the nonlinearly broadened pump spectrum, as well as minimal temporal walk-off.

6.3.1 Standing-Wave Cavity Optical Parametric Oscillator

Initial trials of the SPOPO performance were carried out with a bow-tie configuration standing-wave resonator, as shown in Figure 6.7. The MgO:PPLN was orientated with its optic axis aligned in the plane of the resonator and thus the pump polarization was also set to this axis.

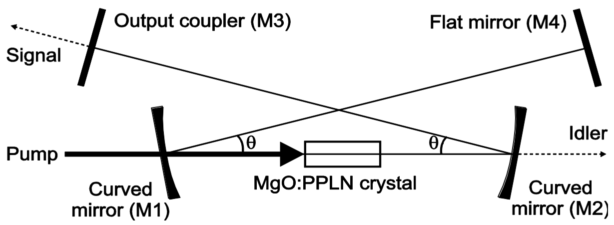

Figure 6.7: Schematic diagram of the standing-wave cavity

If we assume diffraction-limited beams and set the resonated signal and the pump waist spot sizes (radii), ω_s and ω_p, at the centre of the MgO:PPLN crystal to be roughly equal then, given the relationship between these spot sizes and the idler polarization spot size [27], i.e. $\omega i=(\omega_s^{-2}+\omega_p^{-2})^{-1/2}$, we are limited to a range of signal spot sizes between ~90 μm and ~160 μm to avoid clipping of any of the beams by the 0.5 mm by 0.5 mm poling aperture (here we define clipping as occurring when a beam spot size becomes greater than 1/3 of the aperture at any point in the crystal). In practice we used 250 mm radius of curvature mirrors for M1 and M2 (Figure 6.8) and with the cavity length set to match the lowest repetition rate of the pump source (114.8 MHz) the calculated signal waist was ~98 μm with insignificant astigmatism due to the θ=12° folding angle (Figure 6.8). With the focusing lenses available we set the pump beam waist to be 125 μm and hence obtained a calculated idler polarization spot size of 77 μm. Thus the pump focusing is considerably weaker than confocal, (a 56 μm spot size would correspond to confocal focusing over the 4 cm long MgO:PPLN crystal).

All mirrors M1-M4 were highly reflective for the signal wavelength, apart from the output coupler M3, and highly transmissive for the idler in the mid-infrared (CaF_2 substrates are used). The pump input coupler M1 transmitted 92% of the pump light and the idler output coupler M2 transmitted 88% of the generated idler light. A modified Findlay-Clay analysis of the internal losses of the cavity [13], indicated a round-trip signal loss of 9.5%. The MgO:PPLN, with MgF_2 single-layer anti-reflection (AR) coatings on its end-faces, had a measured single-pass transmission of 95% at 1.5 μm. As the round trip involved two passes through the crystal it appears that the internal losses at the signal wavelength were dominated by the AR coatings.

Figure 6.8 shows the initial low-power characterization of the standing-wave SPOPO using an R=95% reflectivity signal output coupler (M3) and a pulse repetition rate of 918.4 MHz (8 pulses circulating in the cavity). Pump depletion of up to 50% was observed with maximum output signal and idler powers of 1.2 W and 1.3 W for a pump power incident on M1 of 11.4 W. The threshold of just over 2 W indicates that even with these relatively large internal losses, the pump source, which is at present scalable to 100 W average power, could provide sufficient peak power to allow SPOPO operation three times above threshold at repetition rates of more than 10 GHz. However, when using a larger output coupling (R=65%) and increased pump power the roll-over of the SPOPO output, which can already be seen in Figure 6.9, became much stronger, with oscillation ceasing at ~21 W of pump power. That thermal effects were, at least in part, responsible for this effect was confirmed by observing that when a 50% duty cycle chopper was placed in the pumping beam to reduce the average power, oscillation was recovered at the high pump power level.

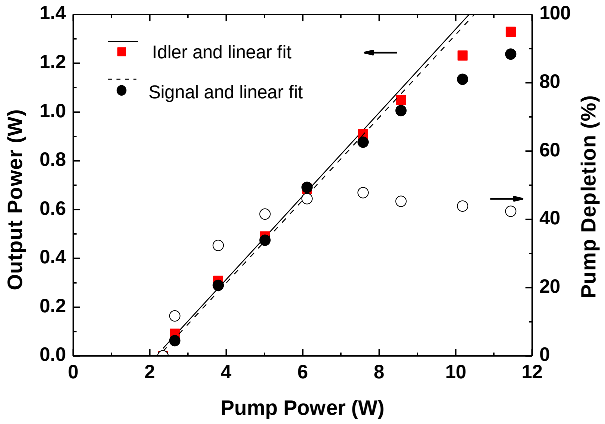

Figure 6.8: Low power characterization of the standing-wave cavity. The linear fits are to the first five data points. The signal output coupler used had a reflectivity of R=95%.

This result is at variance with the simplistic notion that the OPO should not exhibit any significant thermal input. Also, previous reports of high-power operation of periodically-poled $LiTaO_3$ [6], and $LiNbO_3$ [28], did not show such effects. No improvement was seen in this behavior by tuning further away from the mid-infrared transparency boundary to idler wavelengths of less than 3 μm and there was no increase in the pump bandwidth at higher powers in this high repetition rate regime, which might have led to poorer conversion efficiency. As the MgO:PPLN was in contact with a temperature controlled oven (fixed to 0.1 ℃), we would also expect that any physical clipping of the idler beam due to non-diffraction-limited performance would not cause significant variations in temperature. However, further indication of a thermal input to the nonlinear crystal was given by an observed linear tuning of the output signal wavelength by 0.155 nm/W, as the pump power is increased. For a pump power increase from 2.6 W to 23.8 W, the signal wavelength increases by ~3.3 nm, which, if due only to a change in temperature [29], would correspond to a ~6 ℃ rise in temperature within the crystal at the location of the interacting beams.

The $MgO:LiNbO_3$ crystal was in thermal contact with a gold-plated temperature-controlled copper block on one of its 40 mm by 10 mm faces with the other being in contact with an indium-tin-oxide-coated piece of glass (for management of electrostatic effects) such that heat was effectively dissipated from just one side of the crystal. While a full thermal model of this experimental arrangement has not yet been undertaken we note that MgO-doped, or undoped, $LiNbO_3$ has a large value for $(dn_e/dT)/K_c$, where dn_e/dT is the rate of change of the extraordinary refractive index with temperature [30], and K_c is the thermal conductivity. In comparison, the value of $(dn/dT)/K_c$ in a well-known high-power laser material such as YAG is ~20 times smaller. Using these material parameters in a simple cylindrical rod model [31], leads to predictions that if less than 1% of the pump were converted to heat within the volume occupied by the beam then a thermal lens of focal length ~1 cm, sufficient to cause the cavity to become unstable, would be present.

6.3.2 Ring Cavity Optical Parametric Oscillator

In an attempt to reduce the cavity losses and the effect of any thermal aberrations by only having one pass per round trip through the MgO:PPLN, the cavity shown in Figure 6.8 was modified to a ring resonator. In order to continue to match the fundamental repetition rate of 114.8 MHz the overall cavity length was increased by a factor of 2 compared to the standing-wave oscillator and this led to a smaller and more asymmetric calculated signal waist size in the MgO:PPLN of 47 μm (in the plane of the cavity) by 59 μm. To maintain good spatial overlap, the pump waist size was adjusted to 50 μm, leading to an expected idler polarization waist size of ~35 μm and, consequently, an expectation of significant idler clipping due to the increased beam divergence, even if the beam was diffraction-limited. A similar Findlay-Clay analysis to that used for the standing-wave cavity gave a higher value for the round trip losses of 15.7%, despite the single pass through the MgO:PPLN crystal. However, additional losses for the idler in this configuration due to increased diffraction losses and clipping would reduce the parametric gain [32, 33], and hence increase the effective loss as determined by the Findlay-Clay measurement.

Figure 6.9 shows the output power characteristics and pump depletion for 1, 4, and 8 pulses circulating in the cavity for pump average powers up to 24 W, currently limited by the thermal effects in the isolator used between the pump source and the SPOPO. The first observation was that the roll-over effect was not present for the lower repetition rates and while it was still present for the 918.4 MHz results, oscillation was maintained up to the full 24 W of pump power. For 114.8 MHz operation we obtained 7.3 W of signal at 1.54 μm and 3.1 W of idler at 3.4 μm, with a pump depletion that saturated at ~70%. An R=65% output coupler was used for all the results in Figure 6.9 and it is likely that a larger output coupler could have provided greater signal output power for the low repetition rate case, as it operated at 33 times above threshold at maximum power.

The greatly improved performance with the ring resonator suggests that it benefited from only having one pass of the signal through the nonlinear crystal per round trip. Modeling of the ring and standing-wave cavities suggest that they would require thermal lenses of similar strength to drive them into instability and so we speculate that the reduced aberrations imposed on the signal beam by only passing once through the crystal was the more important effect. It may also be the case that the single pass of the signal through the crystal led to less heat being deposited, although the mechanism by which any such absorption occurs is not clear. It is interesting to note that the performance has improved despite the expectation that the idler would not be able to pass through the nonlinear crystal in this configuration, without a significant degree of interception by the surfaces of the MgO:PPLN slab.

The presence of the power roll-over in the high repetition rate results is intriguing as there should be no difference in the thermal load for the different repetition rates. The only change is that the gain is lower due to the reduced peak intensity of the pump pulse, which is reflected in the higher average power threshold.

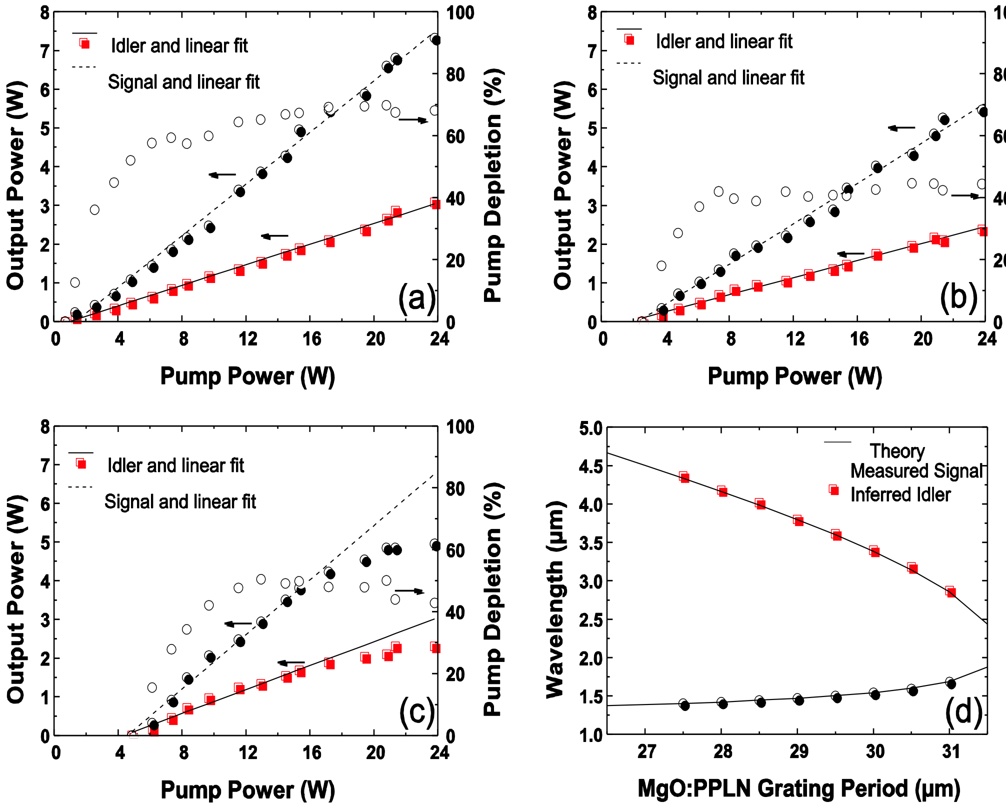

Figure 6.9: Output power characterization of the ring cavity at (a) 114.8 MHz, (b) 459.2 MHz, and (c) 918.4 MHz. The linear fits are to the first ten data points in (c). The signal output coupler used has a reflectivity of R=65%. Wavelength tuning against poled grating period is shown in (d) with the temperature of the crystal held at 150 ℃. The idler wavelengths are inferred from the measured signal wavelengths.

In order to confirm the potential for tunable operation we translated the nonlinear crystal to access gratings with different poling periods. The experimental results, taken at a repetition rate of 918.4 MHz, are shown in Figure 6.9(d) together with the theoretical curve derived from the temperature-dependent Sellmeier equation for MgO-doped congruent $LiNbO_3$ [29]. The temperature of the crystal was set to 150 ℃ and the pump power was adjusted to be approximately 15% higher than the threshold level at each signal wavelength. Tuning was demonstrated between 1.40 µm and 1.68 µm for the signal and 2.87 µm and 4.36 µm for the idler.

Autocorrelation measurements, taken at 918.4 MHz, gave full-width half-maximum pulse durations of ~17 ps (assuming a Gaussian pulse shape) for both signal and idler. Figure 6.10 shows an interferometric autocorrelation of the 3.4 µm idler pulse taken using two-photon absorption in an InGaAs photodiode with an extended sensitivity up to 2.1 µm. The fully modulated fringes suggest a nearly bandwidth-limited pulse, but unfortunately we did not have a suitable spectrometer available to measure the idler spectrum to confirm this.

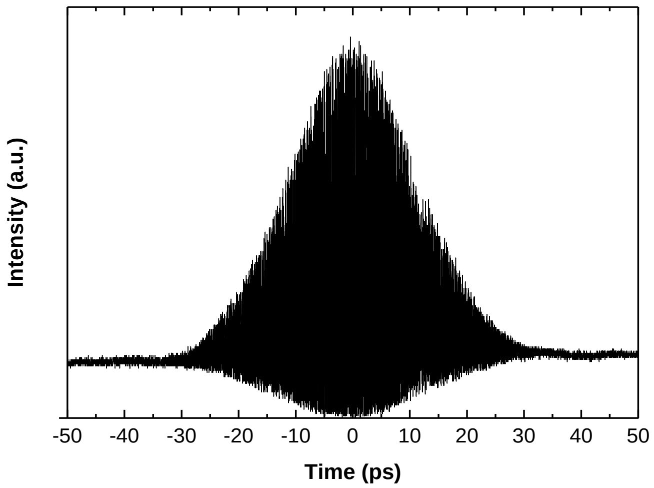

Figure 6.10: Interferometric autocorrelation of the 3.4 μm idler pulse suggesting bandwidth-limited performance. The FWHM pulse duration, assuming a Gaussian temporal pulse shape, is ~17 ps. The individual fringes are too close together to be resolved in this figure.

The beam quality, M^2, for both the signal and idler, again taken at 918.4 MHz, was measured at both medium and high powers. For the signal M^2 measurements, a 100 mm focal length lens was used to produce a beam waist through which a beam profiler was translated, recording the $1/e^2$-beam radius at points along the beam. The M^2 value was then fitted to this data. The beam profiler was not sensitive in the idler spectral region and so a knife-edge method was used to determine the 15% and 85% power transmission points, allowing an estimation to be made of the $1/e^2$-beam radius. This was repeated for several positions along the idler beam spanning the waist region and again an M^2 value was fitted to the data. The results presented in Table 6.1 show that the resonated signal was near diffraction-limited with just a small degradation at higher pump powers. The M^2 of the idler shows a significant departure from diffraction-limited performance, which we expect as the non-resonated beam was composed of an addition of the idler radiation generated from all points along the 4 cm length of nonlinear crystal, which is much greater than the confocal parameter corresponding to the idler polarization waist size. We also note that the M^2 measured in the plane of the resonator (denoted as the x-axis) was consistently worse than in the y-axis. There were various factors that distinguish the two axes and which may be responsible for this difference. These include the asymmetry in the resonated signal spot size due to the angle θ at the curved mirrors, stronger thermal lensing in the x-plane as this corresponds to the heat removal axis due to the slab geometry of the crystal, and the presence of a hard aperture in the x-axis due to the oven.

Table 6.1. M² beam quality measurements

	Signal (1.54 µm)		Idler (3.4 µm)	
Pump Power	M_x^2	M_y^2	M_x^2	M_y^2
11W	1.06	1.01	2.50	1.56
24W	1.20	1.09	3.18	1.58

We also made spectral measurements of the depleted and undepleted pump at high average powers in the two repetition rate extremes, where nonlinear broadening is either absent or at its strongest. The results are shown in Figure 6.11, where we have set the areas under the curves to represent the measured average powers of the input pump and the residual pump after depletion and thus give directly comparable spectra. It appears that depletion occurred across the entire spectrum confirming no limitation due to the phase-matching bandwidth.

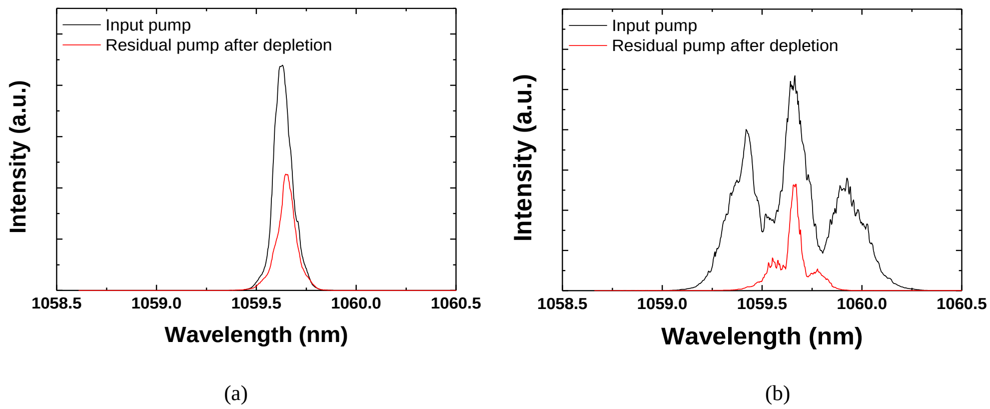

Figure 6.11: Comparison of the spectra of the input pump and the residual pump (after depletion) at 24 W incident average pump power at (a) 918.4 MHz and (b) 114.8 MHz, with the latter spectra showing broadening due to self-phase modulation in the fibre amplifiers. The curves are normalized to the ratio of their measured average powers.

6.4 High power Supercontinuum Generation in PCF

6.4.1 Experimental setup

Figure 6.12 shows the schematic of the setup. The setup is similar to that of the SPOPO except the OPO setup was replaced with 2 m long PCF. The total insertion loss of the isolator, HWP and PBS was approximately 35%. Another HWP before the coupling lens enabled alignment of the polarization axis of the beam to a principal birefringence axis of the PCF.

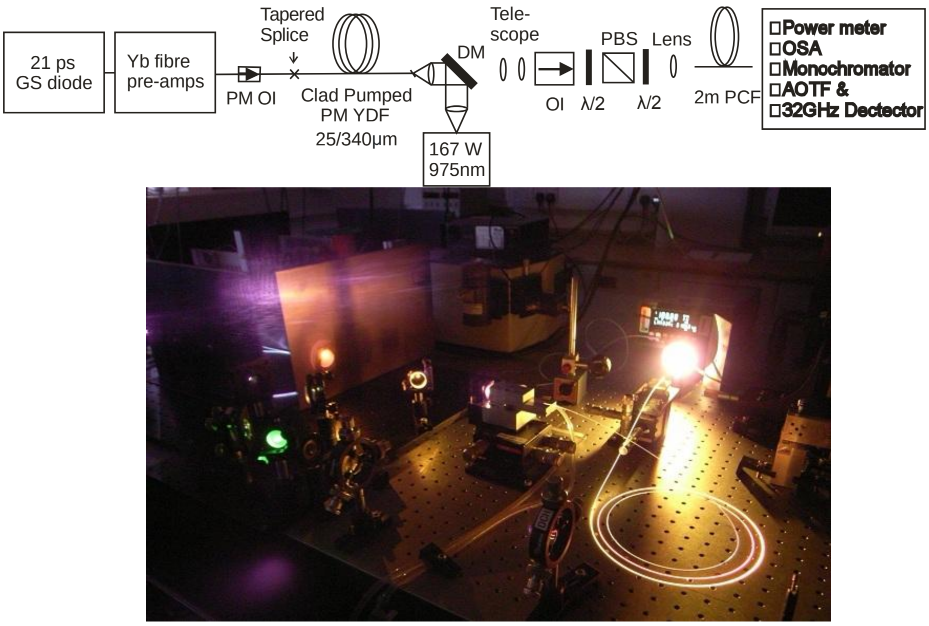

Figure 6.12: Schematic diagram of the Yb^{3+}-doped fibre MOPA and launch to the PCF. Bottom insert shows the SCG setup at 30 W power level

The MOPA system generated linearly polarized, diffraction-limited, 21 ps pulses at user selected repetition rates ranging from 14 MHz to 910 MHz and with an average output power up to 100 W as described previously in Chapter 4. The output beam from the MOPA had an M^2 of ≤1.1 and the stability of the beam quality was ensured by the tapered splice. Spectra were recorded using a fibre-coupled OSA (ANDO AQ6315) in the 350-1750 nm range and a free-space coupled monochrometer in combination with a PbS detector for the 1.75-3.5 µm range.

6.4.2 Fibre characteristics and high average power supercontinuum results

The PCF used for the SCG was an all silica structure fabricated using the stack and draw technique and had a core diameter of ~4.37 µm and a high air-fill-fraction in the cladding as shown by the photograph in Figure 6.13(a). The zero dispersion wavelength is at ~1012 nm such that the wavelength of our picosecond pump source lies in the anomalous dispersion region. The dominant mechanisms leading to spectral broadening are likely to be modulation instability, leading to a soliton continuum and subsequent blue expansion due to soliton trapping [15, 21, 34]. The dispersion data shows the experimentally measured points overlaid on the curve calculated by modeling using a commercial finite element module (COMSOL Multiphysics) based on the optical micrograph of the fibre (shown inset). The pitch (Λ) of the air holes was measured to be 5.29 μm with d/Λ ~ 0.956. Figure 6.13(b) shows the loss of the PCF measured using the cut-back method. The loss was ~0.175 dB/m at the 1.06 μm pump wavelength and ~0.5 dB/m at the OH loss-peak in the 1.35-1.40 μm region.

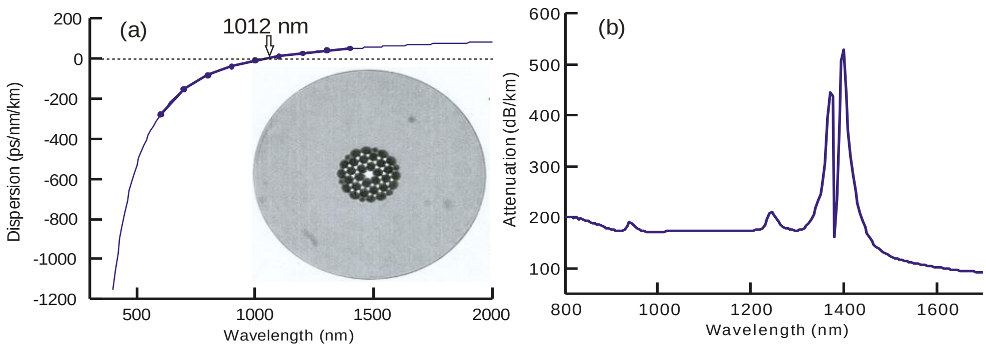

Figure 6.13: (a) Dispersion profile of the PCF. (b) Measured attenuation data.

The launch optics comprised a telescope that matched the beam size to a high-NA aspheric coupling lens at the input of the fibre. Several focal lengths were tested before finally selecting an f= 3.1 mm aspheric lens. Figure 6.14 shows the average output power of the SC source as a function of the incident pump power when operating at the 114.8 MHz repetition rate at which we obtained the highest power continuum of 39 W. The launch efficiency was > 80% at incident powers below 30 W. We believe that the observed roll-off in output power vs. incident pump power was primarily due to beam quality degradation inside the bulk isolator at increasing power. The far field pattern of the output beam is shown inset to Figure 6.14(top). Note that the central region of the image is saturated in order to show the low intensity side-lobes [35]. The lower inset to Figure 6.14 shows the separate components of the visible spectrum that were observed after passing the continuum through a prism.

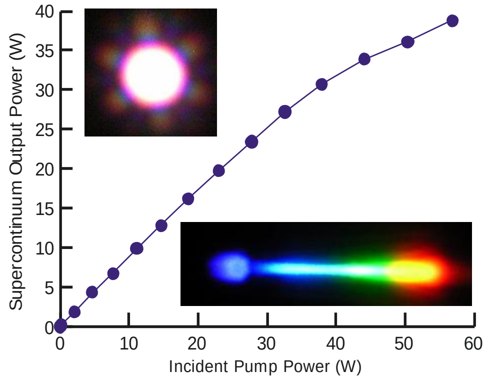

Figure 6.14: Supercontinuum output power vs incident power. Inset shows the far field pattern of the output beam and prism separated white light.

It is found that the highest continuum output power was limited by damage to the fibre output facet. (We are uncertain about the mechanism involved although we note that damage caused by UV absorption is a possible contributing factor [36].) In future an angle-polished end-cap could be used to avoid back-reflections and expand the mode, but we did not have the mechanics available in the short term to achieve the angle necessary for this high NA fibre. We tested the system at high power for ~20 minute periods at SCG powers of up to ~35 W and we did not observe any significant change in the output power, output spectrum or mode shape. At the maximum 39 W power level the heat load on the fibre input prevented us from operating for extended periods because of drifting of the launch optics. However we also ran the system daily for ~20-30 minute periods for over a week of operation with reduced repetition rates at the 20 W level such that the peak power was similar to that of the 39 W SCG results and again we did not observe any photodarkening of the SCG fibre.

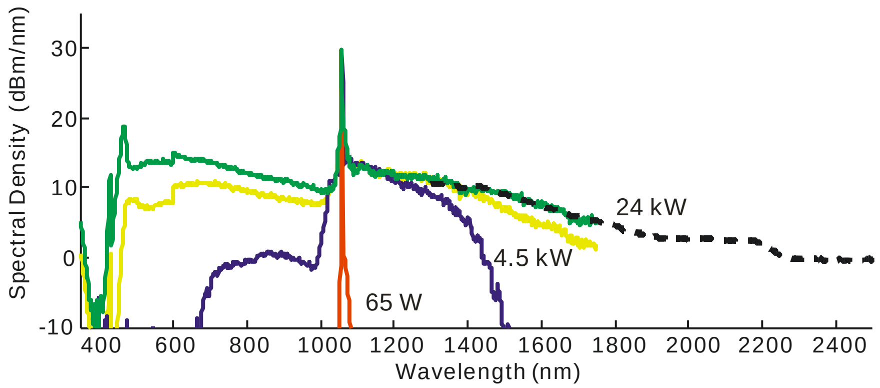

Figure 6.15: Supercontinuum evolution in a 2 m long PCF at 0.15 W, 11 W and 57 W of incident pump power at repetition rate of 114.8 MHz. Solid lines – OSA measurements, dashed line – measurements with monochrometer and PbS detector. (The top lines in green/yellow show spectra with input polarization aligned to orthogonal birefringence axes.)

Figure 6.15 shows the spectral evolution at an incident power level of 0.15 W, 11 W and 57 W at a repetition rate of 114.8 MHz. The labels show the peak powers of the launched pump pulses. We observed that the colour of the continuum spectrum evolved along the fibre and when operating with a maximum average power the continuum was visibly white after 1.5 m. However, optimization using cut-back measurements showed that the spectral flatness improved using a 2.0 m length of PCF and therefore a 2.0 m length was used for the results shown above. Longer fibre lengths produced lower output powers due to the fibre loss. Numerical integration of the continuum spectrum indicated that just 12% of the power remained at the pump wavelength. The spectrum covered the range from 400 nm to 2300 nm with spectral flatness across the visible region of better than 10 dB and a blue peak at a wavelength of 430 nm (shown in Figures. 6.14 and 6.15).

The continuum spectra with various orientations of the half-wave-plate at the fibre input were recorded. We first measured the angles of the fibre birefringence axes by using low energy pulses and an analyzer PBS at the PCF output. The measured birefringent beat length was 35 mm and the weak birefringence was due to the relatively large core. At the maximum 39 W Supercontinuum power level, the broadest continuum was produced with the polarization aligned to one of the principal axes and the narrowest spectrum was produced at the orthogonal axis. The variation in the spectra with the input polarization aligned to the orthogonal birefringence axes can be seen in Figure 6.15.

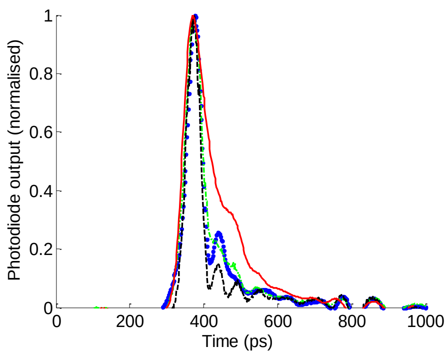

Figure 6.16: Pulse shape of transmitted low power pump (blue dotted line), filtered at 1186.6 nm (green dash dotted line), filtered at 1317.6 nm (black dashes) and broadband (solid red line).

Figure 6.16 shows the temporal profiles of the optical pulses at the output of the 2 m PCF measured using a 32 GHz bandwidth InGaAs photodiode and sampling scope. The broadest pulse corresponds to the full bandwidth of the SC spectrum incident on the diode. When the pulses were coupled onto the orthogonal fibre axis, the main peak was delayed and appeared at the position of the shoulder to the rear of the pulse, so we attribute that shoulder to stray power coupled onto the orthogonal fibre axis. The shorter pulse shown by the blue dotted line in Figure 6.16 was obtained with lower pump power (PCF output of 50 mW). We also filtered the continuum spectra with an acousto-optic tunable filter (AOTF) to produce 1.2 nm bandwidth spectra at 1186.6 nm and 1317.6 nm and the pulse durations were within the measurement resolution (Figure 6.16), confirming that the wavelength shifting had not increased the input duration substantially. (Note that the extended tail was an artifact of the diode/scope system since it was also seen in an impulse response measurement using clean 200 fs pulses.)

For comparison we tested two commercially available silica PCFs produced by NKT Photonics (formerly Crystal Fibre) using our high power MOPA as the seed. The larger core fibre (SC-5.0-1040 data available from www.nktphotonics.com) had a mode field diameter (MFD) of 4 μm and ZDW at 1040 nm and with a 10 m length the maximum transmitted power at the 128 MHz repetition rate was 10 W with a yellow, rather than white colour at the output and a minimum wavelength of 489 nm. We did not perform cut-back measurements on the fibre but we observed the colour evolution on the spool and a minimum length of between 5 m and 7 m was required for the yellow colour to develop. In comparison, the fibre fabricated at Central Glass & Ceramic Research Institute (CGCRI) had a more rapid onset of visible continuum, improved power transmission and blue spectral components extending to 409 nm. The second commercial fibre tested (NL-1050-ZERO-2) had a smaller core with MFD of 2.2 μm and ZDWs at 975 nm and 1125 nm and in this case no visible light was generated at the maximum transmitted power of 1 W (limited by facet damage).

6.4.3 High peak power Supercontinuum results

Since the maximum average power was limited by thermal damage, we tested the fibre with lower repetition rates which produce higher pulse energies for a given average power. This led to an increase in the input peak power density before thermal damage or output facet damage became a problem. In this case the limit on continuum power was dictated by the input facet damage due to the high peak intensity.

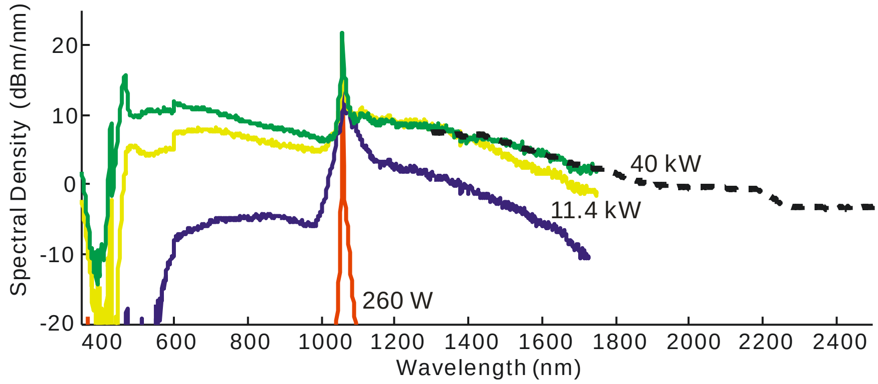

Figure 6.17: Supercontinuum evolution in a 2 m long PCF at 0.15 W, 7 W and 25 W of incident pump power at repetition rate of 28 MHz. (The top lines in green/yellow show spectra with input polarization aligned to orthogonal birefringence axes. Linestyles as in Figure 6.15.)

Figure 6.17 shows the SCG obtained at a repetition rate of 28 MHz. The maximum average power was 20 W and the peak power spectral density across the visible of 26.9 W/nm compared to 12.5 W/nm for the highest average power results in Figure 6.15. The overall profiles of the continuum spectra are similar at both repetition rates but in Figure 6.17, the visible power density is ~10 dBm/nm below the input wavelength peak whereas in Figure 6.15, the visible power density is ~15 dBm/nm below the peak so there is more effective conversion of pump to visible wavelengths at the higher peak power. As with the high average power results (Figure 6.15) the variation in the spectral bandwidth with the input polarization was investigated and we found that with the maximum input peak power of 40 kW, the SCG was broadest and narrowest with the polarization aligned to the fibre's orthogonal birefringence axes with the variation in spectra shown in Figure 6.17. The peak power for facet damage when using the f=3.1 mm launch lens was ~40 kW +/- 3 kW at repetition rates between 14 MHz and 56 MHz. In future, power scaling may therefore be possible by using a mode-expanding end-cap at the input to the fibre in order to reduce the intensity at the air/glass interface.

6.5 Conclusion

In this chapter, various wavelength conversion results based on the high performance picosecond fibre MOPA are presented. Our results span the spectral range spanning the UV to the mid-IR and show the versatility of fibre based laser sources.

A frequency doubled green source at 530 nm pumped with the picosecond source at user selectable repetition rates of up to 910 MHz and an average output power in excess of 100 W at 1.06 μm was demonstrated. Stable, diffraction limited, picosecond pulsed 56

W of green light at 530 nm at an overall conversion efficiency of 56% by using a 15 mm long LBO crystal was generated. The diode-to-green optical power conversion efficiency was 37%. Further power scaling is primarily limited by the spectral integrity of the fundamental light. Newly optimised PM amplifiers offering better spectral integrity should increase the conversion efficiency to 80% according to theory.

I also presented a synchronously pumped picosecond optical parametric oscillator (OPO). At 24 W of pump power, up to 7.3 W at 1.54 µm and 3.1 W at 3.4 µm were obtained. The periodically poled MgO-doped $LiNbO_3$ OPO operates with ~17 ps pulses at a fundamental repetition rate of 114.8 MHz but can be switched to higher repetition rates of up to ~1 GHz. Tunabilty between 1.4 µm and 1.7 µm (signal) and 2.9 µm and 4.4 µm (idler) is demonstrated by translating the nonlinear crystal to access different poling-period gratings and typical M^2 values of 1.1 by 1.2 (signal) and 1.6 by 3.2 (idler) are measured at high power for the singly resonant oscillator.

The picosecond fibre MOPA pumped Supercontinuum source with 39 W output, spanning at least 0.4-2.25 µm at a repetition rate of 114.8 MHz was also presented. The 2 m long PCF had a large, 4.4 µm diameter core and a high-delta design which led to an 80% coupling efficiency, high damage threshold and rapid generation of visible continuum generation from the picosecond input pulses. The high and relatively uniform power density across the visible spectral region was ~31.7 mW/nm corresponding to peak power density of ~12.5 W/nm for the 21 ps input pulses. The peak power density was increased to 26.9 W/nm by reducing the repetition rate to 28 MHz. This represents an increase in both average and peak power compared to previously reported visible Supercontinuum sources from either CW pumped or pulsed-systems at this time. Further power scaling and an extended blue-shift represents a possible direction for future work. Besides considering the structural parameters of the PCF, increasing the blue-shift of the SCG is also possible by modifying the glass composition of the fibre [37]. Extending the mid-IR to longer wavelengths using this approach is also a topic worthy of further study.

References

[1] J. Golden, "Green lasers score good marks in semiconductor material processing," Laser Focus World, vol. 28, pp. 75-6, (1992).

[2] A. Bachmann, S. Wyler, R. Ruszat, R. Casella, T. Gasser, and T. Sulser, "80W high-power KTP laser vaporization of the prostate clinical results after 110 consecutive procedures," Eur Urol. 3 (suppl 2), pp. 145-145, 2004.

[3] F. Kienle, K. K. Chen, S.-u. Alam, C. B. E. Gawith, J. I. Mackenzie, D. C. Hanna, D. J. Richardson, and D. P. Shepherd, "High-power, variable repetition rate, picosecond optical parametric oscillator pumped by an amplified gain-switched diode," Opt. Express, vol. 18, pp. 7602-7610, 2010.

[4] W. E. Glenn, "Solid-state light sources for color projection," Advanced Solid-State Lasers, vol. 10 of OSA Trends in Optics and Photonics Series, pp. 38–42, (1997).

[5] S. Lecomte, R. Paschotta, S. Pawlik, B. Schmidt, K. Furusawa, A. Malinowski, D. J. Richardson, and U. Keller, "Optical parametric oscillator with a pulse repetitionrate of 39 GHz and 2.1-W signal average outputpower in the spectral region near 1.5 μm," Opt. Lett., vol. 30, pp. 290-292, 2005.

[6] T. Südmeyer, E. Innerhofer, F. Brunner, R. Paschotta, T. Usami, H. Ito, S. Kurimura, K. Kitamura, D. C. Hanna, and U. Keller, "High-power femtosecond fiber-feedback optical parametricoscillator based on periodically poled stoichiometric LiTaO3," Opt. Lett., vol. 29, pp. 1111-1113, 2004.

[7] A. Robertson, M. E. Klein, M. A. Tremont, K.-J. Boller, and R. Wallenstein, "2.5GHz repetition-rate singly resonant optical parametric oscillator synchronously pumped by a mode-locked diode oscillator amplifier system," Opt. Lett., vol. 25, pp. 657-659 (2000).

[8] M. V. O'Connor, M. A. Watson, D. P. Shepherd, D. C. Hanna, J. H. V. Price, A. Malinowski, J. Nilsson, N. G. R. Broderick, D. J. Richardson, and L. Lefort, "Synchronously pumped optical parametric oscillator driven by a femtosecond mode-locked fiber laser," Opt. Lett., vol. 27, pp. 1052-1054, 2002.

[9] S. Lecomte, R. Paschotta, M. Golling, D. Ebling, and U. Keller, "Synchronously pumped optical parametric oscillators in the 1.5-μm spectral region with a repetition rate of 10 GHz," J. Opt. Soc. Am. B, vol. 21, pp. 844-850, 2004.

[10] S.-W. Chu, T.-M. Liu, C.-K. Sun, C.-Y. Lin, and H.-J. Tsai, "Real-time second-harmonic-generation microscopy based on a 2-GHz repetition rate Ti:sapphire laser," Opt. Express, vol. 11, pp. 933-938, 2003.

[11] A. Vogel, J. Noack, G. Hüttman, and G. Paltauf, "Mechanisms of femtosecond laser nanosurgery of cells and tissues," Applied Physics B: Lasers and Optics, vol. 81, pp. 1015-1047, 2005.

[12] F. Ganikhanov, S. Carrasco, X. S. Xie, M. Katz, W. Seitz, and D. Kopf, "Broadly tunable dual-wavelength light source for coherent anti-Stokes Raman scattering microscopy," Opt. Lett. , vol. 31, pp. 1292-1294 (2006).

[13] D. C. Hanna, M. V. O'Connor, M. A. Watson, and D. P. Shepherd, "Synchronously pumped optical parametric oscillator with diffraction-grating tuning," J. Phys. D: Appl. Phys. , vol. 34, pp. 2440-2454 2001.

[14] H.S.S.Hung, J.Prawiharjo, D.C.Hanna, and D.P.Shepherd, "Spectral phase and amplitude measurements of parametric transfer in a SPOPO," in CLEO/QELS 2007 Baltimore 6-11 May 2007 CTuM4.

[15] J. M. Dudley, G. Genty, and S. Coen, "Supercontinuum generation in photonic crystal fiber," Reviews of Modern Physics, vol. 78, p. 1135, 2006.

[16] R. R. Alfano, Ed., The Supercontinuum Laser Source. New York: Springer, 2005, p.^pp. Pages.

[17] P. Russell, "Photonic crystal fibers," Science, vol. 299, pp. 358-362, Jan 17 2003.

[18] J. C. Knight, "Photonic crystal fibres," Nature, vol. 424, pp. 847-851, Aug 14 2003.

[19] J. K. Ranka, R. S. Windeler, and A. J. Stentz, "Visible continuum generation in air-silica microstructure optical fibers with anomalous dispersion at 800 nm," Optics Letters, vol. 25, pp. 25-27, 2000.

[20] J. C. Travers, A. B. Rulkov, B. A. Cumberland, S. V. Popov, and J. R. Taylor, "Visible supercontinuum generation in photonic crystal fibers with a 400W continuous wave fiber laser," Optics Express, vol. 16, pp. 14435-14447, 15 September 2008.

[21] J. M. Stone and J. C. Knight, "Visibly "white" light generation in uniform photonic crystal fiber using a microchip laser," Opt. Express, vol. 16, pp. 2670-2675, 2008.

[22] T. Schreiber, J. Limpert, H. Zellmer, A. Tunnermann, and K. P. Hansen, "High average power supercontinuum generation in photonic crystal fibers," Optics Communications, vol. 228, pp. 71-78, 2003.

[23] A. B. Rulkov, M. Y. Vyatkin, S. V. Popov, J. R. Taylor, and V. P. Gapontsev, "High brightness picosecond all-fiber generation in 525-1800nm range with picosecond Yb pumping," Optics Express, vol. 13, pp. 377-381, 2005.

[24] A. Kudlinski, A. K. George, J. C. Knight, J. C. Travers, A. B. Rulkov, S. V. Popov, and J. R. Taylor, "Zero-dispersion wavelength decreasing photonic crystal fibers for ultraviolet-extended supercontinuum generation," Optics Express, vol. 14, pp. 5715-5722, 2006.

[25] Y. Furukawa, K. Kitamura, A. Alexandrovski, R. K. Route, M. M. Fejer, and G. Foulon, "Green-induced infrared absorption in MgO doped LiNbO3," Appl. Phys. Lett. , vol. 78, pp. 1970-1972 (2001).

[26] T. Andres, P. Haag, S. Zelt, J. P. Meyn, A. Borsutzky, R. Beigang, and R. Wallenstein, "Synchronously pumped femtosecond optical parametric oscillator of congruent and stoichiometric MgO-doped periodically poled lithium niobate," Applied Physics B: Lasers and Optics, vol. 76, pp. 241-244, 2003.

[27] M. J. McCarthy and D. C. Hanna, "All-solid-state synchronously pumped optical parametric oscillator," J. Opt. Soc. Am. B, vol. 10, pp. 2180-2190, 1993.

[28] C. W. Hoyt, M. Sheik-Bahae, and M. Ebrahimzadeh, "High-power picosecond optical parametric oscillator based on periodically poled lithium niobate," Opt. Lett., vol. 27, pp. 1543-1545, 2002.

[29] O. Gayer, Z. Sacks, E. Galun, and A. Arie, "Temperature and wavelength dependent refractive index equations for MgO-doped congruent and stoichiometric LiNbO3," Applied Physics B: Lasers and Optics, vol. 91, pp. 343-348, 2008.

[30] L. Moretti, M. Iodice, F. G. D. Corte, and I. Rendina, "Temperature dependence of the thermo-optic coefficients of lithium niobate, from 300 to 515 K in the visisble and infrared regions," J. Appl. Phys., vol. 98, p. 036101, 2005.

[31] W. A. Clarkson, "Thermal effects and their mitigation in end-pumped solid-state laser," J. Phys. D: Appl. Phys. , vol. 34, pp. 2381-2395 2001.

[32] D. D. Lowenthal, "CW periodically poled LiNbO3 optical parametric oscillator model with strong idler absorption," IEEE J. Quantum Electron., vol. QE-34, pp. 1356-1366 1998.

[33] L. Lefort, K. Puech, G. W. Ross, Y. P. Svirko, and D. C. Hanna, "Optical parametric oscillation out to 6.3 μm in periodically poled lithium niobate under strong idler absorption," Appl. Phys. Lett. , vol. 73, pp. 1610-1612 1998.

[34] S. Coen, A. H. L. Chan, R. Leonhardt, J. D. Harvey, J. C. Knight, W. J. Wadsworth, and P. St.J.Russell, "White-light supercontinuum generation with 60-ps pump pulses in a photonic crystal fiber," Optics Letters, vol. 26, pp. 1356-1358, 2001.

[35] N. A. Mortensen and J. R. Folkenberg, "Near-field to far-field transition of photonic crystal fibers: symmetries and interference phenomena," Optics Express, vol. 10, pp. 475-481, 2002.

[36] N. Yamamoto, L. Tao, and A. P. Yalin, "Single-mode delivery of 250 nm light using a large mode area photonic crystal fiber," Optics Express, vol. 17, pp. 16933-16940, 2009.

[37] M. H. Frosz, P. M. Moselund, P. D. Rasmussen, C. L. Thomsen, and O. Bang, "Increasing the blue-shift of a supercontinuum by modifying the fiber glass composition," Optics Express, vol. 16, pp. 21076-21086, 2008.

Chapter 7 Summary and Future Work

Overview

This final chapter summarises the work and results presented throughout this thesis on the advancement of high power pulsed Yb^{3+}-doped fibre MOPAs and describes areas of possible future work. My work towards pulsed fibre MOPA can be conveniently divided into two parts according to the pulse durations targetted; nanosecond and picosecond sources. Section 7.1 will discuss nanosecond systems and their applications and Section 7.2 picosecond systems and their applications. In Section 7.3 I will draw some general conclusions.

7.1 Nanosecond fibre MOPA and applications

In this work, nanosecond pulses generated from a semiconductor laser were amplified in a Yb^{3+}-doped fibre amplifier chain to over 300 W of average power. Shaping of the pulses from the semiconductor seed using an electro-optic modulator allowed various custom defined pulse shapes to be produced at the amplifier output: Square, step, triangular as well as smooth pulse shapes (parabolic and Gaussian) were achieved. A linearly polarized version of the amplifier system was built for a variety of wavelength conversion experiments utilizing the pulse shaping technique to improve the frequency conversion performance.

A high power pulsed fibre laser pumped nanosecond pulsed PPMgLN-based OPO was demonstrated. A total parametric output power of over 9 W was obtained, with over 2.4 W emitted at 3.5 μm. The pulse shaping technique played an important role in avoiding deleterious nonlinear effects and thus allowed the pulsed PM fibre laser to operate at a higher pulse energies/power levels. The main limiting factor for further power scaling in these experiments was risk of damage resulting from the small beam waist inside the crystal. A larger dimension crystal should help in this regard and is planned within the group. A very high power PPMgO:CLN based OPO using an elliptical shape beam has been demonstrated recently [1]; this result suggests that further power scaling should also be possible by applying spatial mode shaping techniques to our current fibre MOPA.

In addition, using the nanosecond fibre MOPA as a pump source, (simultaneous) high power wavelength doubling and frequency doubling experiments were carried out. Up to

12.7 W of mid-IR output at wavelengths around 2 μm from a degenerate PPLN OPO and up to 9.8 W of visible output power at 530 nm from a LBO crystal were achieved. At maximum pump power, conversion efficiencies of 36% for the 2 μm mid-IR output and 27% for the visible output were achieved. The broadband IR output of the OPO had a FWHM spectral bandwidth in excess of 170 nm. The visible output was measured to have an M^2 of 1.2. Temporal pulse-shaping of the MOPA seed pulses allowed for generation of near flat-top output pulses, resulting in enhancement of the SHG conversion efficiency from 30% to 33%. Higher conversion efficiency should be possible by increasing the peak power from the nanosecond fibre MOPA [2]. Unfortunately, the limited time available for these experiments during the LAMPS project meant that we were not able to do these experiments at the time.

We also demonstrated SRS based wavelength shifting to selected individual Raman orders with good adjacent order suppression ratios in an external fibre using pulse shape control implemented in our fibre MOPA. By controlling the pump power whilst maintaining flat-topped pulses the generation of individual Stokes lines up to the 9th order was obtained. Using this concept with optimized fibre designs and lengths as well as other Raman gain media it is possible to envisage a host of tunable lasers operating at discrete tunable wavelengths in the visible/near IR. Visible sources are very useful in the biological and medical research area. The source developed in this work would be suitable for various biomedical experiments [3-5].

7.2 Picosecond fibre MOPA and applications

A fiberized, diode-seeded, YDFA MOPA system generating linearly polarized, diffraction-limited, 21 ps pulses at repetition rates ranging from 56 MHz to 908 MHz and at average output powers of 100 W was developed. The polarization stability is ensured by using PM amplifier fibres and the stability of the mode quality is ensured by using a tapered splice to the final amplifier. At the lowest repetition rate of 56 MHz the 21 ps pulses from our system have a maximum energy of 1.7 μJ, and a peak power of 85 kW. The system demonstrates that an attractive combination of controllable repetition-rate gain-switched diode seed and high-power single-mode PM-fibre amplifiers can create a source suitable for a wide variety of applications. In addition, pulse compression of the pulses to durations as short as 1.1 ps was realized by exploiting the SPM induced spectral broadening that was observed at the highest pulse energies and adding a grating-based compressor at the output. A maximum compression factor of 17 was achieved and a corresponding enhancement in peak power to ~590 kW should be possible with the use of optimized compressor gratings. We used 4.2 ps pulses at a repetition rate of 227 MHz and an average (compressed) output power of 52 W to demonstrate 26 W of visible laser power (50% SHG efficiency).

Based on the PM YDFA seeded by a GS-laser diode, I have also managed to generate 56 W of green light at 530 nm at an overall conversion efficiency of 56% by using a 15 mm long LBO crystal (for 17 ps pulses). Further power scaling is primarily limited by the spectral integrity of the fundamental beam. This high power green source is being investigated for material processing applications; preliminary results show that it allows better quality of various ceramics than utilising the unconverted beam at 1 μm. Further power scaling of the SHG and better conversion efficiency should be possible using higher pump powers and new fibre designs in the final stage of the fibre MOPA [6].

A high power picosecond optical parametric oscillator pumped by this fibre system was also demonstrated. The SPOPO can deliver pulses at 114.8 MHz, 229.6 MHz, 459.2 MHz, or 918.4 MHz simply by controlling the source repetition rate via a pulse picker and having 1, 2, 4, or 8 pulses circulating in the SPOPO cavity, without any need to adjust the cavity length. Output powers as high as 7.3 W at 1.54 μm and 3.1 W at 3.4 μm were observed with 24 W of pump power, and tunability between 1.4 μm and 1.7 μm (signal) and 2.9 μm and 4.4 μm (idler) was demonstrated. The pulse duration for both the signal and idler was ~17 ps. Higher overall efficiency was realized recently [7]. By developing a higher peak power and pulse energy pump laser higher pulse energies and higher efficiencies should be attainable and are being pursued [8].

A picosecond fibre MOPA pumped high power Supercontinuum source covering at least the 0.4-2.25 μm spectral region was also successfully demonstrated. Average output powers as high as 39 W with > 80% launch efficiency and 87% pump depletion were achieved at a pulse repetition rate of 114.8 MHz. A power density of up to 31.7 mW/nm with good uniformity was measured across the full visible spectral range. At a reduced repetition rate of 28 MHz the peak power spectral density in the visible was 26.9 W/nm with 93% pump depletion, an average power of 20 W and an overall conversion efficiency of 74%.

Further Supercontinuum average power scaling is of great interest for applications such as communications, environment measurement and remote sensing. In our case, the limiting factor for power scaling is damage of the output facet of the fibre. The fibre end failure may be due to material absorption at the UV and Mid-IR. Fibre end micro-structure sealing or new fibre designs may help to overcome this problem.

7.3 Conclusions

My project concentrated on scaling the power from pulsed fibre laser whilst maintaining good control of the output pulses (spatial mode quality, pulse shape, polarisation, spectrum etc). Benefiting from the MOPA approach precise control of the seed laser allows high quality output pulses that can be tailored according to the end application requirements. Many applications can benefit in terms of higher efficiency and better output quality because of the enhanced performance of the laser. The pump source can be highly compact and incorporate a minimum number of free-space components.

In conjunction with the various techniques of nonlinear conversion described, the fibre MOPA becomes even more versatile. A wavelength converted source based on nonlinear conversion pumped by a fibre MOPA is suitable for many research and industrial applications.

However, there is still space for improving the performance of fibre lasers, such as increasing the output peak power and output pulse energy. Higher peak power not only helps in industrial applications [9] but also results in better wavelength conversion efficiency [2]. In my experiments, the output peak power of my laser was limited by the design of final stage LMA Yb^{3+}-doped fibre, which has a relatively low pump absorption and conservative mode field diameter. The fibres I used were the best commercially available at the time since my access to experimental fibres from the ORC was limited due to the fire of 2005 that destroyed our in-house fabrication facilities. The relatively long fibre device length (few metres) resulted in modest nonlinear thresholds (10 s of kWs) compared to what is now possible using the latest research fibres and limited the scaling of peak power (and hence pulse energy) in my work. Towards the end of my project improved fibre designs [6, 10] became available within the community and should allow at a factor of 10 improvement in peak power performance if incorporated in my systems. A factor of 100 may ultimately be achievable - although fiberized means to pump these new fibres still need to be developed and fibre performance and reliability confirmed. Future extensions of work should exploit these new fibres along with the latest developments in nonlinear frequency conversion media. The possibility of using my lasers in conjunction with poled optical fibres holds out the promise of a range of truly all fibre sources operating at diverse wavelengths. Further extension of wavelength conversion to the soft X-ray [11, 12] and THz regions [13, 14] is also a promising area for future research, as is coherent/spectral beam combination [15] of multiple pulsed fibre lasers to reach powers far beyond the single fibre limit.

References

[1] Y. Peng, W. Wang, X. Wei, and D. Li, "High-efficiency mid-infrared optical parametric oscillator based on PPMgO:CLN," Opt. Lett., vol. 34, pp. 2897-2899, 2009.

[2] S. Koichi, H. Ryusuke, S. Hiroaki, T. Kazuyoku, Y. Shigeru, and N. Kenzo, "High-peak power pulse amplification using Yb doped fiber and second harmonic generation," 2007, pp. TuA4-8.

[3] E. Auksorius, B. R. Boruah, C. Dunsby, P. M. P. Lanigan, G. Kennedy, M. A. A. Neil, and P. M. W. French, "Stimulated emission depletion microscopy with a supercontinuum source and fluorescence lifetime imaging," Opt. Lett., vol. 33, pp. 113-115, 2008.

[4] V. Kapoor, F. V. Subach, V. G. Kozlov, A. Grudinin, V. V. Verkhusha, and W. G. Telford, "New lasers for flow cytometry: filling the gaps," Nat Meth, vol. 4, pp. 678-679, 2007.

[5] D. M. Owen, E. Auksorius, H. B. Manning, C. B. Talbot, P. A. A. de Beule, C. Dunsby, M. A. A. Neil, and P. M. W. French, "Excitation-resolved hyperspectral fluorescence lifetime imaging using a UV-extended supercontinuum source," Opt. Lett., vol. 32, pp. 3408-3410, 2007.

[6] M. K. H. Fabio Di Teodoro, Joseph Morais, and Eric C. Cheung, "High peak power operation of a 100µm-core, Yb-doped rod-type photonic crystal fiber amplifier," in Fiber Lasers VII: Technology, Systems, and Applications, Proc. of SPIE Vol. 7580, 758006.

[7] O. Kokabee, A. Esteban-Martin, and M. Ebrahim-Zadeh, "Efficient, high-power, ytterbium-fiber-laser-pumped picosecond optical parametric oscillator," Opt. Lett., vol. 35, pp. 3210-3212, 2010.

[8] F. Kienle, P. Siong Teh, S.-U. Alam, C. B. E. Gawith, D. C. Hanna, D. J. Richardson, and D. P. Shepherd, "Compact, high-pulse-energy, picosecond optical parametric oscillator," Opt. Lett., vol. 35, pp. 3580-3582, 2010.

[9] A. Ancona, F. Röser, K. Rademaker, J. Limpert, S. Nolte, and A. Tünnermann, "High speed laser drilling of metals using a highrepetition rate, high average power ultrafastfiber CPA system," Opt. Express, vol. 16, pp. 8958-8968, 2008.

[10] T. Fabio Di, "High-Peak-Power Pulsed Fiber Lasers," in Advanced Solid-State Photonics, OSA Technical Digest Series (CD) 2008, p. WA1.

[11] R. T. C. T.J.Butcher, P.Horak, F.Poletti, J.G.Frey, W.S.Brocklesby, "Spatio-spectral technique to verify pump-pulse propagation model in an Ar-filled capillary in the presence of high harmonic generation," presented at the Photon 10 Southampton 2010.

[12] C. Spielmann, N. H. Burnett, S. Sartania, R. Koppitsch, M. Schnürer, C. Kan, M. Lenzner, P. Wobrauschek, and F. Krausz, "Generation of Coherent X-rays in the Water Window Using 5-Femtosecond Laser Pulses," Science, vol. 278, pp. 661-664, October 24, 1997 1997.

[13] A.Malinowski, D.Lin, K.K.Chen, S.-U.Alam, D.J.Richardson, Z.Zhang, M.Ibsen, R.E.Miles, M.R.Stringer, Y.Zhang, J.Young, P.Wright, and K.Ozanyan, "Fiber MOPA seeded difference frequency generation as a

tuneable source for THz tomography," in The Institute of Engineering and Technology, LONDON, 2010.

[14] M. Tang, H. Minamide, Y. Wang, T. Notake, S. Ohno, and H. Ito, "Tunable terahertz-wave generation from DAST crystal pumped by a monolithic dual-wavelength fiber laser," Opt. Express, vol. 19, pp. 779-786, 2011.

[15] O. Schmidt, C. Wirth, D. Nodop, J. Limpert, T. Schreiber, T. Peschel, R. Eberhardt, and A. Tünnermann, "Spectral beam combination of fiber amplified ns-pulses by means of interference filters," Opt. Express, vol. 17, pp. 22974-22982, 2009.

Appendix Publication list

[1] Kangkang Chen, Shaif-ul Alam, Dejiao Lin, Andrew Malinowski and D. J. Richardson, "100W, Fiberized, Linearly-Polarized, Picosecond Ytterbium Doped Fiber MOPA," in CLEO/QELS Baltimore, 2009.

[2] Kang Kang Chen, Shaif-ul Alam, John Hayes, Dejiao Lin, Andrew Malinowski and David J. Richardson "100W, Single Mode, Single Polarization, Picosecond, Ytterbium Doped Fibre MOPA Frequency Doubled to 530nm" in CLEO PR Shanghai, 2009

[3] Kangkang Chen, Shaif-ul Alam, Christophe A. Codemard, Andrew Malinowski, and David J. Richardson 'Excitation of individual Raman Stokes lines of up-to 9th order using rectangular shaped optical pulses at 530nm' in Photonics West San Francisco, 2010.

[4] Andrew Malinowski, Khu Tri Vu, Kang Kang Chen, Johan Nilsson, Yoonchan Jeong, Shaiful Alam, Dejiao Lin and David J. Richardson "High Power Pulsed Fiber MOPA System Incorporating Electro-Optic Modulator Based Adaptive Pulse Shaping" Optics Express, 2009.

[5] Shaif-ul Alam, Kangkang Chen, John R Hayes, Dejiao Lin, Andrew Malinowski, Howard J. Baker and David J. Richardson "Over 56W of frequency doubled light at 530nm pumped by an all-fiber, diffraction limited, picosecond fibre MOPA" in Photonics West San Francisco, 2010.

[6] James Beedell, Ian Elder, Kang Kang Chen, Shaif-ul Alam, David J. Richardson & Duncan Hand "Visible & mid-IR output using a fibre laser pump source" in SPIE Europe Security & Defence, 2009

[7] Dejiao Lin, Shaif-ul Alam, Kangkang Chen, Andrew Malinowski and D. Richardson, "100W, Fully-Fiberized Ytterbium Doped Master Oscillator Power Amplifier Incorporating Adaptive Pulse Shaping" in CLEO/QELS Baltimore, 2009.

[8] A.Malinowski, K.T.Vu, K.K.Chen, P.Horak, and D.J.Richardson, "Selective generation of individual Raman Stokes wavelengths using shaped optical pulses," in OFC San Diego, 2008.

[9] A.Shirakawa, C.Codemard, J.Ji, K.K.Chen, A.Malinowski, D.J.Richardson, J.K.Sahu, and J.Nilsson, "High-brightness 210 μJ pulsed Raman fiber source," in CLEO/QELS 2008 San Jose 2008.

[10] A.Shirakawa, C.Codemard, J.Ji, K.K.Chen, A.Malinowski, D.J.Richardson, J.K.Sahu, and J.Nilsson, "Brightness-enhancement of pulsed fiber source by double-clad Raman fiber," in The 69th Autumn Meeting of JAP Nagoya, 2008.

[11] Yonghang Shen, Shaif-ul Alam, Kangkang Chen, Dejiao Lin, Shuangshuang Cai, Bo Wu, Peipei Jiang, and Andrew. Malinowski and D. J. Richardson, "PPMgLN based high power optical parametric oscillator pumped by Yb3+-doped fiber amplifier incorporates active pulse shaping," JSTQE, 2008.

[12] S. U. Alam, Kangkang Chen, Dejiao Lin, Yonghang Shen, Shuangshuang Cai, Bo Wu, Peipei Jiang, Andrew. Malinowski and D. J. Richardson, "HIGH POWER, PULSED OPTICAL PARAMETRIC OSCILLATOR AT 3.5 μm PUMPED BY A DIODE SEEDED Yb3+-DOPED FIBER MOPA " in Photonocs IIT, Delhi, 2008.

[13] S. U. Alam, Kangkang Chen, Dejiao Lin, Yonghang Shen, Shuangshuang Cai, Bo Wu, Peipei Jiang, Andrew. Malinowski and D. J. Richardson, "Externally modulated, diode seeded Yb3+-doped fiber MOPA pumped high power optical parametric oscillator " in Photonics West San Jose, California, 2009.

[14] D.J.Richardson, A.Malinowski, S.-U.Alam, J.H.V.Price, K.K.Chen, Y.Jeong, J.Nilsson, J.Sahu, D.N.Payne, "Harnessing the power of light - the fibre laser revolution" JNOG 2008 Lannion France 13-20 Oct 2008 Lu1.0 (Invited)

[15] Alam, S. Lin, D. Malinowski, A. Hayes, J.R. Chen, K.K. Flannagan, J. Geddes, V. Nilsson, J. Richardson, D.J. "Spatially and temporally shaped,100 W, all-fiber, pulsed laser at 1.0 μ m" in CLEO EUROPE， 2009

[16] A.Malinowski, D.Lin, K.K.Chen, S.-U.Alam, D.J.Richardson, Z.Zhang, M.Ibsen, R.E.Miles, M.R.Stringer, Y.Zhang, J.Young, P.Wright, K.Ozanyan. " Fiber MOPA seeded difference frequency generation as a tuneable source for THz tomography" in London The Institute of Engineering and Technology, 21 Jan 2010

[17] Florien Kienle, Kang K. Cheng, Shaif-ul Alam, Corin B. E. Gawith, Jacob I. Mackenzie, David C. Hanna, David J. Richardson, and David P. Shepherd " A High-Power, Variable Repetition Rate, Picosecond Optical Parametric Oscillator Pumped by an Amplified Gain-Switched Diode" Optics Express, 2010.

[18] Kang Kang Chen, Shaif-ul Alam, Jonathan H. V. Price, John R. Hayes, Dejiao Lin, Andrew Malinowski, C. Codemard, Debashri Ghosh, Mrinmay Pal, Shyamal K. Bhadra and David J. Richardson, "Picosecond Fiber MOPA Pumped Supercontinuum Source With 39 W Output Power" in CLEO/QELS 2010 San Jose 2010 CTuX1.

[19] Florian Kienle, Kang K. Chen, Shaif-ul Alam, Corin B. E. Gawith, Jacob I. Mackenzie, David C. Hanna, David J. Richardson, and David P. Shepherd, "A Picosecond Optical Parametric Oscillator Synchronously Pumped by an Amplified Gain-Switched Laser Diode" in CLEO/QELS 2010 San Jose 2010 CThZ7.

[20] Kang Kang Chen, Shaif-ul Alam, Jonathan H. V. Price, John R. Hayes, Dejiao Lin, Andrew Malinowski, Christophe Codemard, Debashri Ghosh, Mrinmay Pal, Shyamal K. Bhadra, and David J. Richardson, " Picosecond Fiber MOPA Pumped Supercontinuum Source with 39 W Output Power " Optics Express, Vol. 18, Issue 6, pp. 5426-5432(2010).

[21] J.R.Hayes, M.N.Petrovich, F.Poletti, P.Horak, N.G.R.Broderick, X.Feng, S.X.Dasgupta, W.H.Loh, D.Ghosh, Pal. M., S.K.Bhadra, K.K.Chen, J.H.V.Price, S.-U.Alam, D.J.Richardson, "Recent advances in microstructured fibers for laser delivery and generation" Photonics West 2010 San Francisco 23-28 Jan 2010

[22] K.K.Chen, S.-U.Alam, J.R.Hayes, D.Lin, A.Malinowski, D.J.Richardson, "100W single mode single polarization picosecond ytterbium doped fibre MOPA frequency doubled to 530nm" Photonex '09 Coventry 14-15 Oct 2009

[23] J.R.Hayes, M.N.Petrovich, F.Poletti, S.Dasgupta, X.Feng, W.H.Loh, N.G.Broderick, K.K.Chen, S.-U.Alam, D.Lin, A.Malinowski, D.J.Richardson,

"Advanced fibre diesigns for high power laser beam delivery and generation" Photonex '09 Coventry 14-15 Oct 2009 (Invited)

[24] Kang Kang Chen, Shaif-ul Alam, John R. Hayes, Howard J. Baker, Dennis Hall, Roy Mc Bride, Jonathan H. V. Price, Dejiao Lin, Andrew Malinowski and David J. Richardson, " 56W frequency doubled source at 530 nm pumped by an all-fiber, single mode, single polarization, picosecond, Yb3+-doped fibre MOPA" IEEE Photonics Technology Letters, 2010.

[25] Peter Horak, Kang Kang Chen, Shaif-ul Alam, Sonali Dasgupta, and David J. Richardson, " High-Power Supercontinuum Generation with Picosecond Pulses" ICTON, 2010

[26] K. K. Chen, J. H. V. Price, S.-U. Alam, J. R. Hayes, D. Lin, A. Malinowski, and D. J. Richardson, "Polarisation maintaining 100W Yb-fiber MOPA producing μJ pulses tunable in duration from 1 to 21 ps," Opt. Express, vol. 18, pp. 14385-14394, 2010.

[27] K. K. Chen, S.-U. Alam, P. Horak, C. A. Codemard, A. Malinowski, and D. J. Richardson, "Excitation of individual Raman Stokes lines in the visible regime using rectangular-shaped nanosecond optical pulses at 530 nm," Opt. Lett., vol. 35, pp. 2433-2435, 2010.

[28] Jindan Shi, Xian Feng, Kangkang Chen, Peh Siong Teh, Peter Horak, Dejiao Lin, Shaif-ul Alam, Wei H. Loh, David J. Richardson, Morten Ibsen, “Efficient near-infrared supercontinuum generation in tellurite holey fiber pumped 320nm within the normal dispersion regime” ACP, 2010.

[29] D.J.Richardson, K.K.Chen, D.Lin, E.L.Lim, P.S.Teh, A.Malinowski, J.H.V.Price, F.Kienle, D.P.Shepherd, S.U.Alam, “Ultrafast fibre lasers for biophotonics” Rank Prize Fund Ultrafast Fibre Lasers for Biophotonics Grasmere 23-26 Aug 2010 (invited)

[30] F.Kienle, K.K.Chen, S.-U.Alam, C.B.E.Gawith, J.I.Mackenzie, D.C.Hanna, D.J.Richardson, D.P.Shepherd A high power, variable repetition rate, picosecond, optical parametric oscillator pumped by an amplified gain-switched diode Rank Prize Funds Symposium on Biophotonics Grasmere, England 23-26 Aug 2010.

[31] F.Kienle, K.K.Chen, S.-U.Alam, C.B.E.Gawith, J.I.Mackenzie, D.C.Hanna, D.J.Richardson, D.P.Shepherd， “Variable repetition rate, high power, picosecond optical parametric oscillator synchronously pumped by a fibre-amplified gain-switched laser diode” International Summer School in Ultrafast Nonlinear Optics SUSSP 66 Edinburgh, Scotland 11-21 Aug 2010.

[32] D.Lin, S.U.Alam, P.S.Teh, K.K.Chen, D.J.Richardson, “Selective excitation of multiple Raman Stokes wavelengths (green-yellow-red) using shaped multi-step pulses from an all-fiber OM MOPA” Optics Expresss, 2011, Vol.19 pp.2085-2092.

[33] D.Lin, P.S.Teh, S.-U.Alam, K.K.Chen, D.J.Richardson, “Simultaneous excitation of selective multiple Raman Stokes wavelengths (green- yellow-red) using shaped multi-setup pulses from a all-fibre MOPA system” Photonics West 2011, San Francisco, 22-27 Jan 2011, 7914-23.

[34] Shaif-ul Alam, Dejiao Lin, Peh Teh, Kang Chen, David Richardson, “A fiber based synchronously pumped tunable Raman laser in the NIR” CLEO EUROPE 2011 CJ1

[35] Shaif-ul Alam, Peh The, Dejiao Lin, Kangkang Chen, David Richardson, “Rapidly tunable, wavelength agile, visible fiber based light source exploiting Raman scattering of multi-step pulses” CLEO 2011 CThEE5

[36] Dejiao Lin, Shaif-ul Alam, Peh Siong The, Kangkang Chen, David Richardson, “Synchronously pumped tunable Raman laser in the visible pumped by an all-fiber PM MOPA at 1060 nm” CLEO 2011 CTuX1

[37] Dejiao Lin, Shaif-ul Alam, Peh Siong The, Kangkang Chen, David Richardson, “Tunable, synchronously-pumped fiber Raman laser in the visible and NIR exploiting MOPA generated rectangular pump pulses” Opt. Lett., accepted, 2010